

*INVESTIGATION OF INFLUENZA VIRUS
PARTICLE AGGREGATION AND PURIFICATION
WITH MAGNETIC SULFATED CELLULOSE
PARTICLES*

Dissertation zur Erlangung des akademischen Grades

Doktoringenieur

(Dr.-Ing.)

von Dipl.-Ing. Michael Martin Pieler

geb. am 11. November 1985 in Wien, Österreich

genehmigt durch die Fakultät für Verfahrens- und Systemtechnik

der Otto-von-Guericke-Universität Magdeburg

Promotionskommission:

Prof. Dr. rer. nat. Franziska Scheffler (Vorsitz)

Prof. Dr.-Ing. Udo Reichl (Gutachter)

Prof. Dr.-Ing. Jürgen Hubbuch (Gutachter)

Priv. Doz. Dr. Egbert Müller (Gutachter)

Eingereicht am: 31. Januar 2017

Promotionskolloquium am: 29. Mai 2017

Investigation of influenza virus particle aggregation and purification with magnetic sulfated cellulose particles

Investigation of influenza virus particle aggregation and purification with magnetic sulfated cellulose particles

Diese Dissertation ist meinem Vater gewidmet.

Investigation of influenza virus particle aggregation and purification with magnetic sulfated cellulose particles

Investigation of influenza virus particle aggregation and purification with magnetic sulfated cellulose particles

“In the beginner’s mind there are many possibilities,
but in the expert’s there are few.”

– Shunryu Suzuki

Investigation of influenza virus particle aggregation and purification with magnetic sulfated cellulose particles

KURZFASSUNG

Ziel dieser Doktorarbeit war es, neue Einblicke in das Influenza-Viruspartikel (VP) Aggregationsverhalten in verschiedenen Puffern für das Downstream Processing (DSP) zu erhalten. Zusätzlich sollte sowohl die Anwendbarkeit von magnetischen sulfatierten Cellulose-Partikeln (MSCP) für die Aufreinigung von Influenza-VP als auch für die kombinierte Aufreinigung und Formulierung von Influenza-VP-basierenden Vakzinen gezeigt werden.

Der erste Teil der Arbeit untersuchte das Influenza-VP Aggregationsverhalten, welches dramatische Effekte auf Vakzin-Herstellungsprozesse sowie auf die Wirksamkeit und die klinische Sicherheit von VP-basierenden Biotherapeutika haben kann. Gewöhnlich sind VP in Puffer-Lösungen suspendiert. Dabei stellen spezielle Salze definierte Puffereigenschaften, wie z.B. pH, Ionenstärke oder Osmolarität, ein. Interessanterweise zeigen gelöste Salze einen wiederkehrenden Trend in chemischen und biologischen Systemen durch ionenspezifische Effekte, die als Hofmeister Serie (HS) bekannt ist. Diese Effekte sind omnipräsent und beeinflussen kolloidale Partikelsysteme in verschiedenster Weise. In dieser Arbeit wurden die Effekte von verschiedenen Anionen (SO_4^{2-} , HPO_4^{2-} , Cl^- , Br^- , NO_3^- und I^-) und Kationen (K^+ , Na^+ , Li^+ , Mg^{2+} und Ca^{2+}) auf die Partikelgrößenverteilungen (PSD) von Influenza A/Puerto Rico/8/1934 H1N1 (A/PR) VP, die in adhärennten und Suspensions- Madin-Darby-Hunde-Nieren (MDCK) -Zellen hergestellt wurden, genauer untersucht. Die geernteten VP wurden inaktiviert, konzentriert und gegen die Puffer dialysiert, welche die Salze für die Untersuchungen beinhalteten. Danach wurden die PSD mit einer optimierten differentiellen zentrifugalen Sedimentations (DCS) Scheibenzentrifugen-Methode gemessen. Die PSD von den VP, die in adhärennten und Suspensionszellen hergestellt wurden, zeigten keine Aggregation in Puffern mit einer Ionenkonzentration höher als 60 mM. Bei geringer konzentrierten Puffern zeigten die in adhärennten Zellen hergestellten VP mehr Aggregation als die in Suspensionszellen hergestellten VP. Zusätzlich zeigten beide VP-Proben Ca^{2+} -induzierte Aggregation, wobei diese bei den in adhärennten Zellen hergestellten VP ausgeprägter war. Außerdem änderten die VP ihren monomeren apparenten hydrodynamischen Durchmesser (AHD) in Abhängigkeit des Ions und dessen Konzentration im Puffer. Die AHD vergrößerten sich mit steigenden Konzentrationen von NaCl , NaNO_3 , KCl , NaBr und $\text{Na}^+/\text{PO}_4^{3-}$, und verkleinerten sich mit steigenden Konzentrationen von CaCl_2 in den Puffern. Diese AHD Änderungen mit verschiedenen Ionen zeigten in manchen Fällen einen HS Trend.

Zusammenfassend konnte gezeigt werden, dass der verwendete Messaufbau für die Optimierung von Prozessen für das DSP, die Formulierung und des Blendings von Virus-basierenden Vakzinen oder viralen Vektoren, bei denen der Aggregationsstatus eine wichtige Rolle spielt, verwendet werden kann.

Im zweiten Teil der Arbeit wurden MSCP für die Aufreinigung von Influenza-VP sowie für die kombinierte Aufreinigung und Formulierung für Influenza Impfstoffe entwickelt und charakterisiert. Das Prinzip basierte dabei auf sulfatierte Cellulose-Liganden der MSCP, die eine

Investigation of influenza virus particle aggregation and purification with magnetic sulfated cellulose particles

pseudo-Affinität zu Influenza-VP haben und daher für eine VP-Aufreinigung ausgenutzt werden können.

Die MSCP-Methode wurde mit einer etablierten Zentrifugationsmethode für die Aufreinigung von A/PR VP, welche in adhärenen und Suspensionszellen hergestellt wurden, verglichen. Die aufgereinigten VP-Proben wurden charakterisiert und auf Protein-Ebene mittels Massenspektrometrie verglichen.

In beiden Methoden wurden zehn Influenza Virus Proteine identifiziert. Die Anzahl der kontaminierenden Wirtszellen-Proteine war für beide Methoden für beide VP-Proben vergleichbar. Jedoch konnte mit der MSCP-Methode die Zeit für die VP-Aufreinigung von 3 h für die Zentrifugationsmethode auf 30 min vor der Analyse mittels Massenspektrometrie verkürzt werden.

Im nächsten Schritt wurde ein MSCP-basierendes Vakzin Aufreinigungs- und Formulierungssystem entwickelt, mit dem das DSP von veterinären Vakzinen und das Hochdurchsatz-Screening von Virus-basierenden Vakzin- und viralen Vektor-Kandidaten vereinfacht werden kann. Das Konzept wurde mit A/PR VP, die in Suspensionszellen hergestellt wurden, implementiert. Die geerntete VP-Brühe wurde geklärt, inaktiviert, konzentriert und diafiltriert um die VP an die MSCP zu binden. Die erhaltenen VP- oder Antigen-beladenen MSCP (aMSCP) wurden anschließend für Immunisierungsstudien direkt in Mäuse injiziert. Diese Studie beinhaltete positive Kontrollen (suspendierte VP und eine suspendierte VP/leere MSCP Interaktions-Kontrolle) und eine negative Kontrolle (Formulierungspuffer). Im Versuch zeigte die mit aMSCP immunisierte Gruppe hohe Anti-Influenza A Antikörper Titer und einen vollen Schutz nach einer letalen Infektion mit Replikations-kompetenten A/PR VP. Die aMSCP immunisierte Gruppe zeigte vergleichbare Resultate wie die positiven Kontrollen (suspendierte VP und eine suspendierte VP/leere MSCP Interaktions-Kontrolle). Im Kontrast dazu zeigte die negative Kontrolle (Formulierungspuffer) keine Anti-Influenza A Antikörper Titer und auch keinen Schutz nach der letalen Infektion. Ergänzend dazu zeigte die Analyse der Nukleoprotein-Genkopienanzahl in den Lungen der aMSCP immunisierten Gruppe eine 400-fache Reduktion im Vergleich zu der negativen Kontroll-Gruppe (Formulierungspuffer). Dies implizierte eine effektive Induktion der antiviralen Immunität durch das MSCP-Vakzin.

Im zweiten Teil konnte gezeigt werden, dass die Aufreinigung und Formulierung eines Influenza Vakzins mittels MSCP schnell und zuverlässig möglich ist und ein voller Schutz gegen eine letale Influenza A/PR Infektion erzielt werden kann. Zusätzlich könnte das MSCP Aufreinigungs- und Formulierungssystem nach der VP-Produktionsphase direkt in einem Bioreaktor implementiert werden, um die benötigten Aufreinigungsschritte weiter zu reduzieren. Solch ein Prozess könnte bei kostengünstigen veterinären Vakzinen und Hochdurchsatz-Screenings für die Evaluierung und Produktion von Virus-basierenden Vakzinen und viralen Vektoren Anwendung finden.

Zusammenfassend konnten in dieser Doktorarbeit neue Erkenntnisse im Bereich der Influenza-VP Aggregation in verschiedenen Puffern gewonnen werden und die Anwendbarkeit von MSCP für die VP-Aufreinigung und -Formulierung gezeigt werden. Der verwendete Puffer-Screening-Ansatz kann

Investigation of influenza virus particle aggregation and purification with magnetic sulfated cellulose particles

einfach für andere VP adaptiert werden. Zusätzlich kann komplementäre Analytik in Kombination mit dem verwendeten Puffer-Screening helfen neue Faktoren der VP-Aggregation aufzudecken. MSCP-Vakzine könnten durch eine topische oder transdermale Applikation weiter optimiert werden.

Investigation of influenza virus particle aggregation and purification with magnetic sulfated cellulose particles

Investigation of influenza virus particle aggregation and purification with magnetic sulfated cellulose particles

ABSTRACT

This doctoral thesis aims to deliver new insights on influenza virus particle (VP) aggregation behavior in different buffers for the downstream processing (DSP). Furthermore, the applicability of magnetic sulfated cellulose particles (MSCP) for new purification processes for influenza VP and combined purification and formulation processes for influenza VP-based vaccines were shown.

The first part of this work investigates influenza VP aggregation, which has dramatic effects on vaccine production processes and the efficacy and clinical safety of virus-based biotherapeutics. Usually, VP are suspended in buffer solutions. In these buffers, specific salts are used to establish defined properties in the solution, e.g., pH, ionic strength, or osmolarity. Interestingly, the dissolved salts show ion-specific effects in a reoccurring trend in chemical and biological systems known as Hofmeister series (HS). These effects are omnipresent and also affect colloidal particle systems in different ways. In this work, the effects of different anions (SO_4^{2-} , HPO_4^{2-} , Cl^- , Br^- , NO_3^- , and I^-) and cations (K^+ , Na^+ , Li^+ , Mg^{2+} , and Ca^{2+}) on the PSD of influenza A/Puerto Rico/8/1934 H1N1 (A/PR) VP produced in adherent and suspension Madin Darby canine kidney (MDCK) cells were investigated. The harvested VP were inactivated, concentrated, and dialyzed against buffers containing the different salts for the screening. After that, the PSD were measured by an optimized differential centrifugal sedimentation (DCS) disc centrifugation method. The PSD for both adherent and suspension cell-derived VP showed no aggregation in buffers with a ion concentration higher than 60 mM. In lower concentrated buffers, the VP produced in the adherent cell line showed more aggregation compared to the VP produced in the suspension cell line. Ca^{2+} also induced aggregation in both VP samples, and more aggregation for the VP produced in the adherent cell line. Moreover, the VP changed their monomeric apparent hydrodynamic diameter (AHD) depending on the ion and its concentration in the buffer. The AHD increased with increasing concentrations of NaCl, NaNO_3 , KCl, NaBr, and $\text{Na}^+/\text{PO}_4^{3-}$, and decreased with increasing concentrations of CaCl_2 in the buffer. The AHD changes with different ions sometimes resembled an HS trend.

Consequently, this setup can be used to optimize virus-based vaccine or viral vector production processes, where the aggregation status is crucial for DSP, formulation, and blending.

In the second part of this work, MSCP were developed and characterized regarding their applicability for influenza VP purification as well as for a combined purification and formulation of influenza vaccines. The principle is based on the sulfated cellulose ligands of the MSCP that have a pseudo affinity to influenza VP, which can be used for VP purification.

The MSCP purification method was compared to an established centrifugation method for the purification of A/PR VP produced in adherent and suspension MDCK cells. The purified VP samples were characterized and compared on the protein level by mass spectrometry.

For both methods, ten influenza virus proteins were identified. The number of contaminating host cell proteins was similar for both purification methods for both VP samples. With the MSCP method,

Investigation of influenza virus particle aggregation and purification with magnetic sulfated cellulose particles

however, the VP purification time could be reduced from 3 h (centrifugation method) to 30 min before mass spectrometry analysis.

In a next step, a MSCP-based vaccine purification and formulation system was designed to simplify the DSP of veterinary vaccines and to enable high-throughput screening applications for virus-based vaccines and viral vector candidates. Proof of concept was carried out with A/PR VP produced in suspension MDCK cells. The harvested VP broth was clarified, inactivated, concentrated, and diafiltered followed by binding the VP to the MSCP. The VP- or antigen-loaded MSCP (aMSCP) were then directly injected into mice for immunization including positive controls (suspended VP and suspended VP/empty MSCP interaction control) and negative controls (formulation buffer). In the experimental setup, the group immunized with aMSCP showed high anti-influenza A antibody titers and full protection after a lethal challenge with replication competent influenza A/PR VP. Furthermore, the group immunized with the aMSCP showed similar results compared to the positive controls (suspended VP and suspended VP/empty MSCP interaction control). In contrast, the negative control group (formulation buffer) showed no anti-influenza A antibody titers and no protection after the lethal challenge. In addition, the analysis of the nucleoprotein gene copy numbers in the lungs of aMSCP immunized mice showed a 400-fold reduction when compared to the negative control (formulation buffer), which implies an efficient induction of antiviral immunity.

In summary, the results of the second part showed that the purification and formulation of an influenza vaccine with MSCP was fast, reliable and elicited full protection in mice against a lethal influenza A/PR infection. Additionally, the MSCP purification and formulation system could be implemented after the VP production phase directly in the bioreactor to further reduce the number of needed process steps. Such a process could be applicable for low-cost veterinary vaccines and high-throughput screening applications for the evaluation and production of virus-based vaccine and viral vector candidates.

Overall, this doctoral thesis revealed new findings in the field of influenza VP aggregation in different buffers and could show the applicability of MSCP for VP purification and formulation setups. The used buffer screening setup can be easily adapted to other VP. Furthermore, complementary analytics in combination with the outlined buffer screening system can help to uncover the underlying factors of VP aggregation. The MSCP system can be potentially improved by a topical or transdermal application.

DANKSAGUNGEN

Ein großes Danke geht an Prof. Dr.-Ing. Udo Reichl und an Prof. Dr. Michael Wolff für die Betreuung und die Möglichkeit diese Dissertation in der Bioprozesstechnik Arbeitsgruppe anzufertigen. Besonderen Dank für die vielen lehrreichen Diskussionen, die eingeräumten Freiräume um Neues zu probieren, und die vielen Möglichkeiten Konferenzen und Kooperationspartner zu besuchen.

Ein weiteres großes Danke geht an die Mitglieder des DSP Teams, vor allem an Pavel Marichal-Gallardo, Matthias Meininger, Anja Bastian, Lisa Fichtmüller, Ana Raquel Fortuna, Laura Fischer und Corina Siewert. Ein besonderes Danke geht dabei an meinen Bürokollegen Pavel, von dem ich in unzähligen Diskussionen viel lernen konnte, und an Anja, Lisa und Corina für die umfassende Unterstützung im Labor.

Ein weiteres großes Danke geht an die gesamte Bioprozesstechnik Arbeitsgruppe, vor allem an Thomas Bissinger, Felipe Tapia, Timo Frensing, Thilo Muth, René Hennig, Robert Kottler, Daniel Vázquez Ramírez, Sascha Young Kupke, Anja Serve, Ilona Behrendt, Claudia Best, Susanne König, Dirk Benndorf und Erdmann Rapp.

Danke an Anja Heyse und Nicole Gebert, die im Zuge ihrer Masterarbeiten einige wichtige Puzzlesteine zu dieser Arbeit beitragen konnten.

Danke an Bianka Stein von der Prozesstechnik Arbeitsgruppe für die Unterstützung bei der Messung des Zeta-Potentials der MSCP.

Danke an Sarah Frentzel vom Universitätsspital der Otto-von-Guericke Universität Magdeburg und Dunja Bruder vom Universitätsspital der Otto-von-Guericke Universität Magdeburg und dem Helmholtz-Zentrum für Infektionsforschung für die interessante und erfolgreiche Zusammenarbeit bei den Immunisierungs-Studien.

Danke an das Bundesministerium für Bildung und Forschung (BMBF) für die Unterstützung meiner Dissertation im Zuge des Projektes 0315640C sowie an die BMBF-Projektpartner: Frank Hämmerling, Christopher Ladd Effio, Prof. Dr. Jürgen Hubbuch (Karlsruhe Institute of Technology); Dr. Boris Hundt, Matthias Proemmel, Sabine Stefaniak (IDT Biologika GmbH); Dr. Louis Villain, Katrin Töppner (Sartorius Stedim Biotech GmbH); Dr. Egbert Mueller, Judith Vajda (Tosoh Bioscience GmbH).

Danke auch an Alexander Förster, Robert Prusas, Pawan Goyal, Jens Bremer, Dustin Lemme und Falko Kaule für die vielen Unternehmungen in der Freizeit.

Danke auch an die Gutachter Prof. Dr.-Ing. Udo Reichl (Otto-von-Guericke-Universität Magdeburg und Max-Planck-Institut für Dynamik komplexer technischer Systeme), Prof. Dr. Jürgen Hubbuch (Karlsruhe Institute of Technology) und Dr. Egbert Müller (Tosoh Bioscience GmbH).

Zu guter Letzt möchte ich noch meinem Vater Josef Arnold Pieler, meiner Freundin Bianca Wuchty, meiner Schwester Manuela Pieler, Renate Klein, Patrick Klein sowie meiner restlichen Familie für ihre Unterstützung danken. Ohne euren Rückhalt wäre dies Alles nicht möglich gewesen!

ERKLÄRUNG

Ich erkläre hiermit, dass ich die vorliegende Arbeit ohne unzulässige Hilfe Dritter und ohne Benutzung anderer als der angegebenen Hilfsmittel angefertigt habe. Die aus fremden Quellen direkt oder indirekt übernommenen Gedanken sind als solche kenntlich gemacht.

Insbesondere habe ich nicht die Hilfe einer kommerziellen Promotionsberatung in Anspruch genommen. Dritte haben von mir weder unmittelbar noch mittelbar geld-werte Leistungen für Arbeiten erhalten, die im Zusammenhang mit dem Inhalt der vorgelegten Dissertation stehen.

Die Arbeit wurde bisher weder im Inland noch im Ausland in gleicher oder ähnlicher Form als Dissertation eingereicht und ist als Ganzes auch noch nicht veröffentlicht.

Magdeburg, am 31.01.2017

Michael M. Pieler

CONTENTS

1 MOTIVATION	1
1.1 INVESTIGATION OF INFLUENZA A VIRUS PARTICLE AGGREGATION	2
1.2 INFLUENZA A VIRUS PARTICLE PURIFICATION WITH MAGNETIC SULFATED CELLULOSE PARTICLES.....	2
2 BACKGROUND	5
2.1 INFLUENZA VACCINES	5
2.2 CELL CULTURE-BASED PRODUCTION OF INFLUENZA VIRUS.....	7
2.3 DOWNSTREAM PROCESSING OF INFLUENZA VIRUS PARTICLES	7
2.4 ANALYTICS DURING THE PRODUCTION OF INFLUENZA VIRUS PARTICLES.....	9
2.4.1 <i>Upstream processing</i>	9
2.4.2 <i>Downstream processing</i>	10
2.4.3 <i>Virus particle aggregation and influenza virus analytics</i>	10
2.5 VIRUS PARTICLE AGGREGATION ANALYTICS.....	11
2.6 IMMUNIZATION STUDIES IN MICE.....	14
3 MATERIALS AND METHODS	15
3.1 BUFFERS AND MEDIA SOLUTIONS	15
3.2 SCREENING BUFFERS	15
3.3 UPSTREAM PROCESSING	16
3.3.1 <i>Adherent MDCK production system</i>	16
3.3.2 <i>Suspension MDCK production system</i>	16
3.3.3 <i>Influenza virus particle production for analytical method comparison</i>	16
3.4 DOWNSTREAM PROCESSING	17
3.4.1 <i>Virus broth clarification and inactivation</i>	17
3.4.2 <i>Tangential flow filtration concentration for aggregation studies</i>	17
3.4.3 <i>Tangential flow filtration concentration and diafiltration for immunization studies</i>	17
3.4.4 <i>Dialysis for buffer exchange</i>	17
3.4.5 <i>Influenza virus purification using centrifugation for analytics</i>	18
3.4.6 <i>Production of magnetic sulfated cellulose particles</i>	18
3.4.7 <i>Virus particle purification using magnetic sulfated cellulose particles for analytics</i>	20
3.4.8 <i>Positive control antigen preparation</i>	21
3.4.9 <i>Antigen purification and formulation using magnetic sulfated cellulose particles</i>	21
3.5 IMMUNIZATION STUDIES.....	21
3.5.1 <i>Mice</i>	22
3.5.2 <i>In vivo titration of the vaccine antigen dose</i>	22
3.5.3 <i>Immunization with antigen-loaded magnetic sulfated cellulose particles</i>	22
3.5.4 <i>Challenge of mice with a lethal virus dose</i>	23
3.6 ANALYTICS	23
3.6.1 <i>Hemagglutination assay</i>	23
3.6.2 <i>Single radial immunodiffusion assay for hemagglutinin antigen quantification</i>	23

3.6.3 Particle size distribution measurements.....	24
3.6.4 Gradient buffer density measurements.....	24
3.6.5 Virus particle density measurements	25
3.6.6 LC-MS/MS-based proteome analysis	26
3.6.7 Blood collection and preparation of sera	26
3.6.8 Detection of anti-A/PR antibodies by ELISA.....	26
3.6.9 Viral load determination by quantitative real-time PCR.....	27
3.6.10 Statistical analysis.....	28
4 RESULTS AND DISCUSSION	29
4.1 INVESTIGATION OF INFLUENZA A VIRUS PARTICLE AGGREGATION	29
4.1.1 Tangential flow filtration concentration.....	29
4.1.2 Virus particle density measurements	29
4.1.3 Specific ion effects on virus particle size distributions.....	31
4.2 INVESTIGATION OF INFLUENZA A VIRUS PARTICLE PURIFICATION USING MAGNETIC SULFATED CELLULOSE PARTICLES.....	41
4.2.1 Production of magnetic sulfated cellulose particles	42
4.2.2 Comparison of magnetic sulfated cellulose particles with an established centrifugation method for analytics	44
4.2.3 Immunization studies in mice using magnetic sulfated cellulose particles.....	50
5 CONCLUSIONS	57
5.1 INVESTIGATION OF INFLUENZA A VIRUS PARTICLE AGGREGATION	57
5.2 INVESTIGATION OF INFLUENZA A VIRUS PURIFICATION AND VACCINE FORMULATION USING MAGNETIC SULFATED CELLULOSE PARTICLES.....	57
6 OUTLOOK	59
6.1 INVESTIGATION OF VIRUS PARTICLE AGGREGATION	59
6.2 VIRUS PARTICLE PURIFICATION AND VACCINE FORMULATION USING MAGNETIC SULFATED CELLULOSE PARTICLES.....	60
7 REFERENCES.....	61
8 APPENDICES.....	73
8.1 MATERIALS AND EQUIPMENT.....	73
8.2 STANDARD OPERATING PROCEDURES USED IN THIS WORK	77
8.3 STANDARD OPERATING PROCEDURE FOR INFLUENZA VIRUS PARTICLES SIZE DISTRIBUTION MEASUREMENTS WITH THE CPS DISC CENTRIFUGE DC24000	78
8.3.1 Introduction.....	78
8.3.2 Information material.....	78
8.3.3 Materials	78
8.3.4 Methods.....	81
8.3.5 Validation.....	87
8.3.6 Data analysis.....	87
8.3.7 Points to consider.....	88

8.4 VALIDATION DATA OF THE VIRUS PARTICLES SIZE DISTRIBUTION MEASUREMENT METHOD WITH THE CPS DISC CENTRIFUGE DC24000	89
8.5 PUBLICATIONS.....	91
8.6 PATENTS.....	93
8.7 ATTENDED CONFERENCES	94
8.7.1 Talks.....	94
8.7.2 Posters.....	94
8.8 SUPERVISED STUDENT PROJECTS.....	95
8.8.1 Master theses.....	95
8.8.2 Bachelor thesis.....	95
8.9 CURRICULUM VITAE	96

LIST OF TABLES

TABLE 1 MEAN MONOMERIC APPARENT HYDRODYNAMIC DIAMETER MAXIMA OF A/PR _{SUS} IN STANDARD BUFFER AND STANDARD BUFFER WITH NaCl.....	32
TABLE 2 MEAN MONOMERIC APPARENT HYDRODYNAMIC DIAMETERS OF A/PR _{SUS} IN STANDARD BUFFER WITH 20 MM SALTS.....	35
TABLE 3 MEAN MONOMERIC APPARENT HYDRODYNAMIC DIAMETERS OF A/PR _{SUS} DIALYZED AGAINST STANDARD BUFFER WITH 540 MM SALTS.....	37
TABLE 4 LIST OF IDENTIFIED INFLUENZA A VIRUS PROTEINS AFTER PURIFICATION WITH MAGNETIC SULFATED CELLULOSE PARTICLES AND A CENTRIFUGATION METHOD FOR ANALYTICS.....	45
TABLE 5 HOST CELL PROTEINS IDENTIFIED IN PURIFIED INFLUENZA A VIRUS PARTICLE SAMPLES.....	46
TABLE 6 HEMAGGLUTINATION ACTIVITY LOSSES DURING ANTIGEN-LOADED MAGNETIC SULFATED CELLULOSE PARTICLES LOADING AND WASHING.....	53
TABLE 7 CHEMICALS USED IN THIS WORK.....	73
TABLE 8 PARTICLE STANDARDS USED IN THIS WORK.....	74
TABLE 9 MAGNETIC PARTICLES USED IN THIS WORK.....	74
TABLE 10 MOLECULAR BIOLOGY, CELL CULTURE AND IMMUNIZATION EXPERIMENTS EQUIPMENT USED IN THIS WORK.....	74
TABLE 11 GENERAL EQUIPMENT USED IN THIS WORK.....	76
TABLE 12 STANDARD OPERATING PROCEDURES USED IN THIS WORK.....	77
TABLE 13 DCS DISC CENTRIFUGE SOP EQUIPMENT.....	79
TABLE 14 DCS DISC CENTRIFUGE SOP CHEMICALS.....	79
TABLE 15 DCS DISC CENTRIFUGE SOP STANDARD PARTICLES.....	80
TABLE 16 DCS DISC CENTRIFUGE SOP STANDARD PROCEDURES.....	81
TABLE 17 DCS DISC CENTRIFUGE SOP SAMPLE PARAMETERS.....	81
TABLE 18 DCS DISC CENTRIFUGE SOP CALIBRATION STANDARD PARAMETERS.....	81
TABLE 19 DCS DISC CENTRIFUGE SOP FLUID PARAMETERS.....	82
TABLE 20 DCS DISC CENTRIFUGE SOP OBSERVED VP DENSITIES.....	82
TABLE 21 DCS DISC CENTRIFUGE SOP CLEANING THE CENTRIFUGE.....	82
TABLE 22 DCS DISC CENTRIFUGE SOP CLEANING THE CENTRIFUGE DISC.....	83
TABLE 23 DCS DISC CENTRIFUGE SOP GRADIENT LAYER COMPOSITION.....	84
TABLE 24 DCS DISC CENTRIFUGE SOP GRADIENT LAYER PREPARATION.....	84
TABLE 25 DCS DISC CENTRIFUGE SOP SAMPLE MEASUREMENT.....	85

TABLE 26 MEASUREMENT DATA LOWER AND UPPER DETECTION LIMIT.....	89
TABLE 27 VALIDATION RESULTS FOR SINGLE MEASUREMENT	90

LIST OF FIGURES

FIGURE 1 ELECTRON MICROSCOPY OF A/PR VIRUS PARTICLES	5
FIGURE 2 DOWNSTREAM PROCESSING TRAIN	9
FIGURE 3 INTEGRAL AND DIFFERENTIAL CENTRIFUGAL SEDIMENTATION	13
FIGURE 4 DISC CENTRIFUGE CONSTRUCTION PRINCIPLE	13
FIGURE 5 SULFATION REACTION APPARATUS SCHEME	19
FIGURE 6 IMMUNIZATION EXPERIMENT FOR THE <i>IN VIVO</i> TITRATION OF THE VACCINE ANTIGEN DOSE	22
FIGURE 7 IMMUNIZATION EXPERIMENT WITH ANTIGEN-LOADED MAGNETIC SULFATED CELLULOSE PARTICLES	23
FIGURE 8 PREPARED VIRUS PARTICLE SAMPLES USED FOR DIALYSIS.	30
FIGURE 9 SEDIMENTATION TIME PLOT OF A/PR _{ADH} SAMPLE SPIKED WITH THE 105 NM AND 239 NM PARTICLE STANDARD.	30
FIGURE 10 PARTICLE SIZE DISTRIBUTIONS OF A/PR _{SUS} IN DIFFERENT NaCl CONCENTRATIONS.....	31
FIGURE 11 MONOMERIC APPARENT HYDRODYNAMIC DIAMETER MAXIMA TRENDS OF A/PR _{SUS} IN STANDARD BUFFER WITH 20, 60, AND 540 mM SALTS.	33
FIGURE 12 PARTICLE SIZE DISTRIBUTIONS OF A/PR _{SUS} DIALYZED AGAINST STANDARD BUFFER WITH 20 mM SALTS WITH DIFFERENT CATIONS.....	34
FIGURE 13 PARTICLE SIZE DISTRIBUTIONS OF A/PR _{SUS} DIALYZED AGAINST STANDARD BUFFER WITH 20 mM SALTS WITH DIFFERENT ANIONS.....	34
FIGURE 14 PARTICLE SIZE DISTRIBUTIONS OF A/PR _{SUS} DIALYZED AGAINST STANDARD BUFFER WITH 60 mM SALTS WITH DIFFERENT CATIONS.....	36
FIGURE 15 PARTICLE SIZE DISTRIBUTIONS OF A/PR _{SUS} DIALYZED AGAINST STANDARD BUFFER WITH 60 mM SALTS WITH DIFFERENT ANIONS.....	36
FIGURE 16 PARTICLE SIZE DISTRIBUTIONS OF A/PR _{SUS} DIALYZED AGAINST STANDARD BUFFER WITH 540 mM SALTS WITH DIFFERENT CATIONS.....	37
FIGURE 17 PARTICLE SIZE DISTRIBUTIONS OF A/PR _{SUS} DIALYZED AGAINST STANDARD BUFFER WITH 540 mM SALTS WITH DIFFERENT ANIONS.....	38
FIGURE 18 PARTICLE SIZE DISTRIBUTIONS OF A/PR _{SUS} DIALYZED AGAINST STANDARD BUFFER WITH 20, 60, AND 540 mM Ca ²⁺	39
FIGURE 19 PARTICLE SIZE DISTRIBUTIONS OF A/PR _{ADH} DIALYZED AGAINST STANDARD BUFFER WITH 20, 60, AND 540 mM Ca ²⁺	39
FIGURE 20 PARTICLE SIZE DISTRIBUTIONS OF A/PR _{SUS} AND A/PR _{ADH} DIALYZED AGAINST STANDARD BUFFER.	40
FIGURE 21 PARTICLE SIZE DISTRIBUTIONS OF A/PR _{SUS} AND A/PR _{ADH} DIALYZED AGAINST STANDARD BUFFER WITH 20 mM NaCl.....	40

FIGURE 22 ADHERENT CELL CULTURE-DERIVED INFLUENZA A VIRUS PARTICLE AGGREGATION USING MAGNETIC SULFATED CELLULOSE PARTICLES BASED ON MAGNE™ PROTEIN A PARTICLES FOR PURIFICATION.....	41
FIGURE 23 OPTIMIZATION OF THE MG 200 MAGNETIC MACROPOROUS CELLULOSE PARTICLES SULFATION PROCESS	42
FIGURE 24 MAGNETIC SULFATED CELLULOSE PARTICLES DISINTEGRATION OVER SULFATION TIME	43
FIGURE 25 COMPARISON OF IDENTIFIED VIRAL AND HOST CELL PROTEINS FOR THE INFLUENZA SAMPLES PURIFIED BY MAGNETIC SULFATED CELLULOSE PARTICLES AND CENTRIFUGATION FOR ANALYTICS	44
FIGURE 26 ANTI-A/PR ANTIBODY RESPONSES MEASURED BY ELISA AFTER IMMUNIZATION FOR THE ESTABLISHMENT OF THE ANTIGEN DOSE IN MICE	51
FIGURE 27 RELATIVE BODY WEIGHT OF MICE AFTER INFECTION WITH A LETHAL DOSE OF ACTIVE A/PR FOR THE ESTABLISHMENT OF THE ANTIGEN DOSE.....	51
FIGURE 28 NUCLEOPROTEIN GENE COPIES IN THE LUNG TISSUES OF MICE AFTER INFECTION WITH A LETHAL DOSE OF ACTIVE A/PR FOR THE ESTABLISHMENT OF THE ANTIGEN DOSE.....	52
FIGURE 29 ANTI-A/PR ANTIBODY RESPONSES MEASURED BY ELISA AFTER IMMUNIZATION OF MICE WITH ANTIGEN-LOADED MAGNETIC SULFATED CELLULOSE PARTICLES AND CONTROLS.....	54
FIGURE 30 RELATIVE BODY WEIGHT AFTER INFECTION WITH A LETHAL A/PR VIRUS DOSE AFTER IMMUNIZATION WITH ANTIGEN-LOADED MAGNETIC SULFATED CELLULOSE PARTICLES AND CONTROLS	55
FIGURE 31 NUCLEOPROTEIN GENE COPIES IN THE LUNG TISSUES OF MICE AFTER INFECTION WITH A LETHAL A/PR VIRUS DOSE AFTER IMMUNIZATION WITH ANTIGEN-LOADED MAGNETIC SULFATED CELLULOSE PARTICLES AND CONTROLS	56
FIGURE 32 WEIGHTED LINEAR REGRESSION FOR SINGLE MEASUREMENTS	90

LIST OF ABBREVIATIONS AND ACRONYMS

Abbreviation/acronym	Description
A/PR	A/Puerto Rico/8/1934 (H1N1)
AHD	apparent hydrodynamic diameter maximum
aMSCP	antigen-loaded magnetic sulfated cellulose particles
AUC	analytical ultracentrifugation
CCC	critical coagulation concentration
CFV	concentrated and filtered virus samples
CSC	critical stabilization concentration
CVH	clarified virus harvests
DCS	differential centrifugal sedimentation
DSP	downstream processing
ELISA	enzyme-linked immunosorbent assay
EM	electron microscopy
FASP	filter aided sample preparation
FCS	fetal calf serum
GB	gradient buffer
HA	hemagglutinin
HAU	hemagglutination units
HS	Hofmeister series
HSPG	heparan sulfate proteoglycans
LC-MS/MS	liquid chromatography-tandem mass spectrometry
MDCK	Madin Darby canine kidney
MOI	multiplicity of infection
MSCP	magnetic sulfated cellulose particles
MWCO	molecular weight cut-off
NA	neuraminidase

Abbreviation/acronym	Description
PBS	phosphate buffer saline
PCR	polymerase chain reaction
PFU	plaque forming unit
PMMA	poly(methyl methacrylate)
PSD	particle size distribution
PVC	polyvinyl chloride
RPM	revolutions per minute
RT	room temperature
SB	standard buffer
SOP	standard operating procedure
SPA	single particle approximation
TCID50	50% tissue culture infective dose
USP	upstream processing
VP	virus particle

LIST OF SYMBOLS

Symbol	Unit	Description
a	kg m^{-3}	linear equation placeholder for the gradient buffer density ρ_{GB}
b	kg m^{-3}	linear equation placeholder for ρ_{Std} minus ρ_{GB} multiplied with $t_{\text{Std}105\text{nm}}$ divided by t_{VP}
D	m	Stokes/hydrodynamic diameter
d	$\text{s}^{-1} \text{m}^{-2}$	y-axis segment of linear equation
e	-	slope of linear equation
F_{C}	kg m rad s^{-1}	centrifugal force
F_{S}	$\text{N} = \text{kg m s}^{-2}$	Stokes force
g	kg m^{-3}	y-axis segment of linear equation
k	$\text{m kg}^{-1} \text{s}^{-1}$	slope of linear equation
R	m	radius from initial settling to detection point
r	m	radius
t	s	sedimentation time
v	m s^{-1}	sedimentation velocity
η	$\text{Pa s} = \text{kg s}^{-1} \text{m}^{-1}$	dynamic viscosity
ρ	kg m^{-3}	density
ω	rad s^{-1}	angular velocity
x	kg m^{-3}	linear equation placeholder for the particle density ρ_{i}
y	$\text{s}^{-1} \text{m}^{-1}$	linear equation placeholder for the inverse product of the sedimentation time t_{i} and the squared Stokes/hydrodynamic diameter D_{i}

LIST OF SYMBOL INDICES

Symbol	Description
F	fluid
GB	gradient buffer
i	placeholder for the 105 or 239 nm particle standard
j	placeholder for the 4 to 16% or the 8 to 20% gradient buffer
P	particle
Std	particle standard

1 MOTIVATION

This doctoral thesis was part of the cooperation project “Optimization of an industrial process for the cell culture-based production of seasonal and pandemic influenza vaccines as an alternative to classic egg-based production processes” funded by the Federal Ministry of Education and Research (BMBF, 0315640C). In the course of this project several unit operations were optimized for the downstream processing (DSP) of cell culture-based influenza virus particles (VP). In addition, analytical methods were developed to obtain more information on VP aggregation, which can dramatically affect DSP unit operations. Furthermore, the binding behavior of VP to sulfated carbohydrates, which were used for chromatographic and magnetic particle unit operations, was investigated.

The shift from egg- to cell culture-based influenza VP production systems in industry is dependent on many factors and the benefits are still discussed in this field. However, an optimized DSP can improve both production approaches and can help to increase the availability of safe and cost-effective vaccines.

The main project of this doctoral thesis was the investigation of influenza A/Puerto Rico/8/1934 H1N1 (A/PR) VP aggregation outlined in section 1.1. There, the effects of different buffers on the particle size distributions (PSD) of influenza VP were characterized in an extensive study. The results obtained represent a basis for the optimization of different DSP unit operations, which usually involve a buffer change.

During the optimization of the buffer exchange method for the experiments addressed above, magnetic sulfated cellulose particles (MSCP) were developed as a potential tool. However, their application for the buffer exchange was limited, as aggregation was observed for some VP samples (see section 4.2). Nevertheless, the MSCP were used in the second main project on influenza VP purification by MSCP outlined in section 1.2. There, the MSCP purification method was compared to a centrifugation method and was used for the purification and formulation of a novel influenza vaccine.

1.1 Investigation of influenza A virus particle aggregation

Aggregation of VP strongly influences production of VP-based biopharmaceuticals as well as their clinical safety and efficacy. In particular, VP aggregation is known to affect *in vitro* VP infectivity assays, quantification [1], inactivation [2–4], and DSP [5]. This wide-ranging impact renders this subject very interesting for research and development of several virus-based biopharmaceuticals, like vaccines or viral vectors for gene-therapies.

VP are typically suspended in buffer solutions to obtain defined properties for specific applications. To establish these buffer features different salts are used to control pH, ionic strength, osmolarity, conductivity, etc., depending on the application. The ions of these salts show ion-specific effects in chemical and biological systems. These effects often resemble a reoccurring trend termed Hofmeister series (HS) [6,7].

Therefore, different ions within the HS were evaluated in the scope of this doctoral thesis for their effects on the PSD of influenza VP. To measure the PSD an optimized differential centrifugal sedimentation (DCS) disc centrifuge method was implemented. The direct HS order of the screened ions was for the anions $\text{SO}_4^{2-} < \text{HPO}_4^{2-} < \text{Cl}^- < \text{Br}^- < \text{NO}_3^- < \text{I}^-$, and for the cations $\text{K}^+ < \text{Na}^+ < \text{Li}^+ < \text{Mg}^{2+} < \text{Ca}^{2+}$ [6,8,9]. The HS order is based on the effect of the specific ion on protein solubility. Ions on the left side of the direct HS increase solvent surface tension and decrease solubility of nonpolar molecules which is referred to as "salting out" or kosmotropic properties. The ions on the right side increase the solubility of nonpolar molecules which is referred to as "salting in" or chaotropic properties [9,7]. HS effects were already described for synthetic nanoparticles [9–15]. However, for VP no systematic experimental evaluation with high resolution PSD measurement methods has been carried out so far. Because of that, the present doctoral thesis aims to deliver new information on the effects of specific ions on the PSD of cell culture-derived influenza VP by assessment with DCS disc centrifugation. Influenza A/PR VP produced in adherent and suspension Madin Darby canine kidney (MDCK) cell line production systems were used for the experimental setup.

1.2 Influenza A virus particle purification with magnetic sulfated cellulose particles

Established large-scale influenza vaccine production processes use sulfated carbohydrate matrices for the chromatographic purification of VP [16–18]. Commercially available resins are based on sulfated cellulose (Cellufine Sulfate resin from JNC Corp.) or sulfated dextran (Capto DeVirs resin from GE Healthcare Bio-Sciences AB) [16–18]. Moreover, new sulfated cellulose membrane adsorbers (SCMA) were developed and demonstrated good purification performance for influenza or Modified Vaccinia Ankara (MVA) VP [19–21].

Interestingly, the binding mode of this pseudo affinity adsorption process used for VP purification is not yet resolved in detail [22]. However, sulfated carbohydrates seem to mimic heparan sulfate proteoglycans (HSPG). These HSPG are involved in a wide range of pathogen-host interactions during infection where they act as a low affinity (co-)receptor for direct internalization or

Chapter 1: Motivation

increase the probability of binding to more specific secondary receptors [23]. This cellular membrane binding mechanism was shown for VP, bacteria, and parasites [23], rendering it an interesting feature usable for the purification of such pathogens.

Traditionally, centrifugation based methods are used for small-scale purification for influenza VP analytics. These centrifugation methods for analytics use cost-intensive high-speed centrifugation equipment and are time- and labor-consuming due to the involved manual steps and their limited scalability [24–27].

Since several years, magnetic particle separation processes are increasingly used due to their easy handling, versatility, and scalability [28]. These separation processes are established for the purification of peptides, proteins, nucleic acids, VP, organelles of animal cells, or entire cells [24,29–33]. The used binding modes range from ionic to specific affinity ligand interactions [24,29–33]. However, magnetic particles making use of sulfated cellulose ligands are not commercially available and were not described in literature so far.

Applications for vaccines have been recently published for nanoparticle vaccines with specific immunomodulating properties or magnetic particle DNA vaccines that enable magnetic transfection [34,35]. However, the DSP of such particle-based vaccines usually employs a purification process followed by the formulation with the particulate carrier. Furthermore, the DSP usually employs a wide range of different techniques, which makes it challenging to be implemented in research facilities working on new vaccine or viral vector candidates for gene therapies as they often lack equipment and know-how. However, some ready-to-use high-throughput DSP tools based on aqueous two-phase extraction have been previously introduced, which could help accelerate the research and development of VP-based biopharmaceuticals [36].

Because of that, MSCP were developed to explore their applicability for influenza VP preparation. The cellulose matrix used for the MSCP is available in abundance, is cost-effective, exhibits low unspecific binding, and was shown to be biocompatible [37–40]. The MSCP obtain their magnetic properties from embedded smaller iron-containing particles. The two developed MSCP systems were based on particles with a size of about 100 μm , which makes them easy separable with cost-effective commercially available permanent magnets [41]. Consequently, no special high-gradient magnetic field separation systems are needed, which is lowering overall costs and therefore applicability.

In the first experimental setup the analytical VP sample preparation by MSCP purification was compared to an established centrifugation method for analytics on protein level by liquid chromatography-tandem mass spectrometry (LC-MS/MS) analytics to obtain detailed information on co-purified protein impurities [24–27].

The second experimental setup was a proof of concept for purifying and formulating a cell-culture derived whole virus influenza A/PR vaccine with MSCP. This involved the specific binding of the inactivated VP to the MSCP to obtain antigen-loaded MSCP (aMSCP). The aMSCP were directly formulated and injected into mice. The biocompatibility and nontoxicity of the cellulose and the incorporated smaller Fe_3O_4 particles of the MSCP makes them suitable for such a process without

Investigation of influenza virus particle aggregation and purification with magnetic sulfated cellulose particles

expected adverse effects [35,37–40]. Furthermore, this purification and formulation setup can be potentially carried out directly after upstream processing (USP) to implement a simple and scalable (high-throughput) DSP. During the *in vivo* immunization studies the anti-A/PR antibody levels were monitored. The mice were challenged after immunization with a lethal dose of replication competent A/PR VP and the weight losses were observed followed by viral load estimation in the lungs to evaluate the protective features of the MSCP vaccine.

2 BACKGROUND

2.1 Influenza vaccines

Influenza VP are characterized by their eight single-stranded negative-sense RNA segments and belong to the *Orthomyxoviridae* virus family [42,43]. Influenza VP can be classified in type A, B, and C [43,44]. Influenza type A and B are responsible for the yearly human epidemics. Influenza VP have a size of 80 to 130 nm and are enveloped with a lipid-bilayer derived from the host cell membrane [45,46].

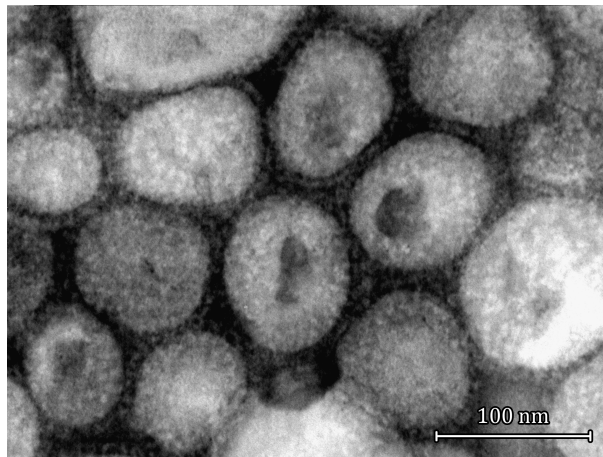


Figure 1 Electron microscopy of A/PR virus particles

A/PR VP were produced in adherent MDCK cells and were purified by sulfated cellulose membrane adsorber (SCMA) chromatography before transmission electron microscopy (TEM). The white spikes around the VP indicate the hemagglutinin (HA) and neuraminidase (NA) surface antigens. TEM was carried out by Christopher Ladd Effio and Mohammad Fotouhi Ardakani (Karlsruhe Institute of Technology, Germany).

The major viral surface proteins hemagglutinin (HA, H) and neuraminidase (NA, N) are incorporated in the VP membrane and are shown in Figure 1. It is generally accepted that HA and

Investigation of influenza virus particle aggregation and purification with magnetic sulfated cellulose particles

NA are the major antigens involved in the immune response during an infection. Influenza A can be divided in two phylogenetic groups: group 1 consisting of H1, H2, H5, H6, H8, H9, H11, H12, H13, H16, H17, and H18, as well as group 2 consisting of H3, H4, H7, H10, H14, and H15. Influenza B can be divided in the Victoria and Yamagata lineages, which are antigenically different [43,47].

The influenza virus strains are named according to their genus/type, the species from which the virus was isolated (omitted if human), the location of the isolate, the number of the isolate, and the year of the isolation [45]. In addition, the HA and NA subtypes are indicated for influenza A viruses. For example, the 8th isolate of an H1N1 subtype influenza A virus isolated from a human in Puerto Rico in 1934 is named A/Puerto Rico/8/1934 (H1N1).

Influenza is considered a major cause for acute febrile respiratory illnesses in humans. The circulating influenza virus strains can change antigenically due to antigenic drift and shift, and are therefore an ongoing health concern [43]. Antigenic drift occurs through point mutations that lead to small gradual antigenic changes in the HA and NA genes and occur in influenza A and B virus [43,48]. The drift generates new strains which cause the seasonal epidemics. Antigenic shift refers to the appearance of a new HA or new HA and new NA that differ from the previous predominant circulating types. These shifts can generate new influenza A viruses by reassortment of strains from different host species and therefore potentially create new pandemic strains [43,45].

The primary strategy to control and prevent influenza outbreaks is vaccination. The available influenza vaccines are based on inactivated influenza VP, live-attenuated influenza VP, or recombinant influenza virus antigens [42,43,49,50].

Inactivated influenza vaccines can be based on whole VP, split VP, or on VP subunits. These vaccines are typically produced in embryonated hen's eggs followed by purification. The traditional trivalent seasonal influenza vaccine is based on inactivated VP consisting of a mixture of influenza A virus (H1N1), influenza A virus (H3N2) and influenza B virus antigens. Recently, quadrivalent influenza vaccines were introduced that contain both influenza B lineages. This is beneficial if two different influenza B virus lineages are circulating in the population, as there is little to no cross-protection between the two influenza B virus lineages [43]. Additionally, there are cell culture systems based on MDCK or Vero cell lines for VP production to overcome limitations of the egg-based system, like a potential supply delay of required eggs in the case of a sudden demand due to a major influenza outbreak [51–53]. Typically, the inactivated vaccines for atypical influenza outbreaks are formulated with additional adjuvants to increase the available doses and to tune the immune response [43,54].

Live-attenuated influenza VP are cold adapted and temperature sensitive, and are administered intranasally. Such vaccines induce strain-specific IgA, which is associated with a protective immune response [43,54]. The used systems are based on the Leningrad or Ann Arbor A virus and B virus strains [54,55].

Recently, recombinant influenza vaccines were licensed. The antigens are based on recombinant hemagglutinin produced in insect cells with the help of baculovirus vectors [43,49,54]. This

Chapter 2: Background

approach has the advantage to circumvent the potentially needed sub-selection and refinement process for production strains used in conventional production processes based on whole VP infecting cells [54]. However, depending on the design of the recombinant influenza vaccine the immune response can differ when compared to vaccines based on whole VP.

Additionally, there are other influenza vaccine concepts that are based on DNA, bacterial production systems, conserved proteins, virus-like particles, or viral-vectors [43,54]. However, these systems play no important role so far and are still in the research and development phase.

2.2 Cell culture-based production of influenza virus

The industrial production of influenza VP is still largely based on the infection of embryonated hens-eggs. However, cell culture-based influenza VP production systems are increasingly used and investigated due to their flexibility, shorter production cycles, greater surge capacity, greater process control, and a more well-characterized reliable product. The cell culture-based production results in a higher similarity between the produced VP and the circulating VP strains, includes no egg-derived contaminants, and potentially enables a faster virus seed generation. However, these advantages come with increased work on process screening and intensification [56].

For the industrial cell culture-based production of influenza vaccines MDCK cells, PER.C6 human embryonated retinal cells, Vero monkey kidney cells, and HEK293 human embryo kidney cells have been evaluated. In addition, Sf9(-derived) insect cells with a baculovirus expression vector system are used for the industrial production of influenza virus antigens or virus-like particles [56].

VP production for vaccines with mammalian cells can be carried out with adherent and suspension cell lines. Adherent cells need a support, which can be provided in roller bottles (see section 3.3.1), where cells attach to the inner surface, or multilayer cultivation systems, which offer increased surface area and control over roller bottles. Furthermore, adherent cells can be grown in shaker flasks, wave bioreactors, and stirred tank bioreactors on porous or non-porous microcarrier beads or in fixed or packed-bed bioreactors on porous carrier materials. In contrast, suspension cells are directly inoculated into the culture media and can be cultivated in shaker flasks (see section 3.3.3), wave bioreactors, or stirred tank bioreactors (see section 3.3.2) without additional cell support [57].

In general, bioreactor systems offer for both cell types increased process control, scale-up options for industrial production, and scale-down options for process characterization. In addition, process intensification can be achieved by fed-batch, perfusion, and continuous bioreactor systems [57].

2.3 Downstream processing of influenza virus particles

The DSP of influenza VP for licensed vaccines involves a clarification, concentration, purification, polishing, and a formulation step, which are commonly based on centrifugation, filtration, and chromatography unit operations [16,58,17,59–63].

Investigation of influenza virus particle aggregation and purification with magnetic sulfated cellulose particles

Clarification can be based on low-speed centrifugation or depth filtration. Concentration can be carried out by micro- or ultrafiltration combined with diafiltration for buffer exchange in dead-end or tangential-flow-filtration (TFF) mode [64]. The purification and polishing can be carried out by high-speed centrifugation using density gradients, also known as “ultracentrifugation” [65,66], and chromatography. The chromatography modes reported in literature for influenza vaccine purification are size exclusion chromatography [67,68], ion exchange chromatography [67,69,70], hydrophobic interaction chromatography [71], (pseudo) affinity chromatography [24,19,72,73], and steric exclusion chromatography [74]. The VP inactivation can be carried out chemically with β -propiolactone [64], ethyleneimine [75,76], or formalin [77]. Furthermore, nuclease treatment can be applied during DSP for host cell DNA depletion [78]. Additionally, work on influenza VP purification by precipitation has been shown with alcohols and polyethylene glycols [79,80]. In addition, magnetic particle systems using anionic interaction based on poly(methyl vinyl ether-maleic anhydride) were recently used for the purification of human influenza A and B VP for research applications [31].

Information on commercially used DSP trains for influenza vaccines based on VP is rare, but two examples from published patents for hens eggs- or cell culture-based [81] and MDCK-based VP [82] are shown in Figure 2. The main difference between the two processes is the used main purification unit operation, i.e., ultracentrifugation or chromatography. In general, the DSP contains as a first step a clarification to separate the VP from bigger impurities of the harvested VP broth, i.e., intact cells and cell fragments. In the shown example, this is carried out by a depth filtration with filter pore sizes in the range of 1.2 to 0.45 μm . This is accompanied by ultrafiltration and diafiltration steps for concentration and buffer exchange. Finally, the process is completed by a sterile filtration with pore sizes in the range of 0.45 to 0.20 μm .

Finally, influenza vaccine preparations are usually formulated in aqueous formulation buffers for intramuscular or intradermal injection using a needle [83], and intranasal delivery [84]. In addition, new applications based on (dissolving) microneedles [85–87] or needle-free administration by epidermal powder immunization [84] have been investigated. The vaccine formulation process suspends the antigens in the formulation buffer for vaccine application and can be based on different unit operations, e.g., dilution, diafiltration, or lyophilization. Furthermore, magnetic particle systems could enable new vaccine formulation (see section 3.4.9 and 4.2.3.2) and application methods (see section 6.2).

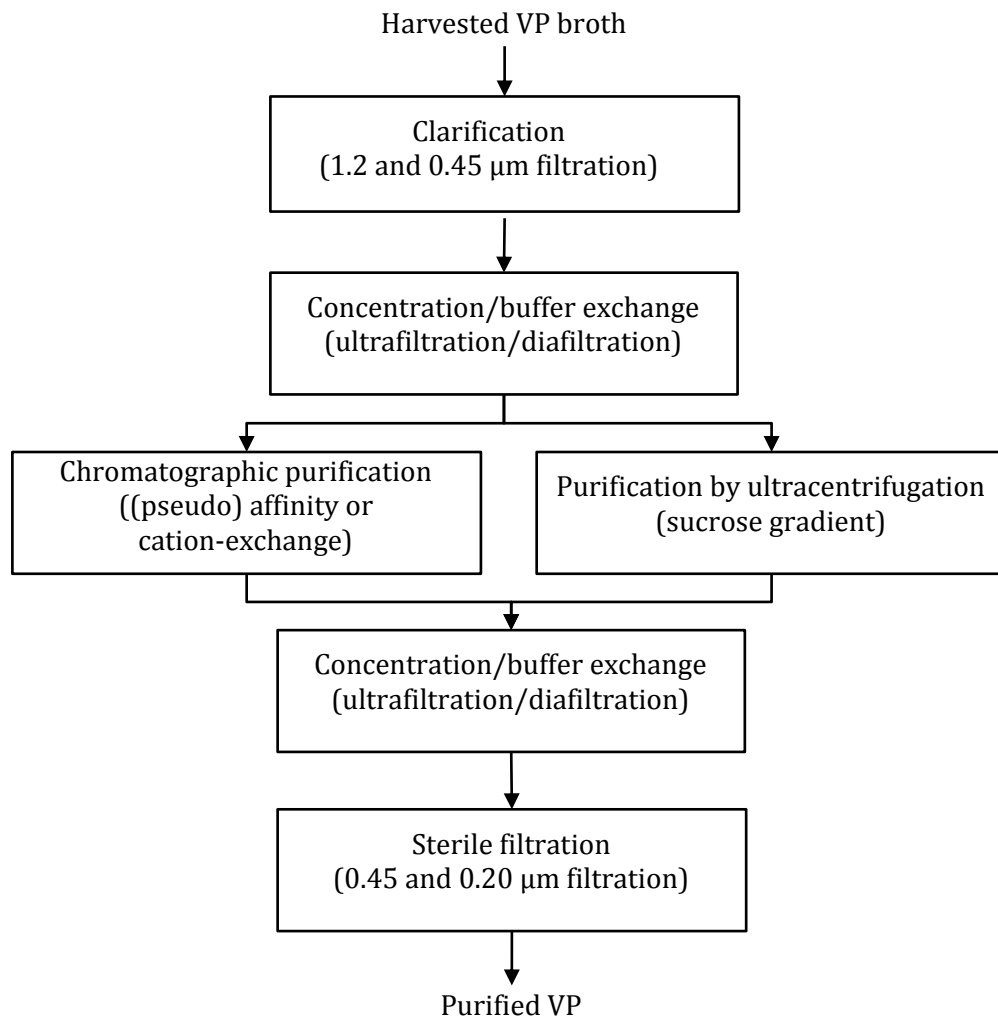


Figure 2 Downstream processing train

The shown downstream processing train covers the steps from the harvested VP broth to the purified VP. The exemplified process does not contain the subsequent process steps for the final vaccine formulation, i.e., inactivation, optional VP splitting, buffer exchange to formulation buffer, fill, and finish (figure adapted from [81,82]).

2.4 Analytics during the production of influenza virus particles

2.4.1 Upstream processing

During the cell culture-based influenza virus production, the hemagglutination assay (see section 3.6.1), the plaque assay, or the 50% tissue culture infective dose (TCID₅₀) are used to monitor virus titers. The hemagglutination assay is based on the ability of infectious, noninfectious or inactivated influenza VP to agglutinate red blood cells. The derived hemagglutination units (HAU) depend on the amount of hemagglutinin on the influenza VP surface and the VP concentration and not on the infectivity or their ability to replicate [88–90].

Investigation of influenza virus particle aggregation and purification with magnetic sulfated cellulose particles

The plaque assay is based on a cell monolayer that is overlaid with an influenza VP sample. Due to the cytopathic effect of the infectious VP, the lysed cells form a circular zone, i.e., the plaque. The derived plaque forming units (PFU) are a quantitative measure of the infectious VP concentration in PFU mL⁻¹ [88]. The TCID₅₀ is based on the VP sample dilution that shows 50% lysis of the infected cells [88,90].

In addition, real-time quantitative PCR can be used during the USP for the quantitation of viral RNA, for potency assays in process development, for characterization of VP stability, for screening of adventitious agents, and for safety assessments [91].

Furthermore, cell count, cell size and cell viability are monitored during USP by microscopy-based methods. The conventional cell-viability assay is based on trypan blue, which is absorbed by dead cells whereas the dye is excluded from living cells due to their intact plasma membrane. This method is usually automated to increase the number of analyzed cells and samples [92]. After the USP the contaminant levels in the VP harvest are analyzed for their protein content by a Bradford assay [93] and for the DNA content by a PicoGreen® assay, measuring the double-stranded DNA [94].

2.4.2 Downstream processing

During the influenza VP DSP the hemagglutination assay (see section 3.6.1) and the single radial immunodiffusion assay (SRID, see section 3.6.2) are used for measuring the HAU and the HA amount of the purified VP, respectively. In contrast to the hemagglutination assay, which is a fast and straightforward procedure, the SRID is more complex. Thus, the SRID is usually not used to obtain recovery balances but to quantify the total HA amount at the end of the DSP. The SRID is the accepted method to formulate vaccines, i.e., to adjust the HA antigen content of seasonal influenza vaccines [95], even though various alternative assays have been evaluated in the past to replace it.

In addition, real-time quantitative PCR can be used during the DSP for the quantitation of VP genomes, process residuals, VP stability, adventitious agents, and for safety assessments [91].

Besides monitoring the product of interest, i.e., the VP, also the depletion of the contaminants has to be determined. The protein impurities are usually measured by a Bradford assay [93]. The DNA impurities are usually measured by a PicoGreen® assay, measuring double-stranded DNA [94], and for low DNA impurity concentrations by a Threshold® Total DNA assay, measuring single-stranded (total) DNA [96].

2.4.3 Virus particle aggregation and influenza virus analytics

In general, the effects of VP aggregation on analytics are not well investigated. Nevertheless, the effects of influenza VP aggregation on the hemagglutination assay [97] and the plaque assay [98] have been described. The experiments on influenza A VP aggregation and the hemagglutination assay showed that VP aggregation reduced the observed HAU and VP aggregate dispersion increased the observed HAU. The plaque assay investigation showed a higher infectivity of

influenza A VP aggregates, which was explained by the complementation of incomplete influenza VP genomes [98].

In addition, there is every reason to assume that VP aggregation affects a range of VP-based methods, e.g., analytics like TCID₅₀, and VP USP and DSP. However, new knowledge on this topic should be obtained in this doctoral thesis on influenza A VP aggregation in different buffers (results see section 4.1).

2.5 Virus particle aggregation analytics

Early work on VP aggregation analytics relied on complex methods to approximate their PSD. The first work revealing the mechanism behind VP aggregation was based on a single particle approximation (SPA) method. This method uses high-speed centrifugation to separate single or monomeric VP from VP aggregates. The SPA method was used to investigate VP aggregation of polio- and reo-VP in water [3,99,100], the effects of specific salts on polio- and reo-VP aggregates at low pH [101], and aggregate mixtures of polio- and reo-VP [102]. The method employs centrifugation of a VP sample applied to a sucrose gradient to separate monomeric VP from VP aggregates. The centrifugation is stopped after a specific time to remove the gradient fluid layers and to analyze them individually via plaque titration or electron microscopy (EM).

Furthermore, a modified SPA method was used to investigate influenza VP aggregation with EM to determine the VP content of influenza vaccines [97]. The obtained data showed that all investigated vaccine preparations contained VP aggregates to some degree. Additionally, it was shown that these VP aggregates could be dissolved in high molality buffers.

Other work investigated the consequences of different human and avian HA and NA combinations on influenza VP aggregation [103]. The experimental setup used a centrifuge with a sucrose gradient to separate monomeric VP from VP aggregates followed by hemagglutination assay of the individual gradient layers. It was shown that the reassortants H3N1, H4N1, H10N1, and H13N1 aggregated whereas natural H1N1 and reassortants based on avian HA and avian NA were found to be mostly monomeric at 4°C. The aggregation at 4°C was found to be reversible at 37°C. Furthermore, the VP aggregates showed a higher infectivity to HAU ratio. The authors explained the aggregation phenomena by the inefficient sialic acid removal from avian HA by human N1.

Moreover, pH-induced aggregation of influenza VP was investigated by UV absorption as well as static and dynamic light scattering [104,105]. In the UV measurement setup, the extinction coefficients of A/PR VP could be determined at a wavelength of 280 nm, which correlated with the VP protein concentration [104]. In addition, the UV spectra allowed monitoring of VP aggregation. The dynamic light scattering showed that the VP samples were not uniform with possible slight aggregation at pH 7.4 and instantaneously aggregated upon acidification to pH 5 [105]. Furthermore, VP aggregation due to acidification developed over minutes to hours.

Investigation of influenza virus particle aggregation and purification with magnetic sulfated cellulose particles

However, these methods failed to give high-resolution PSD to investigate VP aggregation in detail [106]. Finally, size distribution analysis of influenza VP was shown by analytical SEC [107], but was not compared to other high-resolution PSD measurement methods.

One of the most used methods to obtain PSD of nanometer-sized particles is analytical ultracentrifugation (AUC) [108]. AUC has the advantage of obtaining high-resolution PSD but comes with significant investment costs due to the equipment itself and its operation. Therefore, AUC is only used in research in need of its high-end measurement capabilities and detection modes. Because of that, much simpler centrifuges were recently developed to overcome this drawback and make PSD measurements more accessible to a wider user base. Generally, these systems employ limited rotor speeds with a fixed monochromatic detection system [108].

The CPS DC24000 UHR disc centrifuge system from CPS Instruments (LA, USA) is such a system. It uses DCS disc centrifugation to measure PSD. The principle is outlined and compared to traditional integral sedimentation in Figure 3. The disc centrifuge construction principle is shown in Figure 4.

The DCS measurement principle is based on the sedimentation times of the measured particles with unknown size but known buoyant density in a density gradient fluid with known density [109]. With additional characterization parameters, the steady state can be describe by Stokes' law and the centrifugal force shown in Formula 1-2 [110].

$$F_S = 3\pi D\eta v = 3\pi D\eta \frac{dR}{dt}, \quad (1)$$

where F_S is the Stokes force (N), D is the Stokes/hydrodynamic diameter (m), η is the dynamic viscosity (Pa s), and v is the sedimentation viscosity (m s^{-1}).

$$F_C = \frac{\pi}{6} D^3 (\rho_P - \rho_F) \omega^2 r, \quad (2)$$

where F_C is the centrifugal force (kg m rad s^{-1}), D is the Stokes/hydrodynamic diameter (m), ρ_P is the particle density (kg m^{-3}), ρ_F is the fluid density (kg m^{-3}), ω is the angular velocity (rad s^{-1}), and r is the radius of rotation (m). DCS disc centrifugation offers high-resolution PSD measurement capabilities when compared to other PSD measurement technologies, such as nanoparticle tracking analysis and tunable resistive pulse sensing, as well as established static or dynamic light scattering methods [106]. Additionally, DCS with a CPS DC24000 UHR disc centrifuge was already reported for the evaluation of the PSD of recombinant adeno VP [111,112], L1 virus-like particles [113], and influenza VP [110], rendering it the method of choice for investigating influenza VP aggregation for this doctoral thesis [114].

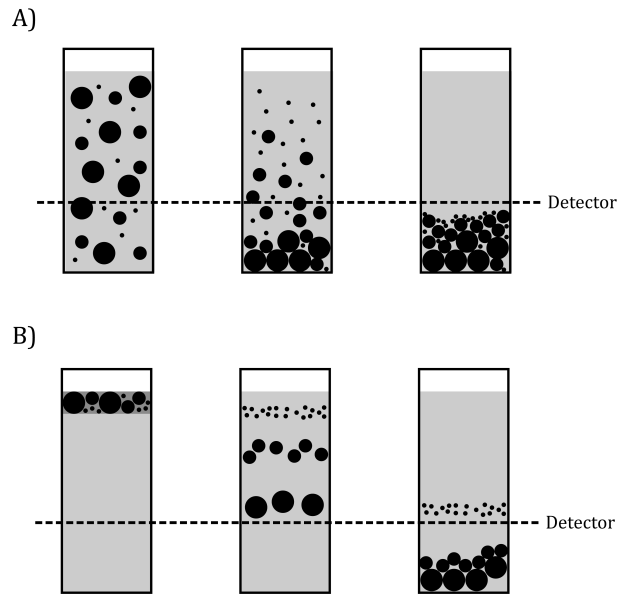


Figure 3 Integral and differential centrifugal sedimentation

(A) For integral sedimentation the sample is centrifuged and bigger particles settle before smaller particles. The method name is derived from the resulting sum or integral of all particles that passed the detector after a certain time. (B) In contrast, for differential centrifugal sedimentation (DCS) the sample is applied on top of a density gradient fluid. The particles are separated in the density gradient based on their size. Therefore, only a fraction or a differential part of the applied particle population is passing the detector. (Note: The description assumes equal buoyant densities of the different-sized particles. The sedimentation process is more complex with mixed particle buoyant densities.) Figures adapted with permission from [109].

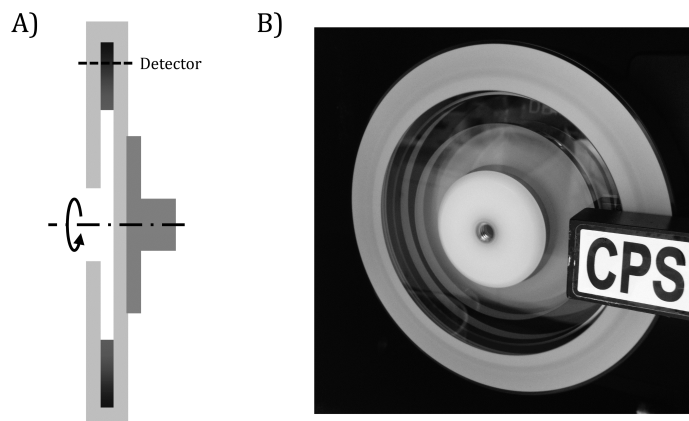


Figure 4 Disc centrifuge construction principle

(A) Schematic cross section of the CPS DC24000 UHR centrifuge disc adapted with permission from [109]. (B) Rotating centrifuge disc with injected gradient buffer pushed to the chamber bottom inside the centrifuge disc. Detector is visible on the right side with the "CPS" label.

2.6 Immunization studies in mice

Influenza animal models are used for the preclinical evaluation of potential vaccines to investigate their safety and efficacy in preventing or moderating infection or disease. For these investigations different animal models with specific advantages and disadvantages are used, i.e., mice, ferrets, cotton rats, hamsters, guinea pigs, and macaques [115].

The mouse model for influenza research is the most widely used animal model due to practical implications, i.e., animal size, mice-specific reagents, possibility of genetic engineering, husbandry requirements, and costs. In addition, the mouse model is considered the best choice for the preliminary assessment of influenza vaccine safety and efficacy. Furthermore, the mouse model allows to use a large number of animals to obtain statistically robust data [115].

The symptoms of a severe influenza-associated disease include in most cases ruffed fur, huddling, lethargy, anorexia, and death. For the assessment of vaccine efficacy, body weight loss and mortality are generally monitored after infection. Of note are differences in the symptoms of an influenza infection in mice and humans. Mice do not develop fever, coughing, or sneezing, and the virus spreads differently in the respiratory tract. In addition, influenza is generally more severe in mice than in humans and the virulence does not always correlate between mice and humans [115].

In the scope of this doctoral thesis, a standard mouse model for influenza research based on C57Bl/6 mice and influenza A/PR was used (see section 3.5).

3 MATERIALS AND METHODS

3.1 Buffers and media solutions

For all aqueous solutions, ultrapure water produced with a Milli-Q Advantage A10 water purification system (Merck KGaA, Darmstadt, Germany) was used. The ultrapure water used for LC-MS/MS sample preparation was filtered through an additional LCPAK0001 filter unit (Merck KGaA, Darmstadt, Germany) to remove trace organic compounds.

The chemicals used for the buffers and the cell culture media had a $\geq 99\%$ purity and were obtained from Sigma-Aldrich Co. LLC. (St. Louis, USA) unless noted otherwise.

3.2 Screening buffers

The following salts were used for the HS ion screening: Na_2SO_4 (S9627), Na_2HPO_4 (S8282), NaH_2PO_4 (S7907), NaCl (S7653), NaBr (71329), NaNO_3 (S8170), NaI (793558), CaCl_2 (C5080), KCl (P9333), LiCl (62476), and MgCl_2 (M2670). The Na^+ and Cl^- salts were used because they are considered reference points in the HS series [11]. The concentrations used for the screening were 20, 60, and 540 mM for all salts. Additionally, NaCl was screened in a concentration of 180, 1020, and 1500 mM. The salts were used in a 10 mM Tris-HCl pH 7.4 standard buffer (SB) at room temperature (RT, 25°C). All concentrations were based on the ion of interest and were not adapted for the counterions [114].

The HS buffers were prepared by dissolving 0.605 g of Tris-base (T6791) and the salt of interest in 450 mL ultrapure water. Then, the pH was titrated with HCl (100317, Merck KGaA, Darmstadt, Germany) to pH 7.4 and the solution was filled up to 500 mL with ultrapure water. The $\text{Na}^+/\text{PO}_4^{3-}$ buffer was also prepared with 0.605 g of Tris-base. The acidic salt NaH_2PO_4 and the basic salt Na_2HPO_4 were weighted in to obtain a neutral pH from the resulting $\text{HPO}_4^{2-}/\text{H}_2\text{PO}_4^-$ buffer system. Because of the additional Tris-base this was followed by titration with HCl to pH 7.4. Finally, 0.05% of NaN_3 (71290) was added to prevent microbial growth followed by a 0.2 μm

Investigation of influenza virus particle aggregation and purification with magnetic sulfated cellulose particles

filtration with a bottle top filter (514-0340, VWR, Radnor, USA) to remove particles and storage at 4°C. All HS buffers were warmed up to RT before being used for dialysis (see section 3.4.4) [114].

3.3 Upstream processing

Influenza VP production was carried out in adherent and suspension MDCK cell lines, shown in detail in section 3.3.1 and 3.3.2, respectively. The virus seed for production was produced in adherent MDCK cells (MDCK_{ADH}, ECACC No. 84121903) with A/PR (3138, Robert Koch Institute, Berlin, Germany) and had a TCID₅₀ of 10⁸ infectious VP mL⁻¹ [116–118].

The VP produced in the adherent system will be named A/PR_{ADH} and for the suspension system A/PR_{SUS} thereafter.

3.3.1 Adherent MDCK production system

MDCK_{ADH} cells were cultivated in GMEM-BHK21 medium (22100-093, Thermo Fisher Scientific Inc., Massachusetts, USA) complemented with 10% v/v fetal calf serum (FCS, F7524), 0.2% w/v lab-FMV-peptone (MC033, Lab M Ltd., Heywood, UK), 1 g L⁻¹ D-(+)-glucose, 4 g L⁻¹ NaHCO₃. VP production in MDCK_{ADH} cells was carried out in 850 cm² roller bottles (680160, Greiner Bio One International GmbH, Frickenhausen, Germany). The cells were washed 3x with phosphate buffer saline (PBS) and fresh medium without FCS and 5 x 10⁵ units trypsin mL⁻¹ (27250-018, from porcine pancreas, Thermo Fisher Scientific Inc., Massachusetts, USA) before infection with 0.5 mL VP seed with a multiplicity of infection (MOI) of 10⁻⁴. 72 hour post infection (hpi) the VP broth was harvested [114,116–118].

3.3.2 Suspension MDCK production system

Suspension MDCK cells (MDCK_{SUS2}) were derived from MDCK_{ADH} cells and were cultivated in a 2x concentrated chemically defined, protein- and peptide-free SMIF8 PGd medium (M008-2b, Service Zellkultur Scharfenberg, Emden, Germany). The medium was supplemented with 5 g L⁻¹ NaCl, 3.66 g L⁻¹ D-(+)-glucose, 2 g L⁻¹ NaHCO₃, 0.242 g L⁻¹ L-glutamic acid, 4 mM L-glutamine, 4 mM pyruvate, 10 mL L⁻¹ 10% Pluronic-F68, and 1 μL L⁻¹ 98% ethanolamine. Cell growth and VP infection was carried out in a 5 L stirred tank bioreactor (CT5-SK, Sartorius Stedim Biotech GmbH, Göttingen, Germany) with 10⁻⁵ units trypsin cell⁻¹ (27250-018, from porcine pancreas, Thermo Fisher Scientific Inc., Massachusetts, USA) and a MOI of 10⁻⁴. The VP broth was harvested 72 hpi [114,116–118].

3.3.3 Influenza virus particle production for analytical method comparison

The influenza VP production for analytical method comparison was carried by Anja Serve (Max Planck Institute for Dynamics of Complex Technical Systems, Magdeburg, Germany) as published in a technical note with shared first authorship (for details on the contributions see section 8.5) [24].

Chapter 3: Materials and Methods

The VP for the experiments in section 3.4.5 and 3.4.7 were produced according to the previous section 3.3.1 with MDCK_{ADH} and a scaled down process based on section 3.3.2. with MDCK_{SUS2} including several modifications: Production was carried out in 250 mL vented shaker flasks for MDCK_{SUS2} with 2×10^{-6} units trypsin cell⁻¹ and an MOI of 0.025. Harvest clarification was carried out by centrifugation at 150 g for 20 min at RT with a Avanti J-20XP tabletop centrifuge [24].

3.4 Downstream processing

3.4.1 Virus broth clarification and inactivation

The obtained VP broth was clarified with a 5 µm (CFAP0508YY, GE Water & Process Technologies, Trevose, USA) and a 0.65 µm depth filter (CFAP9608YY, GE Water & Process Technologies, Trevose, USA) followed by chemical inactivation with β-propiolactone (33672.01, Serva Electrophoresis, Heidelberg, Germany) at a final concentration of 6 mM. Incubation for inactivation was carried out at 37°C for 24 h. After that, the inactivated VP broth was filtered with a 0.45 µm depth filter (CMMP9408YY, GE Water & Process Technologies, Trevose, USA) to obtain the filtered and inactivated VP broth [114]. Successful inactivation was verified before the subsequent steps as described in previous work [64].

3.4.2 Tangential flow filtration concentration for aggregation studies

The filtered and inactivated VP broth (see section 3.4.1) was concentrated by tangential flow filtration to 10⁵ HAU mL⁻¹. For that a ÄKTAcrossflow tangential flow filtration (TFF) system (GE Healthcare Bio-Sciences AB, Uppsala, Sweden) with a Sartocoon Slice 200 Hydrosart cassette (prototype, Sartorius Stedim Biotech GmbH, Göttingen, Germany) made of a cellulose membrane with a 750 kDa molecular weight cut-off (MWCO) was used. After that, the concentrates were filtered with a 0.1 µm filter (SLVV033RS, Merck KGaA, Darmstadt, Germany) to obtain monomeric VP without aggregates and bigger impurities for the subsequent aggregation studies. Finally, the acquired VP samples were aliquoted in 0.5 mL portions and frozen at -80°C [114].

3.4.3 Tangential flow filtration concentration and diafiltration for immunization studies

A VP broth produced and harvested based on the protocol in section 3.3.2 was 20x volumetrically concentrated based on the protocol in section 3.4.2. followed by 10x volume exchange by diafiltration to 50 mM NaCl 10 mM Tris-HCl pH 7.4 preformulation buffer (PFB). The diafiltration to PFB enabled efficient binding of the VP to the MSCP or the sulfated cellulose membrane adsorbers (SCMA) [119].

3.4.4 Dialysis for buffer exchange

Dialysis was used for buffer exchange to investigate VP aggregation in different HS buffers. Therefore, 500 µl of the prepared sample (see section 3.4.2) was transferred into a

Investigation of influenza virus particle aggregation and purification with magnetic sulfated cellulose particles

14 kDA MWCO dialysis tube (0653.1, Carl Roth GmbH & Co. KG, Karlsruhe, Germany) followed by overnight incubation under stirring in 500 mL HS buffer with a dialysis factor of $1:10^3$ [114].

Dialysis tubes with a MWCO of 14 kDa were used to avoid sample concentration due to increased osmotic pressure of higher concentrated HS buffers, which could potentially induce VP aggregation [114].

3.4.5 Influenza virus purification using centrifugation for analytics

The influenza virus purification using centrifugation was carried by Anja Serve (Max Planck Institute for Dynamics of Complex Technical Systems, Magdeburg, Germany) as published in a technical note with shared first authorship (for details on the contributions see section 8.5) [24].

The centrifugation for analytics method involved a first centrifugation step to remove cell debris at 4 000 g for 35 min using an Avanti J-20XP tabletop centrifuge (Beckman Coulter, Inc., Brea, USA). Then, the smaller cell compartments were removed with a centrifugation step at 10 000 g for 45 min. After each step the supernatant was transferred into a new centrifuge tube and the pellet was discarded. Finally, the VP were pelleted with a high-speed centrifugation step at 98 649 g for 1.5 h using an Optima TM LE-80K ultracentrifuge (Beckman Coulter, Inc., Brea, USA) [24–27].

3.4.6 Production of magnetic sulfated cellulose particles

Within this work two different MSCP particle systems were developed and used, which differ in the particle raw material and the sulfation process [24,119,120].

3.4.6.1 Equipment setup and safety precautions for the sulfation reaction

Note: It is highly recommended to consult the supplier's product information before working with the chemicals and the equipment needed for the sulfation reaction to implement all necessary safety measures!

In Figure 5 the sulfation reaction apparatus scheme is shown. Before the apparatus was assembled, all reaction mixture contacting parts needed to be free of residual water. This was achieved by washing all parts with pure acetone followed by full evaporation of the acetone in a chemical hood. This was very important because water can inhibit the sulfation reaction, which can be indicated by the formation of two phases in the reaction mixture. Furthermore, water can react very exothermic with the chlorosulfonic acid (the term "violently" is used in the supplier's product information!).

After the washing and evaporation step, all parts were inspected for defects to avoid potential equipment failure. Then, the sulfation reaction apparatus was assembled in a chemical hood for the sulfation reaction according to section 3.4.6.2 or 3.4.6.3.

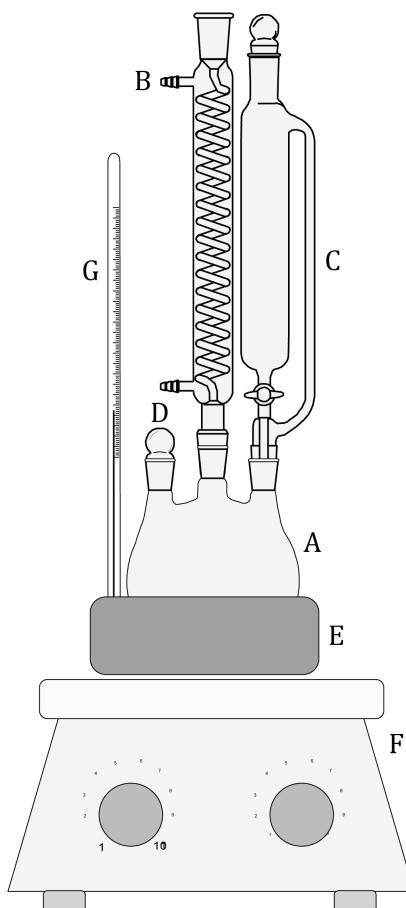


Figure 5 Sulfation reaction apparatus scheme.

Main parts of the sulfation reaction apparatus: (A) three neck round reaction flask, (B) condenser for reflux cooling, (C) dropping funnel for the chlorosulfonic acid, (D) inlet for pyridine or magnetic particles, (E) vessel with appropriate solution for heat contact, (F) heating/cooling unit, and (G) thermometer for temperature monitoring.

3.4.6.2 Magnetic sulfated cellulose particles production based on Magne™ protein A particles

A volume of 30 mL of pyridine (494410) was cooled to or below 0°C before drop wise addition of 3.3 mL chlorosulfonic acid (571024). Slow addition of the acid and proper cooling of the resulting reaction mixture is very important as the dissolution process is very exothermic (see section 3.4.6.1). Then, 20 mL pyridine was added and the reaction mixture was heated to 65°C under stirring to dissolve any resulting crystals of the acid addition. After obtaining a fully homogenous reaction mixture, i.e., no recognizable undissolved crystals by visual inspection, the temperature was reduced to 40°C. Separately, the storage supernatant of 400 mg Magne™ protein A core-shell magnetic cellulose particles (G8781, Promega Corp., Madison, USA) with a size of 30 to 80 μm [41] was removed and the particles were washed twice with 10 mL pyridine to remove residual water followed by resuspension in 10 mL pyridine. Then, the resuspended particles were transferred into the 53.3 mL reaction mixture (18:1 pyridine:chlorosulfonic acid reaction mixture ratio), followed by cooling the reaction mixture to 35°C and incubation for 12 h. If crystal formation occurs during the

Investigation of influenza virus particle aggregation and purification with magnetic sulfated cellulose particles

cooling phase by too low temperatures, the reaction mixture needs to be heated to 65°C and cooled again to 35°C to obtain a homogenous reaction mixture. After the incubation, the reaction mixture was decanted and the MSCP were washed with water. Finally, the obtained MSCP were resuspended in a 20% ethanol water solution to obtain a 50% v/v MSCP suspension for storage [24,120].

3.4.6.3 Magnetic sulfated cellulose particles production based on MG 200 magnetic macroporous cellulose particles

The sulfation of the MG 200 magnetic macroporous cellulose particles (Iontosorb, Ústí nad Labem, Czech Republic) with a diameter of 100 to 250 µm was based on a similar process as outlined in section 3.4.6.2: The reaction mixture consisted of 120 mL pyridine, which were cooled to or below 0°C, before 6 mL chlorosulfonic acid were added dropwise (20:1 pyridine:chlorosulfonic acid reaction mixture ratio). The resulting reaction mixture was heated to 65°C to obtain a homogenous reaction mixture followed by cooling to 42.5°C. Separately, 15 g of MG 200 magnetic macroporous cellulose particles were washed with pyridine to remove residual water. Then, the pyridine-impregnated particles were added to the reaction mixture (without being resuspended in additional pyridine). Next, the reaction mixture was cooled to 42°C and incubated for 15 min. After the reaction, the MSCP were washed with water and were stored in 70% ethanol in water [119,120].

For the optimization of this sulfation process, reaction times of 15, 30 and 45 min were tested and the resulting MSCP were checked for integrity and the dry weight per volume, the zeta potential, and the sulfate content were measured. The zeta potential was measured on a Zetasizer Nano ZS (Malvern Instruments Ltd., Worcestershire, UK). The sulfate content was derived from the SO₂ content measured by IR spectroscopy (Currenta GmbH & Co. OHG, Leverkusen, Germany) of the dried MSCP samples.

3.4.7 Virus particle purification using magnetic sulfated cellulose particles for analytics

For the MSCP purification (MSCP from section 3.4.6.2) 1.75 mL of the 50% v/v MSCP solution was used. The MSCP were washed 3x with 10 mM Tris-HCl pH 7.4. The VP samples obtained according to section 3.3.3 were diluted 1:3 in 10 mM Tris-HCl pH 7.4 to a final volume of 15 mL to enable VP binding to the MSCP. The 15 mL were pipetted onto the MSCP and incubated 1 min under mixing for binding. Then, the supernatant was discarded and the bound VP were eluted in 1 mL 0.6 M NaCl 10 mM Tris-HCl pH 7.4. The MSCP were regenerated with 15 mL 2 M NaCl 10 mM Tris-HCl pH 7.4 for 10 min. The MSCP were equilibrated by washing 3x with 15 ml 10 mM Tris-HCl pH 7.4 before the next VP purification. The MSCP purification was carried out in triplicate for A/PR_{SUS} and A/PR_{ADH} VP [24].

3.4.8 Positive control antigen preparation

In a first step a crude positive control antigen (PCA) was purified by SCMA chromatography from a diafiltered VP sample according to section 3.4.3 [19]. The provided SCMA (prototype, Sartorius Stedim Biotech GmbH, Göttingen, Germany) had a column volume (CV) of 3 mL. The chromatographic purification method consisted of equilibrating the SCMA with 20x CV of PFB, loading of 65 mL of the diafiltered VP sample onto the SCMA, washing the SCMA with 20x CV PFB, and eluting the bound VP with 10x CV of 600 mM NaCl 10 mM Tris-HCl pH 7.4. The elution peak pooling for the crude PCA was based on the light scattering signal indicating the purified VP. Then, the obtained crude PCA was dialyzed overnight to 150 mM NaCl 50 mM Tris-HCl pH 7.4. After that, sucrose was added to a final concentration of 10% w/v and the sample was frozen at -80°C. After freezing, the samples were freeze dried overnight (-49°C, 0.045 mbar, Christ Alpha 1-2 LD, Martin Christ Gefriertrocknungsanlagen GmbH, Osterode am Harz, Germany) and stored again at -80°C to obtain the PCA [119].

The PCA was diluted to the desired HA concentration 200 μL^{-1} formulation buffer (FB) made of PFB with 357 $\mu\text{g mL}^{-1}$ of polyinosinic:polycytidylic acid (poly I:C, high molecular weight, tlr1-pic, Invivogen, San Diego, USA) and 357 $\mu\text{g mL}^{-1}$ of CpG (19404498, Eurofins Genomics GmbH, Ebersberg, Germany) as adjuvants [121]. The formulated PCA was then injected with a \varnothing 0,45 x 12 mm needle using an 1 mL syringe [119].

3.4.9 Antigen purification and formulation using magnetic sulfated cellulose particles

The MSCP antigen purification and formulation process was designed to load 1.0 μg HA per 200 μL aMSCP formulation. The basis for the aMSCP formulations were 500 μL of the MSCP produced according to section 3.4.6.3. The MSCP were washed 5x with PFB to enable VP binding. From the 500 μL diafiltered VP sample according to section 3.4.3 100 μL were kept for SRID analytics and 400 μL , comprising 6.8 μg HA antigen, were loaded onto the conditioned MSCP. For loading, the MSCP were incubated with the antigen solution for 10 min at RT. After incubation, the supernatant was removed (400 μL) to measure the residual HA antigen amount by SRID. With the HA antigen amount in the starting and the end solution, the loaded HA antigen on the aMSCP was calculated. After loading, the aMSCP were washed 5x with 500 μL PFB to remove residual loading material. Finally, the aMSCP were suspended in 700 μL FB to obtain 3x 200 μL for injection with a \varnothing 0,45 x 12 mm needle using an 1 mL syringe [119].

3.5 Immunization studies

The immunization studies were carried out by Sarah Frentzel (Institute of Medical Microbiology and Hospital Hygiene, Infection Immunology Group, University Hospital of the Otto-von-Guericke University Magdeburg, Germany) as published in an research article with shared first authorship (for details on the contributions see section 8.5) [119].

Investigation of influenza virus particle aggregation and purification with magnetic sulfated cellulose particles

3.5.1 Mice

For the immunization studies, eight-week-old female C57Bl/6 mice (Harlan Laboratories, Venray, The Netherlands) were used. The mice were kept in a specific pathogen-free environment according to the guidelines of the regional animal care committee [119].

3.5.2 *In vivo* titration of the vaccine antigen dose

An *in vivo* titration with 1.0, 7.5, and 15.0 μg SCMA purified HA antigen was carried out before the aMSCP immunization experiments. The HA antigen in 100 μL PBS with 50 μg poly I:C and 50 μg CpG was administered intraperitoneally (i.p.) into mice in triplicate for each antigen dose [119].

The immunization experiment contained a first immunization (d1), a second after two weeks (d14) and a third after four weeks (d28). Mice sera were sampled at day 13 (d13), 27 (d27), and 41 (d41) for measuring the anti-A/PR antibody levels via ELISA. At day 42 (d42) the mice were challenged with a lethal A/PR virus dose and their weights were monitored until day 48 (d48, see section 3.5.4). At day 48 they mice were sacrificed and the viral load of the lungs was estimated (see section 3.6.9) [119].

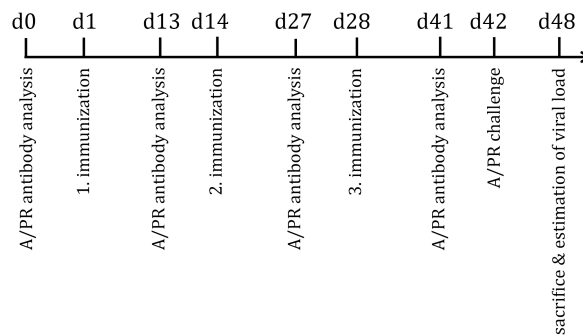


Figure 6 Immunization experiment for the *in vivo* titration of the vaccine antigen dose

Figure adapted with permission from [119].

3.5.3 Immunization with antigen-loaded magnetic sulfated cellulose particles

The aMSCP and controls were injected i.p. into the mice in 200 μL FB comprising 50 μg poly I:C and 50 μg CpG. The immunization setup contained four mice groups ($n = 5$): G1, aMSCP loaded with 1.0 μg HA in FB; G2, 1.0 μg HA PCA in FB (positive control); G3, 1.0 μg HA PCA in FB and blank MSCP in FB injected at two different sites of the abdomen (antigen-particle interaction control); G4, FB (negative control). The immunization experiment consisted of a first immunization (d1) and a second immunization after two weeks (d14). Mice sera were sampled at day 13 (d13) and 27 (d27) for measuring the anti-A/PR antibody levels by ELISA.

Chapter 3: Materials and Methods

At day 28 (d28) the mice were challenged with a lethal A/PR virus dose and their weights were monitored until day 34 (d34, see section 3.5.4). At day 34 they mice were sacrificed and the viral load of the lungs was estimated (see section 3.6.9) [119].

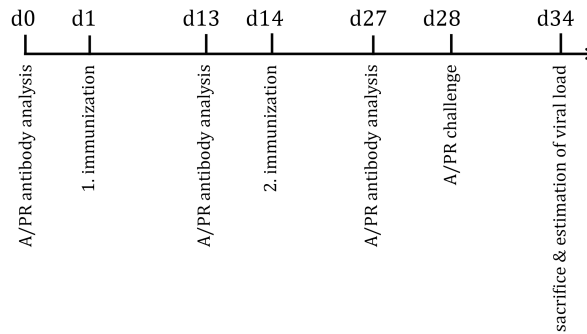


Figure 7 Immunization experiment with antigen-loaded magnetic sulfated cellulose particles

Figure adapted with permission from [119].

3.5.4 Challenge of mice with a lethal virus dose

The mice were challenged with an active MDCK cell-derived influenza A/PR virus two weeks after the last immunization (d42 for the *in vivo* titration, see section 3.5.2, and d28 for the MSCP immunization, see section 3.5.3) [122]. The active A/PR VP were diluted in 25 μ L PBS and were administered to the mice nostrils. The lethal dose was obtained in earlier titration studies. There, a body weight loss of 25% was considered lethal [122]. The mice were anesthetized by i.p. injection of 10% ketamine and 2% xylazin (Ceva Tiergesundheit GmbH, Düsseldorf, Germany) in 0.9% NaCl in water before the intranasal infection. The mice weight was monitored daily after the challenge. The mice were sacrificed by CO₂ euthanasia after six days of the challenge experiment (d48 for the *in vivo* titration, see section 3.5.2, and d34 for the MSCP immunization, see section 3.5.3) [119].

3.6 Analytics

3.6.1 Hemagglutination assay

The hemagglutination assay was used to estimate and compare VP concentrations as described by Kalbfuss et al. [89]. The results are reported in HAU mL⁻¹.

3.6.2 Single radial immunodiffusion assay for hemagglutinin antigen quantification

A SRID based on Wood et al. was used for quantifying the HA amount [123]. For the SRID a 7x7 spot diffusion matrix (1% agarose gel with 64 μ g anti-A/PR serum mL⁻¹, 03/242, NIBSC, Hertfordshire, England) was used. An in house-generated SCMA-purified A/PR standard was used for quantification [73].

Investigation of influenza virus particle aggregation and purification with magnetic sulfated cellulose particles

To measure the HA antigen on the aMSCP from section 3.4.9, sucrose was added to a final concentration of 10% w/v to the samples, followed by freezing at -80°C and freeze drying overnight (-49°C , 0.045 mbar, Christ Alpha 1-2 LD, Martin Christ Gefriertrocknungsanlagen GmbH, Osterode am Harz, Germany). The PCA samples were directly used in the SRID assay [119].

The relative standard deviation (RSD) of the derived HA antigen on the aMSCP by SRID measurements was $\leq \pm 17\%$ ($n = 17$) [119].

3.6.3 Particle size distribution measurements

For measuring the PSD of the A/PR_{ADH} and A/PR_{SUS} VP samples a DCS disc centrifuge method was used with several optimizations [109,110]. For the PSD measurements, the CPS DC24000 UHR disc centrifuge (CPS Instruments Inc., LA, USA) was used with a 4 to 16 % w/v sucrose (1.07654, Merck KGaA, Darmstadt, Germany) gradient. The gradient consisted of nine steps, i.e., 4, 5.5, 7, 8.5, 10, 11.5, 13, 14.5, and 16% sucrose, with a volume of 1.6 mL per step. The gradient steps were injected successively into the running centrifuge disc at a disc speed of 24 000 revolutions per minute (RPM) to build up the 14.4 mL gradient. After gradient layer injection, the gradient quality was assessed by injecting 100 μL of the 239 nm particle standard (0.3 - 0.5% solid content, polyvinyl chloride (PVC), particle density $\rho_P = 1.385 \text{ g mL}^{-1}$, CPS Instruments Inc., LA, USA) diluted 1:4.25 in the corresponding gradient buffer. If the 239 nm particle standard injection was accepted by the CPS software and showed a symmetric and sharp peak, the gradient was used for the subsequent measurement after 10 min of equilibration. After that, 100 μL of the 239 nm particle standard dilution was injected again for calibration followed by injection of 100 μL VP sample. (The double injection of the standard particles helped to identify unusable gradients before the gradient equilibration and reduced gradient evaporation to maximize its life time.) The gradient solution was removed after each measurement from the centrifuge disc. Then, the disc was cleaned with (warm) water followed by drying and cleaning with pure ethanol. The PSD measurements were carried out in triplicate unless noted otherwise [114].

Previous work used a dodecane layer on top of the gradient, which was injected on the gradient [110]. This minimized gradient evaporation and prolonged its life time. However, no dodecane layer was used in the implemented setup to avoid conformational changes of proteins adsorbed to dodecane-in-water emulsion interfaces [114,124,125].

3.6.4 Gradient buffer density measurements

The gradient buffer density ρ_{GB} in combination with the particle density ρ_P directly affects particle sedimentation times and therefore the measured apparent hydrodynamic particle diameter D_p . Therefore, correct ρ_{GB} values are of great importance for obtaining correct PSD. Because of that, an previously outlined ρ_{GB} measurement method employing two differently sized and dense particle standards was implemented [110]. When ρ_{GB} is directly determined in the measurement system, the solution injected with the standard particles for verifying gradient quality and for calibration, the viscosity changes of the gradient buffer due to temperature changes, the gradient buffer

Chapter 3: Materials and Methods

evaporation over time, and the unused gradient fraction below the detector beam are considered. Therefore, the ρ_{GB} values measured with this method are closer to the real ρ_{GB} values than conventional mass measurement of a defined volume of the gradient buffer [114].

To derive the ρ_{GB} , 100 μL gradient buffer without sucrose was spiked with a 105 nm (5% (w/w) solid content, poly(methyl methacrylate) (PMMA), particle density $\rho_P = 1.19 \text{ g ml}^{-1}$, 1:8 final dilution, PMMA-R-KM215, Microparticles GmbH, Berlin, Germany) and the 239 nm particle standard ($\rho_P = 1.385 \text{ g mL}^{-1}$, 1:16 final dilution) and was measured according to section 3.6.3. Afterwards, the ρ_{GB} was determined by linear regression from the particle standard sedimentation times, the particle density ρ_P , and the hydrodynamic particle diameters D_P as shown in Formula 3-5 [110]. The measurements to determine ρ_{GB} were carried out in triplicate [114].

$$x_i = \rho_i; y_i = \frac{1}{t_i(D_i)^2}; i = 105 \text{ or } 239 \text{ nm particle standard}, \quad (3)$$

where x_i is the linear equation placeholder for the particle density ρ_i (kg m^{-3}) and y_i ($\text{s}^{-1} \text{ m}^{-2}$) is the linear equation placeholder for the inverse product of the sedimentation time t_i (s) and the squared Stokes/hydrodynamic diameter D_i (m).

$$\Delta y = k\Delta x + d \rightarrow k = \frac{\Delta y}{\Delta x} \rightarrow d = y_i - kx_i, \quad (4)$$

where k is the linear equation placeholder for the slope ($\text{m kg}^{-1} \text{ s}^{-1}$), and d is the linear equation placeholder for the y-axis segment ($\text{s}^{-1} \text{ m}^{-2}$).

$$y = 0 \rightarrow \frac{-d}{k} = \frac{-y_i + \frac{\Delta y x_i}{\Delta x}}{\frac{\Delta y}{\Delta x}} = \rho_{GB}, \quad (5)$$

where ρ_{GB} is the gradient buffer density (kg m^{-3}).

3.6.5 Virus particle density measurements

Determining the VP buoyant density ρ_{VP} is based on a similar setup as shown in section 3.6.4 and can be carried out simultaneously. Therefore, a VP sample was spiked with the 105 nm and the 239 nm particle standard (final dilutions were adapted to the VP samples) and was measured in two gradient buffers with different densities, i.e., the 4 to 16% w/v standard gradient buffer and a 8 to 20% w/v gradient buffer. After that, ρ_{VP} can be derived by linear regression from the sedimentation times of the 105 nm particle standard and the VP in the two different gradient buffers as outlined in Formula 6-8 [110]. For the linear regression, the 105 nm particle standard was used as a reference because its hydrodynamic size and buoyant density is closer to that of the influenza VP. The measurements to determine ρ_{VP} were carried out in PBS in triplicate [114].

$$a_j = \rho_j; b_j = (\rho_{Std105nm} - \rho_j) \frac{t_{Std105nm}}{t_{VP}}; j = 4 \text{ to } 16\% \text{ or } 8 \text{ to } 20\% \text{ gradient buffer}, \quad (6)$$

where a_j is the linear equation placeholder for the gradient buffer density ρ_{GB} (kg m^{-3}) and b_j (kg m^{-3}) is the linear equation placeholder for the 105 nm standard particle density ρ_{Std} (kg m^{-3})

Investigation of influenza virus particle aggregation and purification with magnetic sulfated cellulose particles

minus the gradient buffer density ρ_{GB} (kg m^{-3}) multiplied with the sedimentation time t_{Std105nm} of the 105 nm standard particles (s) divided by sedimentation time t_{VP} of the VP.

$$\Delta b = e\Delta a + g \rightarrow e = \frac{\Delta b}{\Delta a} \rightarrow g = b_j - ea_j, \quad (7)$$

where e is the linear equation placeholder for the slope (-), and g is the linear equation placeholder for the y-axis segment (kg m^{-3}).

$$b = 0 \rightarrow \frac{-g}{a} = \frac{-b_j + \frac{\Delta ba_j}{\Delta a}}{\frac{\Delta b}{\Delta a}} = \rho_{VP}, \quad (8)$$

where ρ_{VP} is the VP buoyant buffer density (kg m^{-3}).

3.6.6 LC-MS/MS-based proteome analysis

The LC-MS/MS based proteome analysis was carried by Anja Serve (Max Planck Institute for Dynamics of Complex Technical Systems, Magdeburg, Germany) as published in a technical note with shared first authorship (for details on the contributions see section 8.5) [24].

Briefly, pelleted VP were lysed and heat inactivated at 80°C for 5 min. Then, 55 μg protein were precipitated and resuspended in a urea-containing buffer. Finally, the proteins of the solutions were bound to centrifugal filter units, washed several times, digested, and the flow-throughs were collected for LC-MS/MS analysis with an UltiMate 3000 RSLCnano splitless liquid chromatography system coupled online to a LTQ-Orbitrap Elite hybrid MS (Thermo Fisher Scientific Inc., Massachusetts, USA) [24].

3.6.7 Blood collection and preparation of sera

The blood collection and sera preparation was carried out by Sarah Frentzel (Institute of Medical Microbiology and Hospital Hygiene, Infection Immunology Group, University Hospital of the Otto-von-Guericke University Magdeburg, Germany) as published in an research article with shared first authorship (for details on the contributions see section 8.5) [119].

The mice sera were prepared from mice blood samples, which were collected by retrobulbar bleeding one day before the immunizations and at the end of the immunization schedule. Mice were anesthetized by inhalation of isoflurane (N01AB06, Baxter AG, Volketswil, Switzerland) to obtain the blood samples. Then, the blood samples were incubated for 20 min at RT followed by 20 min at 4°C. After that, blood samples were centrifuged at 14 000 RPM for 10 min at 4°C. Finally, the supernatants, i.e., mice sera, were stored at -20°C [119].

3.6.8 Detection of anti-A/PR antibodies by ELISA

A traditional sandwich ELISA setup was used for the detection of the anti-A/PR antibodies in sera of immunized mice. The immobilization of the capture antibody was carried out with 100 μl anti-A/PR serum (03/242, NISBC, Hertfordshire, England) diluted 1:1000 in 50 mM Na_2CO_3 pH 9.6 coating buffer (CB) followed by overnight incubation at 4°C in Nunc MaxiSorp 96-well ELISA

Chapter 3: Materials and Methods

plates (Thermo Fisher Scientific Inc., Massachusetts, USA). After that, the plates were blocked with 200 μL 10% fetal calf serum (Sigma-Aldrich Co. LLC., St. Louis, USA) for 1 h at RT. Then, the plates were washed 5x with washing buffer (WB) made of 0.05% Tween-20 in PBS. Afterwards, plates were incubated with 100 μL inactivated and clarified virus harvest produced according to section 3.4.1 for 2 h at RT. Next, the plates were 5x washed with WB followed by application of 100 μL diluted mice sera and incubation for 2 h at RT. Then, the plates were washed 7x with WB. For the positive control 100 μL PBS with 0.5 $\mu\text{g mL}^{-1}$ monoclonal anti-influenza virus type A hemagglutinin antibody C102 (3IH4, HyTest Ltd., Turku, Finland) was used. 100 μL PBS was used for the negative control. After that, 100 μL of 1:5 000 in PBS diluted anti-mouse IgG whole molecule-peroxidase antibody (A3415, Sigma-Aldrich Co. LLC, St. Louis, USA) was added and incubated for 1.5 h at RT. Next, a 7x wash with WB was carried out. Subsequently, 100 μL of 3,3',5,5'-tetramethylbenzidine liquid substrate (T5569, Sigma-Aldrich Co. LLC., St. Louis, USA) was added and the enzymatic reaction was stopped after 15 min with 50 μL 2 M H_2SO_4 (Merck KGaA, Darmstadt, Germany). Finally, the absorbance after the color reaction was measured at a wavelength of 450 nm (OD 450nm). The RSD for the anti-A/PR antibodies ELISA was $\leq \pm 15\%$ (n = 3) [119].

3.6.9 Viral load determination by quantitative real-time PCR

The viral load determination by quantitative real-time PCR was carried out by Sarah Frentzel (Institute of Medical Microbiology and Hospital Hygiene, Infection Immunology Group, University Hospital of the Otto-von-Guericke University Magdeburg, Germany) as published in an research article with shared first authorship (for details on the contributions see section 8.5) [119].

The viral load estimation after the challenge experiment was based on the nucleoprotein (NP) gene copy numbers obtained by quantitative real-time PCR. For that, the lung tissue of the challenged mice was perfused with ice-cold PBS after the mice were sacrificed at day 6 post infection (p.i.) by CO_2 inhalation. After that, the lung tissue was removed and stored in RNAlater (76106, Qiagen GmbH, Hilden, Germany) at -20°C . After the freezing step the tissue was homogenized followed by RNA isolation with the RNeasy Mini Kit (74106, Qiagen GmbH, Hilden, Germany). The residual DNA was digested with an RNase-free DNase (79254, Qiagen GmbH, Hilden, Germany) and the resulting RNA preparation was eluted in 50 μL nuclease free water. The RNA amount was quantified by a NanoDrop ND-1000 spectrophotometer (Thermo Fisher Scientific Inc., Massachusetts, USA). For the cDNA synthesis 1 μg RNA was used. For the reverse transcription reaction 1.5 μg random primers and 0.25 μg oligo-dT in a total volume of 12 μL water were used. The RNA samples were heated up to 70°C for 10 min and afterwards cooled down on ice for 10 min. After that, the reverse transcription reaction mix was added, containing 1 μL SuperScript II reverse transcriptase, 1 μL 10 mM dNTP mix, 4 μL 5x first-strand buffer, and 2 μL 0.1 M dithiothreitol (18064-071, Thermo Fisher Scientific Inc., Massachusetts, USA). Next, the RNA samples were incubated for the reverse transcriptase reaction at 42°C for 1 h in a thermocycler (Peqlab, Erlangen, Germany). After the reaction, the cDNA amount was estimated with the spectrophotometer. From each reaction 25 ng cDNA was used for the quantitative real-time PCR carried out in triplicate on a LightCycler

Investigation of influenza virus particle aggregation and purification with magnetic sulfated cellulose particles

480 system using a LightCycler 480 SYBR Green I Master reaction mix (Roche Diagnostics GmbH, Mannheim, Germany). The NP gene primers were used at a concentration of 500 nM: sense primer 5'GAGGGGTGAGAATGGACGAAAAAC-3'; anti-sense primer 5'- CAGGCAGGCAGGCAGGACTT-3'. For generating a standard curve an external NP gene copy standard was used. The RSD for the quantitative real-time PCR was $\leq \pm 37\%$ (n = 3) [119].

3.6.10 Statistical analysis

3.6.10.1 Particle size distribution measurements

For the PSD single or triplicate measurements were carried out. The statistical analysis of the mean apparent hydrodynamic diameter maxima of the monomeric VP peak (AHD) of triplicates was carried out using a two-sample *F*-test assuming equality of variances followed by a two-sample student's *t*-test. The results were considered to be statistically significant at a 95% confidence interval ($p < 0.05$) [114].

3.6.10.2 Immunization studies

The statistical analysis of the immunization data with an unpaired, two-tailed student's *t*-test and a two-way ANOVA with Bonferroni post-test using GraphPad Prism v 5.04 (GraphPad Software Inc., La Jolla, CA, USA) was carried out by Sarah Frentzel (Institute of Medical Microbiology and Hospital Hygiene, Infection Immunology Group, University Hospital of the Otto-von-Guericke University Magdeburg, Germany) as published in an research article with shared first authorship (for details on the contributions see section 8.5) [119].

The results of the immunization experiments are shown as mean \pm standard error of the mean (SEM).

4 RESULTS AND DISCUSSION

4.1 Investigation of influenza A virus particle aggregation

The obtained data was first published in Engineering in Life Sciences [114] and parts of the original publication are used hereafter (for details on the contributions see section 8.5 and 8.8.1).

4.1.1 Tangential flow filtration concentration

The filtered and inactivated VP broth produced with the MDCK_{SUS2} production system was concentrated 10x by volume to acquire 9.6×10^4 HAU mL⁻¹ after concentration, filtration, 0.5 mL aliquotation, freezing and thawing (A/PR_{SUS}). The filtered and inactivated VP broth of the MDCK_{ADH} cultivation was concentrated 40x by volume to obtain a HA activity of 1.3×10^5 HAU mL⁻¹ (A/PR_{ADH}). Therefore, the concentrated A/PR_{ADH} samples were diluted 1:1.4 with PBS to obtain HA activities of approximately 10^5 HAU mL⁻¹ for both samples for the subsequent dialysis [114].

During the sample preparation for dialysis no critical aggregation was observed for A/PR_{ADH} and A/PR_{SUS} VP samples. Nevertheless, the A/PR_{SUS} sample still showed minor levels of dimers, which could not be removed completely by the 0.1 µm filtration shown in Figure 8. The observed monomeric AHD maxima of the VP peak was at 89 nm for A/PR_{ADH}, and at 83 nm for A/PR_{SUS}, respectively [114].

4.1.2 Virus particle density measurements

To obtain accurate PSD, the VP buoyant density ρ_{VP} of both VP samples was measured. The obtained ρ_{VP} were 1.18 g mL^{-1} for A/PR_{ADH} and 1.17 g mL^{-1} for A/PR_{SUS}, respectively [114], and are in good agreement with reported values for MDCK-derived influenza A VP measured with the same method with 1.18 and 1.19 g mL^{-1} by Neumann et al. [110].

The measured sedimentation times in the two gradients are exemplified for a spiked A/PR_{ADH} sample in Figure 9.

Investigation of influenza virus particle aggregation and purification with magnetic sulfated cellulose particles

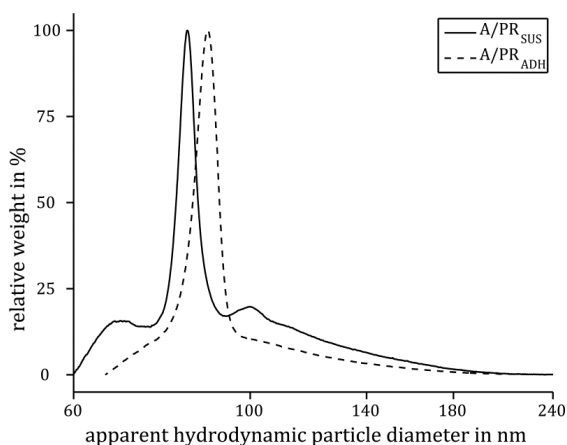


Figure 8 Prepared virus particle samples used for dialysis.

Virus particles produced in the adherent (A/PR_{ADH}) and suspension (A/PR_{SUS}) cultivations after sample preparation for dialysis, i.e., concentration to approximately 10^5 HAU mL^{-1} , $0.1 \mu\text{m}$ filtration, 0.5 mL aliquotation, freezing at -80°C and thawing. The monomeric peak of the A/PR_{ADH} sample is about 89 nm and for A/PR_{SUS} at about 83 nm . The A/PR_{SUS} sample still shows a minor dimer peak at about 100 nm after $0.1 \mu\text{m}$ filtration ($n = 1$).

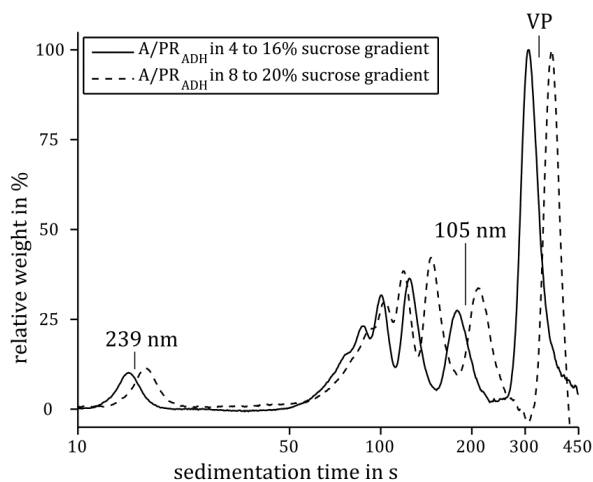


Figure 9 Sedimentation time plot of A/PR_{ADH} sample spiked with the 105 nm and 239 nm particle standard.

The 105 nm particle standard shows aggregates up to tetramers, which are observable as additional peaks on the left sides of the indicated 105 nm particle standard monomer peaks. Peak identity was confirmed by separate PSD measurements of the VP samples and the particle standards (data not shown). Figure adapted with permission from [114].

4.1.3 Specific ion effects on virus particle size distributions

A/PR_{SUS} was screened in standard buffer (SB) consisting of 10 mM Tris-HCl pH 7.4 and SB with all HS salts in a concentration of 20, 60, and 540 mM. Furthermore, SB with NaCl was additionally screened in a concentration of 180, 1020, and 1500 mM. A/PR_{ADH} was screened in SB, SB with 20 mM NaCl and SB with 20, 60, 540 mM CaCl₂ [114].

In a first step, A/PR_{SUS} was screened in all NaCl concentrations shown in Figure 10. Dimers in the size range of 100 to 110 nm were present in low levels in all samples (indicated by the white arrow), which were expected because of the incomplete dimer removal by the 0.1 μm filtration during the sample preparation shown in Figure 8. However, A/PR_{SUS} dialyzed against SB showed high aggregation with the monomeric peak at 81 nm, dimeric at 101 nm, trimeric at 115 nm, and (perhaps) a tetrameric at about 123 nm indicated by the black arrows above the solid line in Figure 10.

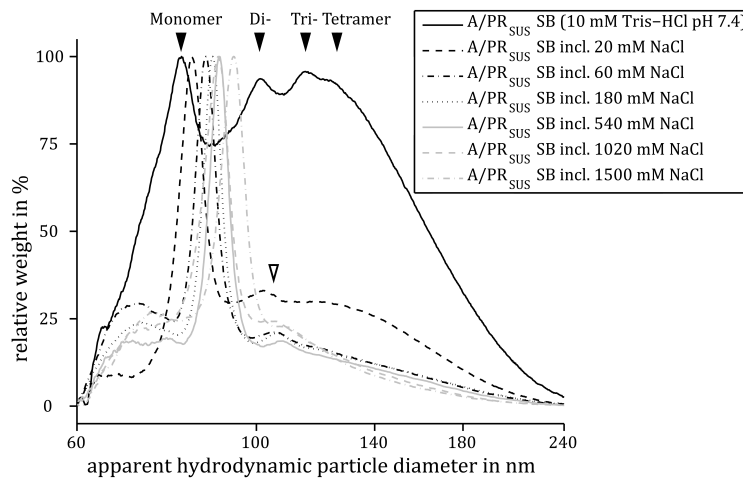


Figure 10 Particle size distributions of A/PR_{SUS} in different NaCl concentrations.

The A/PR_{SUS} virus particles were screened in standard buffer (SB) and SB with 20, 60, 180, 540, 1020 and 1500 mM NaCl. Black arrows indicate the presence of mono- (81 nm), di- (101 nm), tri- (115 nm), and (perhaps) tetramers (about 123 nm) in SB. The white arrow indicates the low presence of dimers in the other buffers. Figure adapted with permission from [114].

Generally, particle aggregation can be described by two different critical concentrations: the critical coagulation concentration (CCC) and the critical stabilization concentration (CSC) [9–12]. The CSC and the CCC are splitting the reaction controlled or slow regimes from the diffusion controlled or fast regimes [9,11]. Additionally, the charge of the particles plays an important role: aggregation of highly charged particles is slow in high salt solutions whereas aggregation of weakly charged particle is fast [9]. Furthermore, the CCC decreases with increasing counterion valence, which is known as Schulze-Hardy rule [9].

The change of the aggregation status between SB with and without 20 NaCl suggests a CSC below 20 mM NaCl. Based on this observation, the VP must be highly charged and hydrophilic [11]. Of note

Investigation of influenza virus particle aggregation and purification with magnetic sulfated cellulose particles

is that all PSD still show the VP monomer. This can be explained by slow VP aggregation or disintegration of VP aggregates during the measurement in the sucrose gradient. However, sucrose gradients were also used in previous experimental setups from literature that investigated aggregation of influenza and adeno VP [97,112]. The experimental setup for the adeno VP used a 8 to 24% sucrose gradient with a similar DCS method and compared it to a conventional AUC method using a ProteomeLab XL-A or XL-I centrifuge (Beckman Coulter, Inc., Brea, USA) without sucrose gradient [112]. These measurements revealed a consisted minor reduction of VP aggregates, suggesting that DCS disc centrifugation is not changing the aggregation status [114].

The AHD values of the monomer (81 nm), dimer (101 nm), and trimer (115 nm) nicely agree to theoretical values based on deformable spheres: monomer/dimer = 81/101 nm = 1/1.25 and monomer/trimer = 81/115 nm = 1/1.42 [126]. This good fit can be explained by previous reports that showed the deformability of influenza A VP in AUC at high g-forces [127]. However, the deformable sphere model was not fitting all aggregation observations (data not shown), which indicates different VP deformabilities in different buffers [114].

Table 1 Mean monomeric apparent hydrodynamic diameter maxima of A/PR_{SUS} in standard buffer and standard buffer with NaCl.

NaCl concentration in standard buffer in mM	AHD in nm*
0	80.92 ± 0.44
20	83.24 ± 0.50
60	86.53 ± 0.46
180	88.25 ± 0.18
540	90.00 ± 0.22
1020	89.32 ± 0.89
1500	93.74 ± 0.19

*** Data shown as monomeric AHD mean ± standard error of the mean (n = 3). Table adapted with permission from [114].**

VP aggregation in low salt solutions was previously reported in literature for influenza A VP, influenza B VP, polio VP, and reo VP by EM [97,99]. However, in these studies aggregates consisting of several hundred VP were detected, which can be linked to the used EM sample preparation by centrifugation [114].

Chapter 4: Results and Discussion

Furthermore, the AHD increased with increasing NaCl concentrations for SB without NaCl and SB with 20, 60, and 180 mM NaCl ($p < 0.05$). Between SB with 540 and 1020 mM NaCl no difference was observable between the adjacent AHD ($p > 0.05$, see Table 1) [114].

Trends of the monomeric AHD of A/PR_{SUS} in SB with 20, 60, and 540 mM of NaCl, NaNO₃, KCl, NaBr, Na⁺/PO₄³⁻, LiCl, and CaCl₂ are shown in Figure 11. There, the monomeric AHD increased with increasing salt concentrations, except for LiCl with no clear trend, and CaCl₂ with decreasing monomeric AHD with increasing salt concentrations [114].

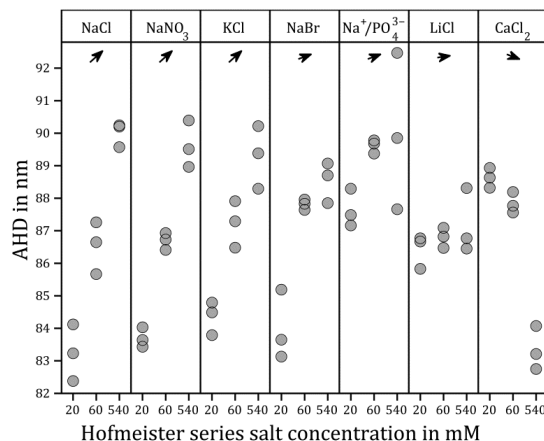


Figure 11 Monomeric apparent hydrodynamic diameter maxima trends of A/PR_{SUS} in standard buffer with 20, 60, and 540 mM salts.

Monomeric apparent hydrodynamic diameter maxima (AHD) trends are indicated by the arrows below the header. AHD measurements with SB containing 540 mM of MgCl₂, Na₂SO₄, and NaI were not successful due to too low differences between the virus particle buoyant density and the gradient buffer density. Figure adapted with permission from [114].

The results of A/PR_{SUS} screened against SB with 20 mM HS ions are shown in Figure 12 for the cations and in Figure 13 for the anions. The monomeric AHD showed a direct HS trend for the cations with Na⁺ < K⁺ < Li⁺ < Mg²⁺ and Ca²⁺ (Table 2) [114].

Additionally, a direct AHD HS trend was visible for the halogen anions with Cl⁻ < Br⁻ < I⁻ (Table 2). However, in both cases, the differences between the neighboring AHD were not significant ($p > 0.05$). Furthermore, there were no visible differences in the aggregation behavior. Only, Li⁺ showed slightly elevated aggregation levels in the range of 100 to 240 nm (Figure 12). In addition, the Ca²⁺-containing buffer induced aggregates up to 560 nm, which are shown Figure 18 [114].

Investigation of influenza virus particle aggregation and purification with magnetic sulfated cellulose particles

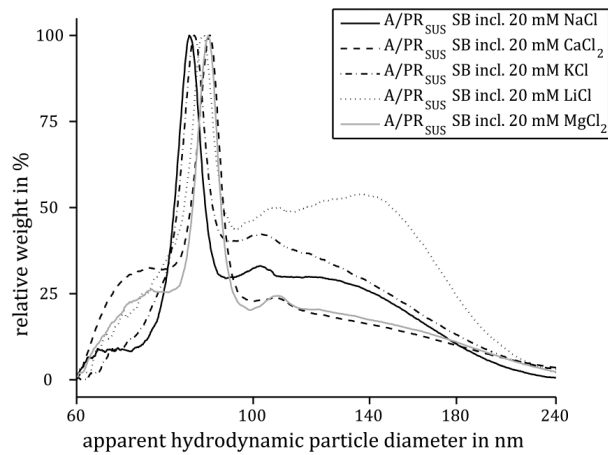


Figure 12 Particle size distributions of A/PR_{SUS} dialyzed against standard buffer with 20 mM salts with different cations.

Figure adapted with permission from [114].

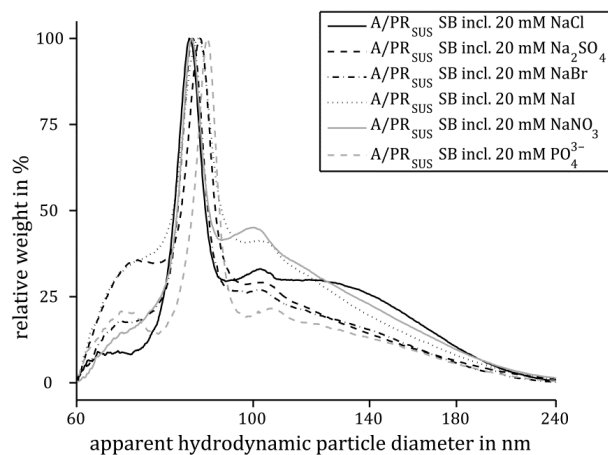


Figure 13 Particle size distributions of A/PR_{SUS} dialyzed against standard buffer with 20 mM salts with different anions.

Figure adapted with permission from [114].

Table 2 Mean monomeric apparent hydrodynamic diameters of A/PR_{SUS} in standard buffer with 20 mM salts.

HS ion	AHD in nm*
Na ⁺	83.24 ± 0.50
K ⁺	84.36 ± 0.30
Li ⁺	86.42 ± 0.30
Mg ²⁺	87.57 ± 0.71
Ca ²⁺	88.63 ± 0.18
Cl ⁻	83.24 ± 0.50
Br ⁻	83.99 ± 0.62
I ⁻	85.03 ± 1.09

* Data shown as monomeric AHD ± standard error of the mean (n = 3). Table adapted with permission from [114].

Dialysis against SB containing 60 mM HS salts showed no observable aggregation in the range of 60 to 240 nm and is visualized in Figure 14 for the cations and in Figure 15 for the anions. However, with Ca²⁺ there was again aggregation observable up to 560 nm (Figure 18). All monomeric AHD differed by not more than 5 nm without significant differences (p > 0.05, data not shown). Interestingly, this range was slightly higher for the different anions compared to the cations and is shown in Figure 15. This is interesting because influenza A VP carry a negative net-charge at pH 7.4 based on reported isoelectric points in the range of 5.0 to 7.0 [17,128]. Therefore, the broader AHD range for the negatively net-charged VP in different anion buffers could indicate a coion interaction between them [114].

Investigation of influenza virus particle aggregation and purification with magnetic sulfated cellulose particles

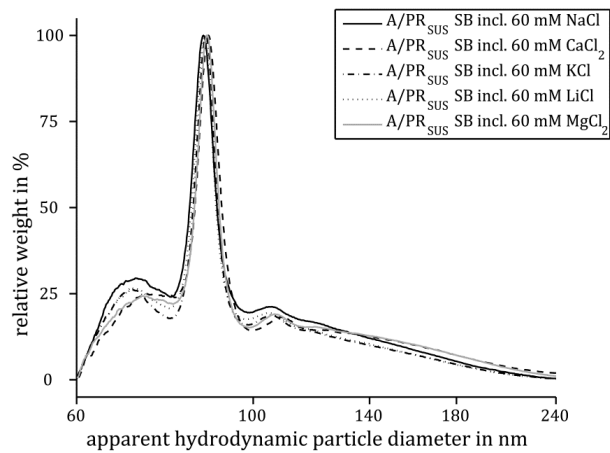


Figure 14 Particle size distributions of A/PR_{SUS} dialyzed against standard buffer with 60 mM salts with different cations.

Figure adapted with permission from [114].

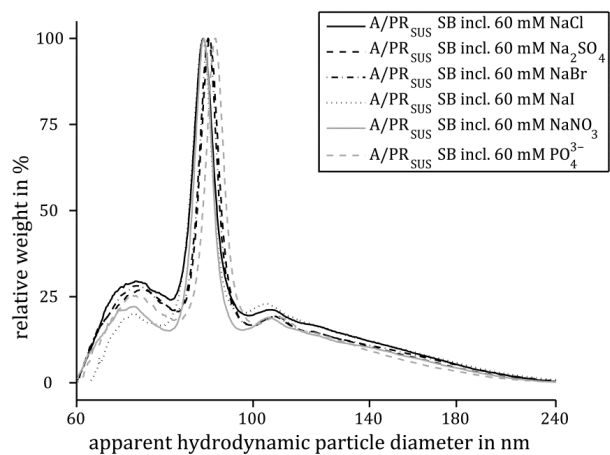


Figure 15 Particle size distributions of A/PR_{SUS} dialyzed against standard buffer with 60 mM salts with different anions.

Figure adapted with permission from [114].

Chapter 4: Results and Discussion

Dialysis against SB containing 540 mM HS salt showed a similar picture to the previously screened 60 mM concentration. The 9x higher concentration increased the monomeric AHD range for different cations shown in Figure 16. Ordering the monomeric AHD resulted in a reverse or indirect HS with $\text{Ca}^{2+} < \text{Li}^+ < \text{K}^+ < \text{Na}^+$. However, the differences between the adjacent AHD were only significant for Li^+ and Ca^{2+} ($p < 0.05$). The Ca^{2+} -containing buffer resulted again in aggregates up to 560 nm (Figure 18). This, and the previous discussed data show that the A/PR_{SUS} VP are stable in all screened SB with 20, 60, or 540 mM HS salt with the exception of SB with Ca^{2+} in all screened concentrations. This observed effect can be linked to a high hydrophilicity of the VP indicated by the numerous non-aggregating ions [11]. The observed stronger effects of the cations on the monomeric AHD can be linked to the negative net-charge of the VP [17,128].

Table 3 Mean monomeric apparent hydrodynamic diameters of A/PR_{SUS} dialyzed against standard buffer with 540 mM salts.

HS ion	AHD in nm*
Na^+	90.00 ± 0.22
K^+	89.30 ± 0.56
Li^+	87.18 ± 0.57
Ca^{2+}	83.34 ± 0.39

* Data is shown as monomeric AHD mean \pm standard error of the mean ($n = 3$). Table adapted with permission from [114].

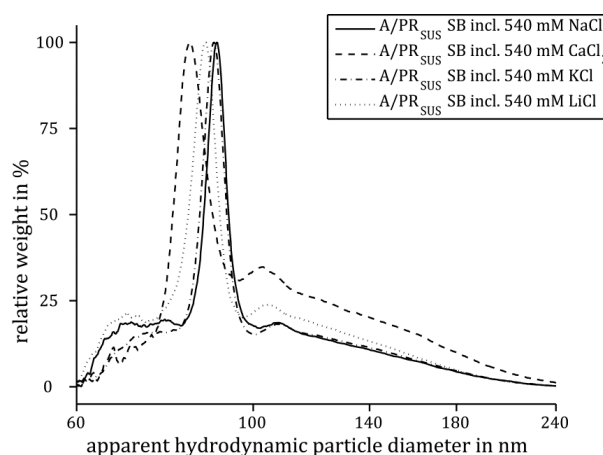


Figure 16 Particle size distributions of A/PR_{SUS} dialyzed against standard buffer with 540 mM salts with different cations.

Figure adapted with permission from [114].

Investigation of influenza virus particle aggregation and purification with magnetic sulfated cellulose particles

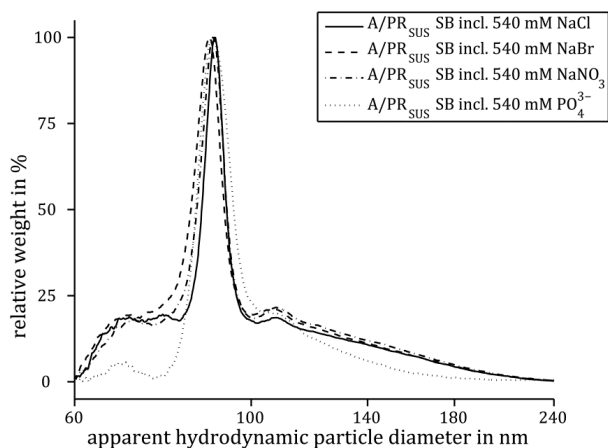


Figure 17 Particle size distributions of A/PR_{SUS} dialyzed against standard buffer with 540 mM salts with different anions.

Figure adapted with permission from [114].

Furthermore, A/PR_{ADH} was compared to A/PR_{SUS} in SB with 20, 60, and 540 mM Ca²⁺ to observe differences in the Ca²⁺-induced aggregation behavior. The A/PR_{ADH} VP showed a higher propensity for aggregation at all screened Ca²⁺ concentrations (Figure 19) compared to A/PR_{SUS} VP (Figure 18). Of note is the potential 16-mer visible at 214 nm for A/PR_{ADH} in SB with 20 mM Ca²⁺ in Figure 19. The observed aggregation behavior for both samples can be linked to the Schulze-Hardy rule and the increased counterion valence of Ca²⁺. Conversely, this was not observed for Mg²⁺. Therefore, the observed effect of Ca²⁺ cannot be only based on an increased ion valence. Controversially, Ca²⁺ seems to stabilize other hydrophilic colloidal particle systems [11]. Further factors contributing to the aggregation effects of Ca²⁺ could be remaining host-cell membrane components like cadherins. These cadherins play an important role in Ca²⁺-dependent mammalian cell adhesion [129]. Another explanation could be a decreased NA activity of A/PR_{AHD} that can result in higher VP aggregation [45,103]. Additionally, a shift to smaller monomeric AHD was visible for both VP samples when dialyzed against SB with 540 mM Ca²⁺ when compared to lower Ca²⁺ concentrations in Figure 18 and Figure 19 [114].

Because of the observed differences in the aggregation behavior of A/PR_{SUS} and A/PR_{ADH} the samples were screened in SB without additional salts shown in Figure 20 and SB with 20 mM NaCl shown in Figure 21. SB without additional salts showed high aggregation for both VP samples. However, aggregates were bigger and more abundant for the A/PR_{ADH} sample. Moreover, A/PR_{ADH} showed aggregation up to tetra- and pentamers in SB with 20 mM NaCl. Conversely, A/PR_{SUS} showed no sign of increased aggregation in the same buffer. A possible explanation of this can be glycosylation differences of the viral HA, which is located in high-abundance in the VP membrane. This is in agreement with previous work on HA glycosylation differences for influenza VP produced in suspension and adherent MDCK host-cell lines [130].

Chapter 4: Results and Discussion

Differences in the glycosylation could potentially affect VP hydrophilicities and therefore aggregation behavior.

Additionally, the observed monomeric AHD for both samples were similar in SB. Conversely, in SB with 20 mM NaCl, the monomeric AHD of A/PR_{ADH} (80 nm) was smaller than for A/PR_{SUS} (83 nm) [114].

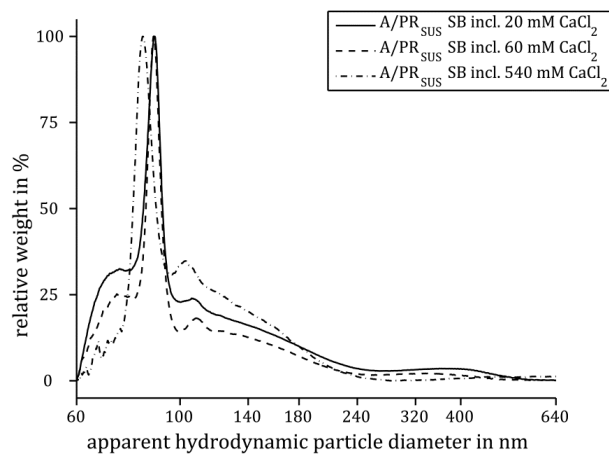


Figure 18 Particle size distributions of A/PR_{SUS} dialyzed against standard buffer with 20, 60, and 540 mM Ca²⁺.

Figure adapted with permission from [114].

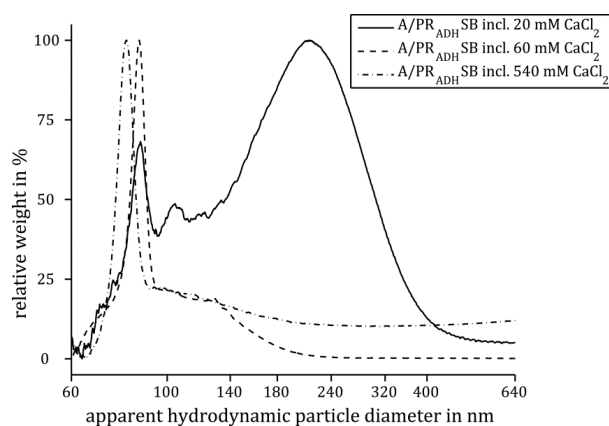


Figure 19 Particle size distributions of A/PR_{ADH} dialyzed against standard buffer with 20, 60, and 540 mM Ca²⁺.

Figure adapted with permission from [114].

Investigation of influenza virus particle aggregation and purification with magnetic sulfated cellulose particles

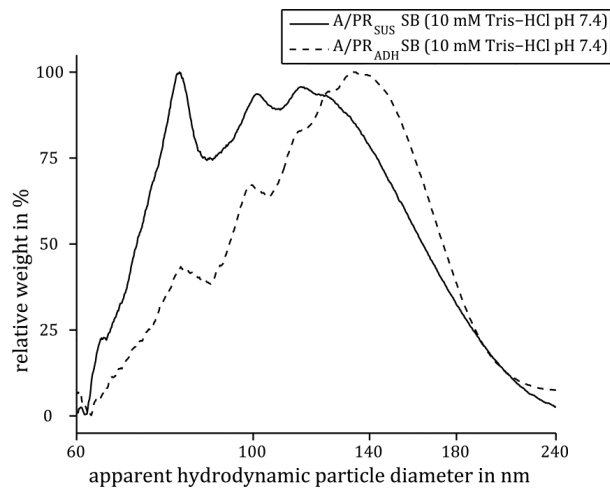


Figure 20 Particle size distributions of A/PR_{SUS} and A/PR_{ADH} dialyzed against standard buffer.

Figure adapted with permission from [114].

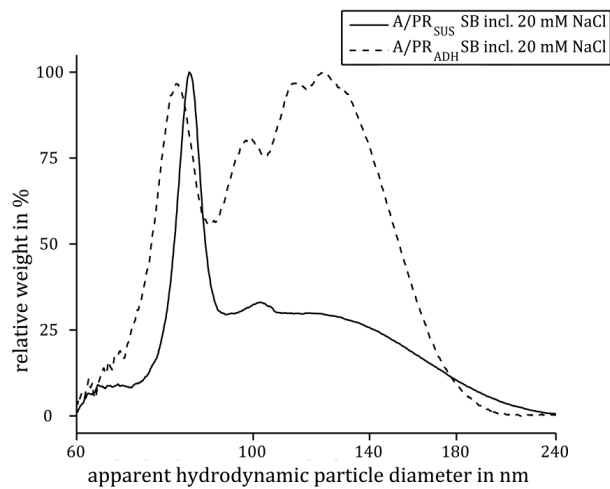


Figure 21 Particle size distributions of A/PR_{SUS} and A/PR_{ADH} dialyzed against standard buffer with 20 mM NaCl.

Figure adapted with permission from [114].

4.2 Investigation of influenza A virus particle purification using magnetic sulfated cellulose particles

For the A/PR VP purification by MSCP two different particle types were used: MSCP based on Magne™ protein A particles and MG 200 magnetic macroporous cellulose particles.

The MSCP based on the Magne™ protein A particles were developed to allow a fast buffer change compared to dialysis for the VP aggregation studies in section 4.1. However, buffer change experiments with A/PR_{ADH} carried out according to section 3.4.7 resulted in high aggregation levels, shown in Figure 22. Because of this clear disadvantage for aggregation studies, the MSCP based on Magne™ protein A particles were only used for comparing a MSCP purification process with an established centrifugation method for analytics, which is described in section 4.2.2.

MSCP based on MG 200 magnetic macroporous cellulose particles were used for the purification and formulation experiments described in section 4.2.3. The MSCP based on MG 200 magnetic macroporous cellulose particles cost less and can be produced in larger quantities compared to the MSCP based on Magne™ protein A particles, which was an advantage due to the needed amounts for the carried-out experiments.

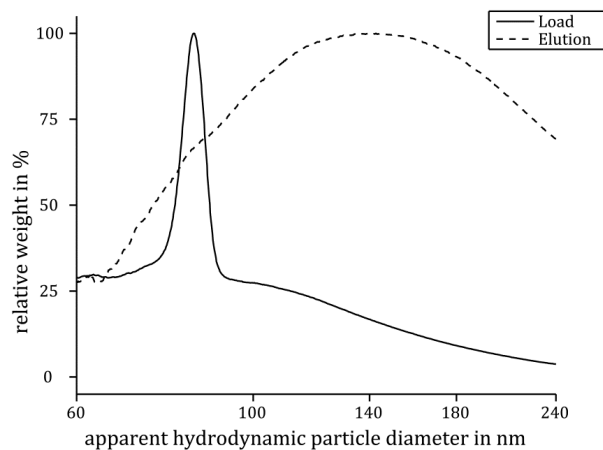


Figure 22 Adherent cell culture-derived influenza A virus particle aggregation using magnetic sulfated cellulose particles based on Magne™ protein A particles for purification

4.2.1 Production of magnetic sulfated cellulose particles

4.2.1.1 Magnetic sulfated cellulose particles based on Magne™ protein A particles

The MSCP production based on Magne™ protein A particles was carried as outlined in section 3.4.6.2. The production process was not further optimized because of the particles limited applicability due to the high raw-material costs.

4.2.1.2 Magnetic sulfated cellulose particles based on MG 200 magnetic macroporous cellulose particles

To optimize the sulfation process of the MG 200 magnetic macroporous cellulose particles, reaction times of 15, 30, and 45 min were screened for the resulting dry weights and zeta potentials (M.Sc. thesis, N. Gebert, see section 8.8.1) as well as for the sulfate contents (Figure 23).

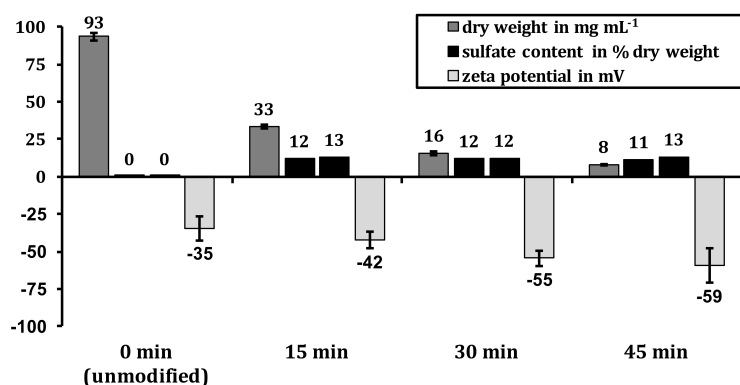


Figure 23 Optimization of the MG 200 magnetic macroporous cellulose particles sulfation process

Dry weight in mg/mL shown as mean \pm standard deviation (n = 3); sulfate content in % dry weight shown as single measurements (n = 2); zeta potential in mV shown as mean \pm standard deviation (n = 52).

The dry weight decreased over the reaction time due to particle disintegration. The zeta potential decrease can be attributed to the sulfation process resulting in more negatively charged MSCP over time. However, the sulfate content is stable after 15 min. Therefore, the zeta potential decrease can be attributed to some degree to particle fragments that dissociated from the MSCP during the sulfation process, which were not present anymore in the sulfate content determination due to the washing steps of the MSCP sample preparation.

The MSCP disintegration over the sulfation reaction time is also shown in Figure 24. Because the MSCP disintegration was not visible and the sulfate content did not increase after 15 min (Figure 23), the 15 min reaction time was used for the final MSCP sulfation process.

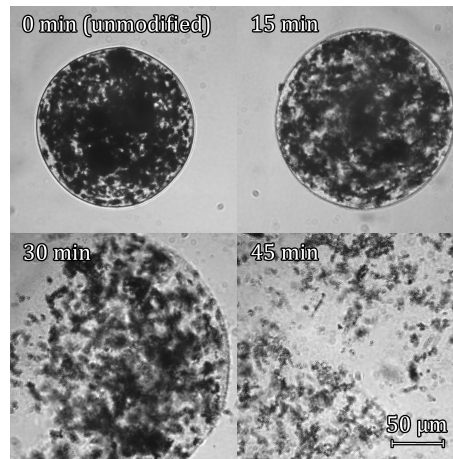


Figure 24 Magnetic sulfated cellulose particles disintegration over sulfation time

The MSCP disintegration was visualized by light microscopy and was substantial after 30 min of sulfation reaction time.

4.2.2 Comparison of magnetic sulfated cellulose particles with an established centrifugation method for analytics

The obtained data was first published in Analytical Chemistry [24] and parts of the original publication are used hereafter (for details on the contributions see section 8.5).

A/PR_{SUS} and A/PR_{ADH} VP produced according to section 3.3.3 were used for the investigation of the MSCP purification performance. The MSCP were based on Magne™ protein A particles and were compared to an established centrifugation method for analytics [26,27,131]. For the LC-MS/MS analysis of the purified VP samples an optimized filter aided sample preparation (FASP) was used to generate tryptic peptides from the lysates [24,132]. The combination of FASP with LC-MS/MS enabled the analysis of the influenza VP proteomes, which may contain additional membrane or internalized host cell protein impurities. With this setup, all ten most abundant influenza A virus proteins could be detected in the purified samples of both purification methods. The corresponding data is visualized in Figure 25 and shown in Table 4 [24].

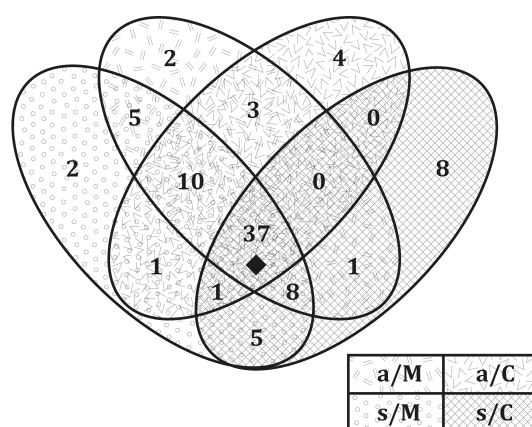


Figure 25 Comparison of identified viral and host cell proteins for the influenza samples purified by magnetic sulfated cellulose particles and centrifugation for analytics

Sample and method abbreviations: a, A/PR_{ADH}; s, A/PR_{SUS}; M, MSCP method; C, centrifugation method for analytics. Identified ten most abundant influenza A virus proteins are marked with a diamond (◆). Figure reproduced in part with permission from [24] (Copyright 2015 American Chemical Society).

Table 4 List of identified influenza A virus proteins after purification with magnetic sulfated cellulose particles and a centrifugation method for analytics

Protein name (abbreviation)	Coverage %				Unique peptides			
	a/M	s/M	a/C	s/C	a/M	s/M	a/C	s/C
Haemagglutinin (HA)	58	47	47	49	58	30	27	28
Matrix protein 1 (M1)	77	67	66	72	65	18	17	18
Matrix protein 2 (M2)	56	49	47	49	8	5	4	5
Neuraminidase (NA)	34	31	30	34	20	11	10	12
Nonstructural protein 1 (NS1)	82	76	68	74	34	19	14	17
Nuclear export protein (NEP)	33	22	22	27	5	3	3	3
Nucleoprotein (NP)	72	74	72	72	82	38	34	37
Polymerase acidic protein (PA)	51	49	46	54.9	40	29	27	35
Polymerase basic protein 1 (PB1)	30	36	30	41.6	24	22	18	26
Polymerase basic protein 2 (PB2)	48	47	39	53	42	33	21	37

Sample and method abbreviations: a, A/PR_{ADH}; s, A/PR_{SUS}; M, MSCP method; C, centrifugation method for analytics. The coverage percentage is the amino acids number of identified peptides divided by the total amino acids number of the protein. Table reproduced in part with permission from [24] (Copyright 2015 American Chemical Society).

Investigation of influenza virus particle aggregation and purification with magnetic sulfated cellulose particles

The obtained viral proteomes also contained low abundant proteins like influenza A matrix protein 2 (M2) and the non-structural protein 1 (NS1) when compared to previous literature [42,133]. Moreover, host cell proteins were detected in all purified A/PR samples. This was also previously shown in literature and seems to be due to host cell proteins incorporated into the VP [133]. Overall, in the purified samples 56 to 69 host cell proteins were identified including cytoplasmic and membrane-bound proteins shown in detail in Table 5. Nevertheless, these host cell proteins are not necessarily incorporated into the VP structure and can be also co-purified with the VP [24].

Table 5 Host cell proteins identified in purified influenza A virus particle samples

Protein name	Occurrence
40S ribosomal protein S11	a/M, a/C
40S ribosomal protein S17	a/M, s/M, a/C
40S ribosomal protein S18	a/M, s/M, a/C
40S ribosomal protein S3	a/M, s/M, a/C, s/C
60S ribosomal protein L12	a/M, s/M, a/C
60S ribosomal protein L13a	a/M, s/C
60S ribosomal protein L15	a/M, s/M
60S ribosomal protein L4	a/M, s/M, a/C, s/C
Actin, cytoplasmic 1	a/M, s/M, a/C, s/C
a-centractin	a/C
Annexin A2	a/M, s/M, a/C, s/C
Annexin A4	a/M, s/M, a/C, s/C
Annexin A13	a/M, s/M, a/C, s/C
Cadherin-1	s/C
Calcyphosin	a/C
Calnexin	a/M, s/M, s/C
Catenin beta-1	a/M, s/M, a/C, s/C
Cathepsin D	a/C
Cathepsin L1	a/C
Caveolin-1	a/M, s/M, s/C
CD44 antigen (fragment)	s/C

Chapter 4: Results and Discussion

Protein name	Occurrence
Cell division control protein 42 homolog	a/M, s/M, a/C, s/C
Claudin-3	s/M, s/C
Clusterin	a/M, s/M, a/C, s/C
Desmin	a/M, s/M, a/C
Dihydrolipoyl dehydrogenase, mitochondrial	a/M, s/M
DLA class I histocompatibility antigen, A9/A9 α chain	a/M, s/M, a/C, s/C
DLA class II histocompatibility antigen, DR-1 β chain	s/M, s/C
DnaJ homolog subfamily B member 11	a/M, s/M, s/C
Dolichyl-diphosphooligosaccharide-protein glycosyl-transferase 48 kDa subunit	a/M, s/M, s/C
Dystrophin	a/M
Endoplasmic reticulum chaperone protein	a/M, s/M, s/C
Ferritin heavy chain	s/C
Ferritin light chain	s/C
Galectin-3	a/M, s/M, a/C, s/C
Glyceraldehyde-3-phosphate dehydrogenase	a/M, s/M, a/C, s/C
GTP-binding nuclear protein Ran	a/M, s/M, a/C, s/C
Guanine nucleotide-binding protein G(i) subunit α -2	a/M, s/M, a/C, s/C
Guanine nucleotide-binding protein G(I)/G(S)/G(T) subunit β -1	a/M, s/M, a/C, s/C
Guanine nucleotide-binding protein G(s) subunit α	a/M, s/M, a/C, s/C
Guanine nucleotide-binding protein subunit α -11(F)	s/C
Heat shock 70 kDa protein 1	a/M, s/M, a/C, s/C
Heat shock 70 kDa protein 4	a/M, s/M, a/C
Heat shock protein β -1	a/M, s/M

Investigation of influenza virus particle aggregation and purification with magnetic sulfated cellulose particles

Protein name	Occurrence
Hypoxanthine-guanine phosphoribosyltransferase	s/M, a/C
Intercellular adhesion molecule 1(fragment)	a/M, s/M
Interferon-induced GTP-binding protein Mx1	a/M, s/M, a/C
Keratin, type I cytoskeletal 10	a/M, s/M, a/C, s/C
Keratin, type I cytoskeletal 9	a/M
Keratin, type II cytoskeletal 1	a/M, s/M, a/C, s/C
Keratin, type II cytoskeletal 2	a/M, s/M, a/C
Myosin-9	a/M, s/M, a/C, s/C
Na-cytochrome b5 reductase 3	s/M
Nucleoside diphosphate kinase A	a/M, s/M, s/C
Nucleoside diphosphate kinase B	a/M, s/M, a/C, s/C
Phosphatidylethanolamine-binding protein 1	a/M, s/M, a/C, s/C
Podocalyxin	a/M, s/M, a/C, s/C
Protein transport protein Sec61 subunit α isoform 1	s/M, s/C
Pyruvate kinase PKLR	a/M, s/M, a/C, s/C
Rab GDP dissociation inhibitor α	a/M, s/M, a/C
Rab GDP dissociation inhibitor β	a/M, s/M, a/C, s/C
Ras-rel. C3 botulinum toxin substrate 1	a/M, s/M, s/C
Ras-rel. protein Rab-10	s/M, s/C
Ras-rel. protein Rab-1A	a/M, s/M, a/C, s/C
Ras-rel. protein Rab-5C	a/M, s/M, a/C, s/C
Ras-rel. protein Rab-7A	a/M, s/M, a/C, s/C
Ras-rel. protein Rab-11A	a/M, s/M, a/C, s/C
Ras-rel. protein Rab-8A	s/M, a/C, s/C
Ribosomal protein L18	a/M, s/M, a/C, s/C
Sarcoplasmic/endoplasmic reticulum calcium ATPase 2	a/M, s/M

Chapter 4: Results and Discussion

Protein name	Occurrence
Serine/threonine-protein phosphatase PP1- β catalytic subunit	a/M, s/M, a/C, s/C
Serum albumin	a/M, s/M, a/C
Sodium/myo-inositol cotransporter	s/M, s/C
Sodium/potassium-transporting ATPase subunit α -1	a/M, s/M, a/C, s/C
Sodium/potassium-transporting ATPase subunit β -1	a/M, s/M, s/C
Spliceosome RNA helicase	a/C
Sulfotransferase 1A1	a/M, a/C
Superoxide dismutase [Cu-Zn]	a/M, s/M, a/C, s/C
Syntaxin-binding protein 2	a/C
Testin	a/M, a/C
Transforming protein RhoA	a/M, s/M, a/C, s/C
Translocon-associated protein subunit α	s/M
Triosephosphate isomerase	a/M, s/M, a/C, s/C
Tyrosine-protein kinase Yes	a/M, s/M, a/C, s/C
Ubiquitin-60S ribosomal protein L40	a/M, s/M, a/C, s/C
Vasodilator-stimulated phosphoprotein	a/M, s/M, a/C, s/C
Vesicular integral-membrane protein VIP36	s/C

Sample and method abbreviations: a, A/PR_{ADH}; s, A/PR_{SUS}; M, MSCP method; C, centrifugation method for analytics. Table reproduced in part with permission from [24] (Copyright 2015 American Chemical Society).

In summary, all ten most abundant influenza A/PR proteins were found in all purification runs with 37 host cell proteins for both methods and VP samples visualized in Figure 25 [24]. Some host cell proteins were only found in one host cell line, e.g., testin was only identified with the MDCK_{ADH} cell line and claudin-3 was only identified with the MDCK_{SUS2} cell line. In general, the identified host cell proteins were similar for both host cell lines and methods with 75 host cell protein hits for the MSCP method and 78 host cell protein hits for the centrifugation method for analytics. For the MSCP method 60 host cell proteins were identified for both host cell lines with six hits only identified for A/PR_{ADH} and nine hits only for A/PR_{SUS}. Moreover, the centrifugation method for analytics identified 38 host cell proteins for both host cell lines with 18 hits only identified for

Investigation of influenza virus particle aggregation and purification with magnetic sulfated cellulose particles

A/PR_{ADH} and 22 hits only for A/PR_{SUS}. This demonstrates a similar purification performance of both methods in terms of host cell protein occurrence in the purified samples [24].

A major advantage of the MSCP method was the fast processing time, which only needed 20% of the centrifugation method for analytics processing time. This can be attributed to the long centrifugation times involved and the limited sample number that can be processed simultaneously with the centrifuge rotor [24]. Furthermore, the found contaminating host cell protein number in the samples could be reduced by additional washing steps for both methods with the drawback of increased processing time. The processing time will increase a few minutes for every additional washing step for the MSCP method. Contrary, for the centrifugation method, every additionally washing step will increase the processing time by approximately 90 min [24].

4.2.3 Immunization studies in mice using magnetic sulfated cellulose particles

The obtained data was first published in Vaccine [119] and parts of the original publication are used hereafter (also see section 8.5).

4.2.3.1 Establishment of the antigen dose needed to induce antiviral immunity in mice

In a first step, the HA antigen dose resulting in an effective antiviral immunity was estimated from using soluble HA antigen with adjuvants. From this dose finding experiment, the antigen amount for the subsequent aMSCP immunization experiment was derived. For this 1.0, 7.5, and 15.0 µg HA antigen were tested with Poly I:C and CpG in mice. The immunization scheme consisted of a first injection (d1) followed by a second injection after two weeks (d14) and a third injection after four weeks (d28). Mice were bled retrobulbar to obtain sera for the anti-A/PR antibody ELISA one day before the first injection (d0), the second (d13), the third (d27), and six weeks after the first injection (d42). First anti-A/PR antibody responses were already observable at day 13 (d13) derived from a single immunization. The highest anti-A/PR antibody response was present with 7.5 µg and 15.0 µg HA antigen. After 42 days (d42) and the three antigen injections, the resulting anti-A/PR antibody responses showed similar levels, demonstrating that all three HA antigen doses were able to induce a strong immune response [119]. The anti-A/PR antibody responses are shown in detail in Figure 26.

The mice immunized with 1.0 µg HA antigen were infected intranasally with a lethal dose of active A/PR after the immunization (d42) to evaluate if the lowest antigen dose offers protection. After infection, the mice body weights were measured for 6 days p.i.. After that, the NP gene copies in the mice lungs were measured to indicate the viral load. In these subsequent experiments the groups were compared to the negative control group, which was mock-immunized with PBS. The group immunized with 1.0 µg HA antigen showed no relative body weight loss with $98.65 \pm 1.06\%$ shown in Figure 27 and no signs of disease. In contrast, the negative control group immunized with PBS showed signs of a influenza infection-associated disease after the challenge paired with a significant relative body weight loss with $88.0 \pm 3.07\%$ after 4 days p.i. [119].

Chapter 4: Results and Discussion

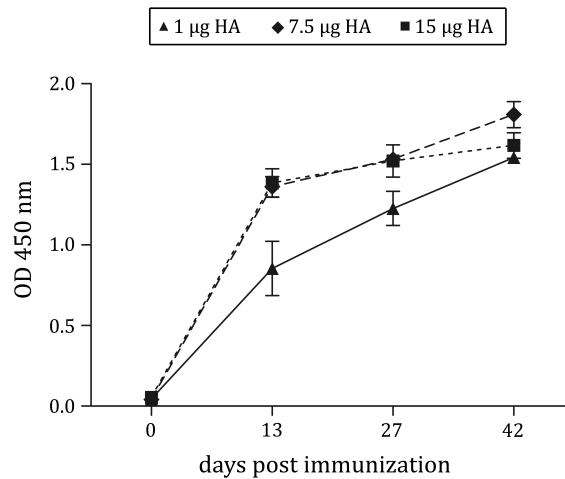


Figure 26 Anti-A/PR antibody responses measured by ELISA after immunization for the establishment of the antigen dose in mice

Anti-A/PR antibody responses of 1:1 000 diluted mice sera before and after immunization with 1.0, 7.5 and 15.0 µg hemagglutinin (HA) antigen measured by ELISA (n = 3 mice per group, data shown as mean ± standard error of the mean). Figure adapted with permission from [119].

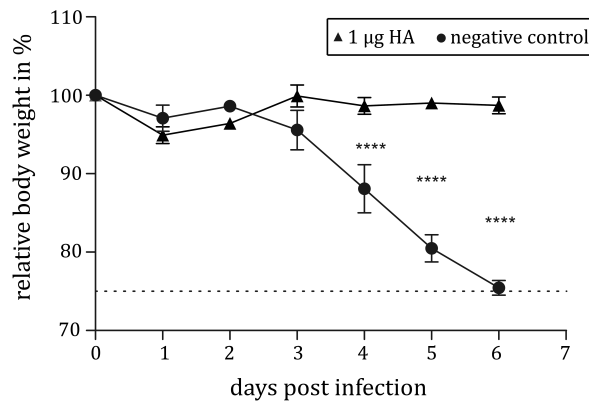


Figure 27 Relative body weight of mice after infection with a lethal dose of active A/PR for the establishment of the antigen dose

Mice groups immunized three times with 1.0 µg hemagglutinin antigen or phosphate buffer saline as a negative control were infected with a lethal dose of active influenza A/PR virus 42 days post the first immunization. The relative body weight loss was monitored until day 6 post infection (n= 3-4 mice per group, values are shown as mean ± standard error of the mean; **** indicates significant differences to the negative control, p < 0.0001). Figure adapted with permission from [119].

Investigation of influenza virus particle aggregation and purification with magnetic sulfated cellulose particles

Additionally, a high viral replication was found in the lung tissues of the mock-immunized mice, which is in agreement with the body weight loss. There, a 392-fold NP gene copy increase was observed for the negative control group with 142067 ± 93981 NP gene copies 25 ng^{-1} cDNA when compared to 363 ± 101 NP gene copies 25 ng^{-1} cDNA of the $1.0 \mu\text{g}$ HA antigen immunized group shown in Figure 28 [119].

In summary, the obtained results for an antigen dose of $1.0 \mu\text{g}$ HA showed full protection against a lethal A/PR virus infection. Therefore, the same amount was used subsequently for the aMSCP immunization experiment.

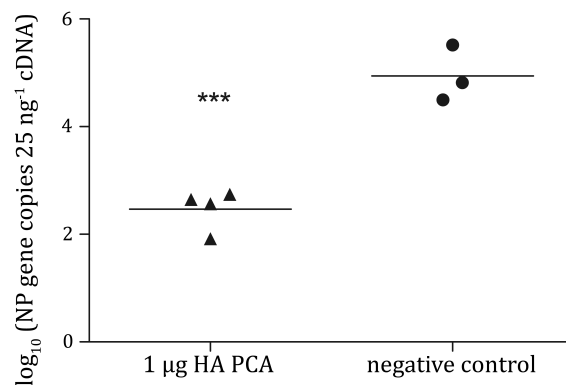


Figure 28 Nucleoprotein gene copies in the lung tissues of mice after infection with a lethal dose of active A/PR for the establishment of the antigen dose

6 days post infection the nucleoprotein gene copy number was measured by quantitative real-time PCR to estimate the viral load in the lung tissues of the challenged mice (horizontal line indicates the mean; *** indicates significant difference, $p = 0.0007$). Figure adapted with permission from [119].

4.2.3.2 Immunogenicity of antigen-loaded magnetic sulfated cellulose particles

The aMSCP immunization experiment was carried out with a antigen dose of $1.0 \mu\text{g}$ HA, which was inducing a potent immune response in the previous experiment (see section 4.2.3.1). Therefore, aMSCP loaded with $1.0 \mu\text{g}$ HA antigen were injected into mice on day 1 (d1) and after two weeks (d14) without a third immunization. It was refrained from the third immunization because of the high anti-A/PR antibody responses after two injections with $1.0 \mu\text{g}$ HA antigen in the previous experiment shown in Figure 26. Mice were bled retrobulbar to obtain sera for the anti-A/PR antibody ELISA one day before the first injection (d0), the second (d13), and one day before four weeks after the first injection (d27). For the immunizations two aMSCP batches were produced: First batch with an average of $2.1 \mu\text{g}$ HA antigen per injection (Injection 1 A $2.06 \mu\text{g}$ HA $200 \mu\text{L}^{-1}$, Injection 1 B $2.07 \mu\text{g}$ HA $200 \mu\text{L}^{-1}$) and a second batch with an average of $1.2 \mu\text{g}$ HA per injection (Injection 2 A $1.19 \mu\text{g}$ HA $200 \mu\text{L}^{-1}$, Injection 2 B $1.24 \mu\text{g}$ HA $200 \mu\text{L}^{-1}$). Antigen loss during aMSCP loading was tested beforehand by HA activity of the washing and formulation supernatants and was negligible with about 11% total HAU shown in detail in Table 6 [119].

Table 6 Hemagglutination activity losses during antigen-loaded magnetic sulfated cellulose particles loading and washing

Sample	Total HAU	HAU %
diafiltered A/PR _{SUS} sample	25,464	100%
supernatant after loading	3,640	14%
Wash 1	1,436	6%
Wash 2	420	2%
Wash 3	234	1%
Wash 4	162	1%
Wash 5	123	0%
aMSCP suspension in formulation buffer	497	2%

Immunizations resulted in high anti-A/PR antibody responses with aMSCP (G1) and the antigen-containing controls, i.e., 1.0 µg HA antigen positive control (G2) and the antigen-particle interaction control (1.0 µg HA antigen and empty MSCP injected at two different sites of the abdomen, G3) shown in Figure 29. As expected, no antibody response was observable with the mock-immunized control group (G4). The similar antibody responses from the aMSCP (G1) and the free antigen (G2 and G3) could be explained by a desorption of the aMSCP-bound antigen after injection into the mice [119].

Investigation of influenza virus particle aggregation and purification with magnetic sulfated cellulose particles

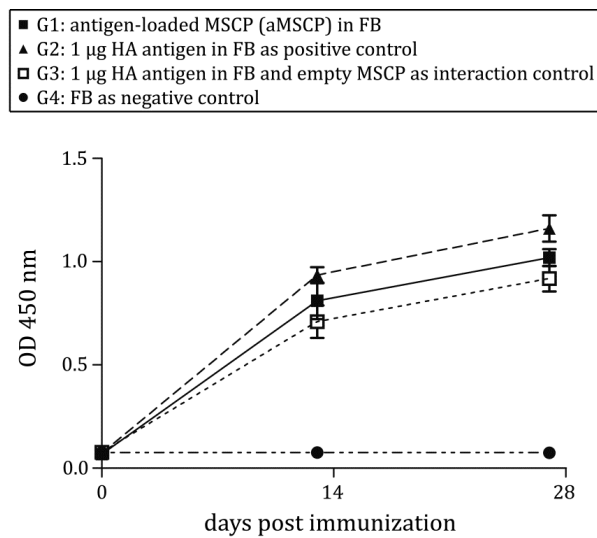


Figure 29 Anti-A/PR antibody responses measured by ELISA after immunization of mice with antigen-loaded magnetic sulfated cellulose particles and controls

Anti-A/PR antibody levels of antigen-loaded magnetic sulfated cellulose particles (aMSCP) group G1, positive control G2, and antigen-particle interaction control G3. 1:1 000 diluted mice sera were analyzed by ELISA (n = 5 mice per group, data shown as mean ± standard error of the mean). Figure adapted with permission from [119].

4.2.3.3 Infection of mice with a lethal influenza virus dose

To evaluate the protection of the MSCP-purified and formulated vaccine, all four groups (G1-4) were challenged by intranasal infection with a lethal dose of active A/PR after immunization (d28). After this challenge the health status including the body weight was monitored until 6 days p.i. [119].

Already at day 3 p.i. the mock-immunized group G4 showed a significant relative body weight loss with $93.5 \pm 0.9\%$ ($p < 0.001$). The relative body weight of the mock-immunized control G4 decreased to $76.8 \pm 1.9\%$ at day 6 p.i. and the mice showed signs of lethargy, anorexia, and ruffed fur confirming a severe influenza infection-associated disease. In comparison, the relative body weight of the aMSCP group G1 with $101.7 \pm 1.2\%$, the positive control G2 with $103.3 \pm 1.2\%$, and the antigen-particle interaction control G3 with $103.0 \pm 2.5\%$ remained stable over the 6 days p.i. without any signs of disease. This indicated an effective protection in all antigen-containing groups. All relative body weight courses are shown in detail in Figure 30 [119].

At day 6 p.i. all mice were sacrificed to determine the viral load of the lung tissue by quantitative real-time PCR of the viral NP gene. The obtained NP gene copies are in agreement with the observed relative body weight changes after the challenge. There, the aMSCP-immunized group G1 showed with $0.9 \times 10^4 \pm 0.2 \times 10^4$ NP gene copies a 408-fold lower NP gene copy number compared to the mock-immunized group G4 with $3.8 \times 10^6 \pm 1.2 \times 10^6$ NP gene copies. Furthermore, the

Chapter 4: Results and Discussion

positive control G2 showed a 138-fold decrease with $2.7 \times 10^4 \pm 1.1 \times 10^4$ NP gene copies and the antigen-particle interaction control G3 a 316-fold decrease with $1.2 \times 10^4 \pm 0.5 \times 10^4$ NP gene copies, when compared to the negative control G4. The NP gene copies are visualized in Figure 31 [119].

In summary, the immunization with aMSCP exhibited full protection in mice against a lethal influenza A/PR infection. Additionally, the immune response was similar to the positive control G2 and antigen-particle interaction control G3 [119].

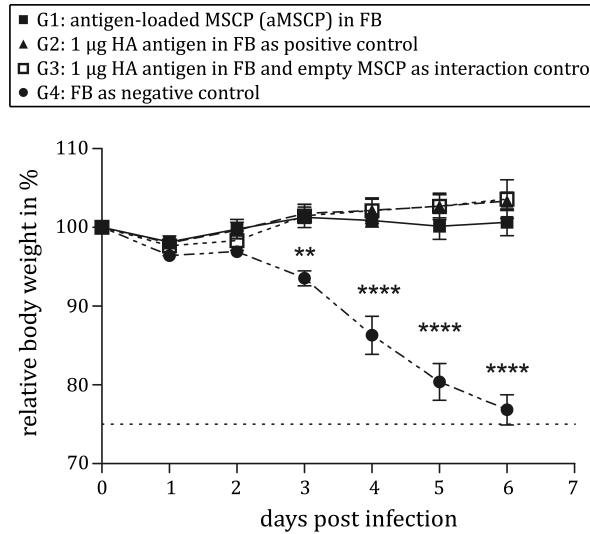


Figure 30 Relative body weight after infection with a lethal A/PR virus dose after immunization with antigen-loaded magnetic sulfated cellulose particles and controls

Relative body weights over time after challenge with a lethal A/PR virus dose 28 days post the first immunization (n = 4-5 mice per group, data shown as mean \pm standard error of the mean; shown significant differences compared to the negative control: **, p < 0.001, ****, p < 0.0001). Figure adapted with permission from [119].

Investigation of influenza virus particle aggregation and purification with magnetic sulfated cellulose particles

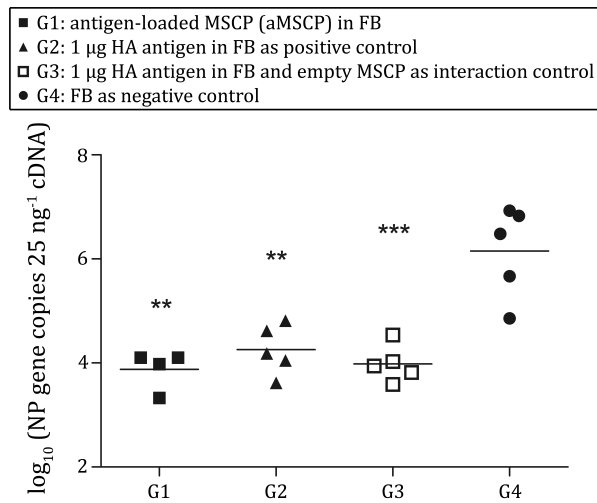


Figure 31 Nucleoprotein gene copies in the lung tissues of mice after infection with a lethal A/PR virus dose after immunization with antigen-loaded magnetic sulfated cellulose particles and controls

Quantitative real-time PCR of the nucleoprotein gene to estimate the viral load in the lung tissues after 6 days post infection (n = 4-5 mice per group, horizontal line indicates the mean; shown significant differences compared to the negative control group: **, p ≤ 0.002; ***, p ≤ 0.0009). Figure adapted with permission from [119].

5 CONCLUSIONS

5.1 Investigation of influenza A virus particle aggregation

The effect of specific HS ions on the PSD of influenza A/PR produced in a suspension (A/PR_{SUS}) and an adherent MDCK cell line (A/PR_{ADH}) was successfully evaluated with an optimized DCS disc centrifugation method.

The VP produced in both cell lines showed aggregation in low salt and Ca²⁺-containing buffers. However, the VP were stable in buffers with a concentration of 60 and 540 mM for all screened HS ions. Furthermore, A/PR_{SUS} was shown to be stable in 60, 180, 540, 1020, and 1500 mM NaCl. Interestingly, A/PR_{ADH} showed aggregation in 20 mM NaCl in contrast to A/PR_{SUS}, which was stable in the same buffer. Additionally, A/PR_{ADH} showed aggregation with larger aggregates in Ca²⁺-containing buffers at all screened concentrations compared to A/PR_{SUS}. If the higher aggregation propensity of A/PR_{ADH} can be linked to the MDCK production cell line or the cultivation media needs to be further evaluated in detail.

Moreover, the high resolution DCS method allowed observing trends in the monomeric AHD of the VP partly reflecting an HS trend.

In summary, buffer and cell line changes can impact VP aggregation and should be assessed in detail for effects on DSP and vaccine formulation in research and development to avoid problems.

5.2 Investigation of influenza A virus purification and vaccine formulation using magnetic sulfated cellulose particles

First, the developed MSCP purification was compared to an established centrifugation method regarding the analytics of influenza VP. Both methods performed similarly for the purification of A/PR_{ADH} and A/PR_{SUS} in terms of the number and identity of protein impurities. However, the MSCP method allowed a faster purification in less than 20% of the time needed for the centrifugation method.

The easy handling and scalability of the MSCP in combination with the potential wide range of VP,

Investigation of influenza virus particle aggregation and purification with magnetic sulfated cellulose particles

bacteria, and parasites binding to the used sulfated cellulose pseudo affinity ligand makes the MSCP an interesting tool for analytical sample preparation.

Second, the proof of concept of a combined MSCP purification and formulation process for an influenza A/PR whole virus vaccine was successfully demonstrated. The mice immunized with the aMSCP showed strong anti-A/PR antibody responses that conferred full protection against a lethal A/PR virus challenge.

The immunization experiment involved a conventional DSP employing clarification, inactivation, concentration, and diafiltration of the harvested A/PR broth. After that standard process, the additional VP purification by chromatography in bind and elute mode (carried out with an SCMA) was replaced by binding the VP to the MSCP. Furthermore, an optimized USP can enable a simplified DSP with MSCP to reduce the number of needed unit operations. This could enable the purification and formulation of new vaccine candidates for veterinary applications as well as viral vectors for gene therapy in research and development. Moreover, MSCP can be used in high-throughput screenings with existing high-throughput magnetic particle handling systems. These advantages could help accelerate the research and development of virus-based products.

The injected MSCP, consisting of cellulose with integrated Fe₃O₄ particles, were not degraded in the course of the immunization and challenge experiments. Additionally, no adverse effects were observed in mice immunized with aMSCP. This can be linked to the biocompatibility and nontoxicity of cellulose and Fe₃O₄ particles in biological systems [35,37–40]. However, potential beneficial or adverse effects of the MSCP in veterinary applications have to be evaluated in future studies.

In summary, the purified and formulated MSCP vaccine induced protective immunity against a lethal A/PR virus challenge.

6 OUTLOOK

6.1 Investigation of virus particle aggregation

The outlined DCS disc centrifugation measurement setup for screening different buffer conditions is already used for the optimization of DSP unit operations for influenza VP purification, where buffer changes play an integral part. In addition, the method can be easily adapted to other VP, with restrictions on very small and light VP, which would dramatically increase the measurement time and could lead to instabilities in the outlined measurement system. Nevertheless, this could be potentially addressed with a modified measurement setup.

In principle, measuring the PSD of VP to reveal their aggregation behavior is only the first step to understand the underlying causes. To identify the involved VP features, e.g., the zeta potential, hydrophilicity [134], glycosylation [26], lipid composition [135], and other (maybe still unknown) VP features, additional analytics is needed. Such a comprehensive approach could help to pinpoint the VP features responsible for the observed behavior, i.e., aggregation and size changes, and could show potential starting points for process optimization. In a first step, this could help to improve unit operations and, in a second step, could potentially reveal interesting possibilities for the optimization of vaccine production systems in general.

The observed VP size changes based on different buffer compositions and concentrations needs further investigation. The size changes observed by DCS disc centrifugation could be verified by conventional AUC or other PSD measurement methods, e.g., nanoparticle tracking analysis and tunable resistive pulse sensing. If the presence of VP size changes could be confirmed, new analytical tools would be needed to investigate their effect on VP-based systems.

In summary, the work on the aggregation behavior of influenza A VP provides a stable foundation for future PSD-based VP research. Due to the increased work on VP-based therapeutics, this field will very likely receive greater interest in the future.

6.2 Virus particle purification and vaccine formulation using magnetic sulfated cellulose particles

The MSCP purification method was successfully applied for influenza A VP and is currently tested with other VP, e.g., MVA, yellow fever, and adeno-associated VP. Depending on the results with other VP, the MSCP could be used in a wide range of (high-throughput) applications for VP purification and vaccine formulation.

Furthermore, the outlined MSCP vaccine system can be further optimized in different ways. The cellulose backbone of the MSCP could be potentially degraded by co-injection of a cellulose-digesting enzyme mixture, which was shown previously for dextran microparticles [59]. However, a more elegant approach would be to circumvent the MSCP injection at all by topical application on the skin. One possibility for this could be nonablative fractional laser (NAFL) pretreated skin or intradermal or transdermal applications employing a topical application followed by antigen transfer by microneedles through the skin barrier [136–138].

In summary, the work on the MSCP is an interesting starting point for future investigations in need of (small scale) VP purification. The easy usability and scalability makes the MSCP useful for research and development as well as for veterinary vaccine applications.

7 REFERENCES

- [1] G.K. Hirst, M.W. Pons, Mechanism of influenza recombination: II. Virus aggregation and its effect on plaque formation by so-called noninfective virus, *Virology*. 56 (1973) 620–631. doi:10.1016/0042-6822(73)90063-9.
- [2] C. Wallis, J.L. Melnick, Virus aggregation as the cause of the non-neutralizable persistent fraction, *J. Virol.* 1 (1967) 478–488.
- [3] D.C. Young, D.G. Sharp, Poliovirus aggregates and their survival in water., *Appl. Environ. Microbiol.* 33 (1977) 168–177.
- [4] M.J. Mattle, B. Crouzy, M. Brennecke, K. R. Wigginton, P. Perona, T. Kohn, Impact of Virus Aggregation on Inactivation by Peracetic Acid and Implications for Other Disinfectants, *Environ. Sci. Technol.* 45 (2011) 7710–7717. doi:10.1021/es201633s.
- [5] J.O. Konz, A.L. Lee, J.A. Lewis, S.L. Sagar, Development of a Purification Process for Adenovirus: Controlling Virus Aggregation to Improve the Clearance of Host Cell DNA, *Biotechnol. Prog.* 21 (2008) 466–472. doi:10.1021/bp049644r.
- [6] W. Kunz, P. Lo Nostro, B.W. Ninham, The present state of affairs with Hofmeister effects, *Curr. Opin. Colloid Interface Sci.* 9 (2004) 1–18. doi:10.1016/j.cocis.2004.05.004.
- [7] W. Kunz, Specific ion effects in colloidal and biological systems, *Curr. Opin. Colloid Interface Sci.* 15 (2010) 34–39. doi:10.1016/j.cocis.2009.11.008.
- [8] Y. Zhang, P.S. Cremer, Interactions between macromolecules and ions: the Hofmeister series, *Curr. Opin. Chem. Biol.* 10 (2006) 658–663. doi:10.1016/j.cbpa.2006.09.020.
- [9] T. Oncsik, G. Trefalt, M. Borkovec, I. Szilagyi, Specific Ion Effects on Particle Aggregation Induced by Monovalent Salts within the Hofmeister Series, *Langmuir*. (2015). doi:10.1021/acs.langmuir.5b00225.

Investigation of influenza virus particle aggregation and purification with magnetic sulfated cellulose particles

- [10] T. Oncsik, G. Trefalt, Z. Csendes, I. Szilagyi, M. Borkovec, Aggregation of Negatively Charged Colloidal Particles in the Presence of Multivalent Cations, *Langmuir*. 30 (2014) 733–741. doi:10.1021/la4046644.
- [11] T. López-León, M.J. Santander-Ortega, J.L. Ortega-Vinuesa, D. Bastos-González, Hofmeister Effects in Colloidal Systems: Influence of the Surface Nature, *J. Phys. Chem. C*. 112 (2008) 16060–16069. doi:10.1021/jp803796a.
- [12] T. López-León, A.B. Jódar-Reyes, J.L. Ortega-Vinuesa, D. Bastos-González, Hofmeister effects on the colloidal stability of an IgG-coated polystyrene latex, *J. Colloid Interface Sci*. 284 (2005) 139–148. doi:10.1016/j.jcis.2004.10.021.
- [13] M. Pavlovic, R. Huber, M. Adok-Sipiczki, C. Nardin, I. Szilagyi, Ion specific effects on the stability of layered double hydroxide colloids, *Soft Matter*. 12 (2016) 4024–4033. doi:10.1039/C5SM03023D.
- [14] T. Oncsik, A. Desert, G. Trefalt, M. Borkovec, I. Szilagyi, Charging and aggregation of latex particles in aqueous solutions of ionic liquids: towards an extended Hofmeister series, *Phys. Chem. Chem. Phys*. 18 (2016) 7511–7520. doi:10.1039/C5CP07238G.
- [15] R. Tian, G. Yang, H. Li, X. Gao, X. Liu, H. Zhu, Y. Tang, Activation energies of colloidal particle aggregation: towards a quantitative characterization of specific ion effects, *Phys. Chem. Chem. Phys*. 16 (2014) 8828–8836. doi:10.1039/C3CP54813A.
- [16] M.W. Wolff, U. Reichl, Downstream Processing: From Egg to Cell Culture-Derived Influenza Virus Particles, *Chem. Eng. Technol*. 31 (2008) 846–857. doi:10.1002/ceat.200800118.
- [17] M.W. Wolf, U. Reichl, Downstream processing of cell culture-derived virus particles, *Expert Rev. Vaccines*. 10 (2011) 1451–1475. doi:10.1586/erv.11.111.
- [18] GE Healthcare Bio-Sciences AB, Application Note - Capto DeVirS, (2009). https://www.gelifesciences.com/gehcls_images/GELS/Related%20Content/Files/1314716762536/litdoc28961649AA_20110830172123.pdf.
- [19] L. Opitz, J. Hohlweg, U. Reichl, M.W. Wolff, Purification of cell culture-derived influenza virus A/Puerto Rico/8/34 by membrane-based immobilized metal affinity chromatography, *J. Virol. Methods*. 161 (2009) 312–316. doi:10.1016/j.jviromet.2009.06.025.
- [20] M.W. Wolff, C. Siewert, S. Lehmann, S.P. Hansen, R. Djurup, R. Faber, U. Reichl, Capturing of cell culture-derived modified Vaccinia Ankara virus by ion exchange and pseudo-affinity membrane adsorbers, *Biotechnol. Bioeng*. 105 (2010) 761–769. doi:10.1002/bit.22595.
- [21] M.W. Wolff, C. Siewert, S.P. Hansen, R. Faber, U. Reichl, Purification of cell culture-derived modified vaccinia ankara virus by pseudo-affinity membrane adsorbers and hydrophobic interaction chromatography, *Biotechnol. Bioeng*. 107 (2010) 312–320. doi:10.1002/bit.22797.

Chapter 7: References

- [22] P.F. O'neil, E.S. Balkovic, Virus harvesting and affinity-based liquid chromatography, *Bio/Technology*. 11 (1993) 173–178.
- [23] A.H. Bartlett, P.W. Park, Heparan Sulfate Proteoglycans in Infection, in: M.S.G. Pavão (Ed.), *Glycans Dis. Ther.*, Springer Berlin Heidelberg, 2011: pp. 31–62. http://link.springer.com/chapter/10.1007/978-3-642-16833-8_2 (accessed January 26, 2015).
- [24] A. Serve, M.M. Pieler, D. Benndorf, E. Rapp, M.W. Wolff, U. Reichl, Comparison of influenza virus particle purification using novel magnetic sulfated cellulose particles with an established centrifugation method for analytics, *Anal. Chem.* (2015). doi:10.1021/acs.analchem.5b02681.
- [25] J.V. Roedig, E. Rapp, Y. Genzel, U. Reichl, Impact of different influenza cultivation conditions on HA N-Glycosylation, *BMC Proc.* 5 (2011) P113. doi:10.1186/1753-6561-5-S8-P113.
- [26] R. Hennig, E. Rapp, R. Kottler, S. Cajic, M. Borowiak, U. Reichl, N-Glycosylation Fingerprinting of Viral Glycoproteins by xCGE-LIF, in: B. Lepenies (Ed.), *Carbohydr.-Based Vaccines*, Springer New York, New York, NY, 2015: pp. 123–143. http://link.springer.com/10.1007/978-1-4939-2874-3_8 (accessed February 11, 2016).
- [27] J. Schwarzer, E. Rapp, U. Reichl, N-glycan analysis by CGE-LIF: Profiling influenza A virus hemagglutinin N-glycosylation during vaccine production, *ELECTROPHORESIS*. 29 (2008) 4203–4214. doi:10.1002/elps.200800042.
- [28] U.A. Peuker, O. Thomas, T.J. Hobley, M. Franzreb, S. Berensmeier, M. Schäfer, B. Hickstein, M.C. Flickinger, *Bioseparation, Magnetic Particle Adsorbents*, in: *Encycl. Ind. Biotechnol.*, John Wiley & Sons, Inc., 2009. <http://onlinelibrary.wiley.com/doi/10.1002/9780470054581.eib642/abstract> (accessed June 29, 2016).
- [29] I. Safarik, M. Safarikova, Magnetic techniques for the isolation and purification of proteins and peptides, *Biomagn. Res. Technol.* 2 (2004) 7. doi:10.1186/1477-044X-2-7.
- [30] S. Berensmeier, Magnetic particles for the separation and purification of nucleic acids, *Appl. Microbiol. Biotechnol.* 73 (2006) 495–504. doi:10.1007/s00253-006-0675-0.
- [31] A. Sakudo, K. Baba, M. Tsukamoto, A. Sugimoto, T. Okada, T. Kobayashi, N. Kawashita, T. Takagi, K. Ikuta, Anionic polymer, poly(methyl vinyl ether–maleic anhydride)-coated beads-based capture of human influenza A and B virus, *Bioorg. Med. Chem.* 17 (2009) 752–757. doi:10.1016/j.bmc.2008.11.046.
- [32] A. Sakudo, K. Baba, M. Tsukamoto, K. Ikuta, Use of anionic polymer, poly(methyl vinyl ether-maleic anhydride)-coated beads for capture of respiratory syncytial virus, *Bioorg. Med. Chem. Lett.* 19 (2009) 4488–4491. doi:10.1016/j.bmcl.2009.05.127.
- [33] I. Šafařík, M. Šafaříková, Use of magnetic techniques for the isolation of cells, *J. Chromatogr. B. Biomed. Sci. App.* 722 (1999) 33–53. doi:10.1016/S0378-4347(98)00338-7.
- [34] L. Zhao, A. Seth, N. Wibowo, C.-X. Zhao, N. Mitter, C. Yu, A.P.J. Middelberg, Nanoparticle vaccines, *Vaccine*. 32 (2014) 327–337. doi:10.1016/j.vaccine.2013.11.069.

Investigation of influenza virus particle aggregation and purification with magnetic sulfated cellulose particles

- [35] S.D. Xiang, C. Selomulya, J. Ho, V. Apostolopoulos, M. Plebanski, Delivery of DNA vaccines: an overview on the use of biodegradable polymeric and magnetic nanoparticles, *Wiley Interdiscip. Rev. Nanomed. Nanobiotechnol.* 2 (2010) 205–218. doi:10.1002/wnan.88.
- [36] C. Ladd Effio, L. Wenger, O. Ötes, S.A. Oelmeier, R. Kneusel, J. Hubbuch, Downstream processing of virus-like particles: Single-stage and multi-stage aqueous two-phase extraction, *J. Chromatogr. A.* 1383 (2015) 35–46. doi:10.1016/j.chroma.2015.01.007.
- [37] T. Miyamoto, S. Takahashi, H. Ito, H. Inagaki, Y. Noishiki, Tissue biocompatibility of cellulose and its derivatives, *J. Biomed. Mater. Res.* 23 (1989) 125–133. doi:10.1002/jbm.820230110.
- [38] G. Helenius, H. Bäckdahl, A. Bodin, U. Nannmark, P. Gatenholm, B. Risberg, In vivo biocompatibility of bacterial cellulose, *J. Biomed. Mater. Res. A.* 76A (2006) 431–438. doi:10.1002/jbm.a.30570.
- [39] J.C. Fricain, P.L. Granja, M.A. Barbosa, B. de Jéso, N. Barthe, C. Baquey, Cellulose phosphates as biomaterials. In vivo biocompatibility studies, *Biomaterials.* 23 (2002) 971–980. doi:10.1016/S0142-9612(01)00152-1.
- [40] L. Zhang, T.J. Menkhous, H. Fong, Fabrication and bioseparation studies of adsorptive membranes/felts made from electrospun cellulose acetate nanofibers, *J. Membr. Sci.* 319 (2008) 176–184. doi:10.1016/j.memsci.2008.03.030.
- [41] Development of High Capacity Magnetic Beads for Antibody and Protein Purification Poster, PS209 - Development of High Capacity Magnetic Beads for Antibody and Protein Purification Poster.pdf.
<http://worldwide.promega.com/~media/Files/Resources/Posters/Development%20of%20High%20Capacity%20Magnetic%20Beads%20for%20Antibody%20and%20Protein%20Purification%20Poster.pdf> (accessed April 2, 2014).
- [42] M.L. Shaw, K.L. Stone, C.M. Colangelo, E.E. Gulcicek, P. Palese, Cellular Proteins in Influenza Virus Particles, *PLoS Pathog.* 4 (2008) e1000085. doi:10.1371/journal.ppat.1000085.
- [43] J.Y. Noh, W.J. Kim, Influenza Vaccines: Unmet Needs and Recent Developments, *Infect. Chemother.* 45 (2013) 375–386. doi:10.3947/ic.2013.45.4.375.
- [44] M.R. Hilleman, Realities and enigmas of human viral influenza: pathogenesis, epidemiology and control, *Vaccine.* 20 (2002) 3068–3087. doi:10.1016/S0264-410X(02)00254-2.
- [45] Fields Virology, 4th Edition, Fourth edition, Lippincott Williams & Wilkins, New York, NY, 2001.
- [46] C. Tidona, G. Darai, *The Springer Index of Viruses*, Springer, 2011.
- [47] J.A. McCullers, T. Saito, A.R. Iverson, Multiple Genotypes of Influenza B Virus Circulated between 1979 and 2003, *J. Virol.* 78 (2004) 12817–12828. doi:10.1128/JVI.78.23.12817-12828.2004.

Chapter 7: References

- [48] T. Francis, A new type of virus from epidemic influenza, *Science*. 92 (1940) 405–408. doi:10.1126/science.92.2392.405.
- [49] M.M.J. Cox, J.R. Hollister, FluBlok, a next generation influenza vaccine manufactured in insect cells, *Biologicals*. 37 (2009) 182–189. doi:10.1016/j.biologicals.2009.02.014.
- [50] B. Buckland, R. Boulanger, M. Fino, I. Srivastava, K. Holtz, N. Khramtsov, C. McPherson, J. Meghrouh, P. Kubera, M.M.J. Cox, Technology transfer and scale-up of the Flublok® recombinant hemagglutinin (HA) influenza vaccine manufacturing process, *Vaccine*. 32 (2014) 5496–5502. doi:10.1016/j.vaccine.2014.07.074.
- [51] J.A. Tree, C. Richardson, A.R. Fooks, J.C. Clegg, D. Looby, Comparison of large-scale mammalian cell culture systems with egg culture for the production of influenza virus A vaccine strains, *Vaccine*. 19 (2001) 3444–3450. doi:10.1016/S0264-410X(01)00053-6.
- [52] A. Doroshenko, S.A. Halperin, Trivalent MDCK cell culture-derived influenza vaccine Optaflu® (Novartis Vaccines), *Expert Rev. Vaccines*. 8 (2009) 679–688. doi:10.1586/erv.09.31.
- [53] O. Kistner, M.K. Howard, M. Spruth, W. Wodal, P. Brühl, M. Gerencer, B.A. Crowe, H. Savidis-Dacho, I. Livey, M. Reiter, I. Mayerhofer, C. Tauer, L. Grillberger, W. Mundt, F.G. Falkner, P.N. Barrett, Cell culture (Vero) derived whole virus (H5N1) vaccine based on wild-type virus strain induces cross-protective immune responses, *Vaccine*. 25 (2007) 6028–6036. doi:10.1016/j.vaccine.2007.05.013.
- [54] A. Shaw, New technologies for new influenza vaccines, *Vaccine*. 30 (2012) 4927–4933. doi:10.1016/j.vaccine.2012.04.095.
- [55] H.F. Maassab, Adaptation and growth characteristics of influenza virus at 25 degrees c, *Nature*. 213 (1967) 612–614.
- [56] E. Milián, A.A. Kamen, Current and Emerging Cell Culture Manufacturing Technologies for Influenza Vaccines, *BioMed Res. Int.* 2015 (2015). doi:10.1155/2015/504831.
- [57] L.E. Gallo-Ramirez, A. Nikolay, Y. Genzel, U. Reichl, Bioreactor concepts for cell culture-based viral vaccine production, *Expert Rev. Vaccines*. 14 (2015) 1181–1195. doi:10.1586/14760584.2015.1067144.
- [58] P. Gagnon, M.C. Flickinger, Chromatographic Purification of Virus Particles, in: *Encycl. Ind. Biotechnol.*, John Wiley & Sons, Inc., 2009. <http://onlinelibrary.wiley.com/doi/10.1002/9780470054581.eib583/abstract> (accessed December 4, 2015).
- [59] M.C. Flickinger, *Downstream Industrial Biotechnology: Recovery and Purification*, John Wiley & Sons, 2013.
- [60] M. Li, Y.X. Qiu, A review on current downstream bio-processing technology of vaccine products, *Vaccine*. 31 (2013) 1264–1267. doi:10.1016/j.vaccine.2012.12.056.

Investigation of influenza virus particle aggregation and purification with magnetic sulfated cellulose particles

- [61] E.P. Wen, R. Ellis, N.S. Pujar, *Vaccine Development and Manufacturing*, John Wiley & Sons, 2014.
- [62] B. Kalbfuss-Zimmermann, U. Reichl, E. P. Wen, R. Ellis, N. S. Pujar, *Viral Vaccines Purification*, in: *Vaccine Dev. Manuf.*, John Wiley & Sons, Inc., 2014: pp. 97–180. <http://onlinelibrary.wiley.com/doi/10.1002/9781118870914.ch5/summary> (accessed February 9, 2015).
- [63] P. Nestola, C. Peixoto, R.R.J.S. Silva, P.M. Alves, J.P.B. Mota, M.J.T. Carrondo, Improved virus purification processes for vaccines and gene therapy, *Biotechnol. Bioeng.* 112 (2015) 843–857. doi:10.1002/bit.25545.
- [64] B. Kalbfuss, Y. Genzel, M. Wolff, A. Zimmermann, R. Morenweiser, U. Reichl, Harvesting and concentration of human influenza A virus produced in serum-free mammalian cell culture for the production of vaccines, *Biotechnol. Bioeng.* 97 (2007) 73–85. doi:10.1002/bit.21139.
- [65] C.B. Reimer, R.S. Baker, T.E. Newlin, M.L. Havens, Influenza Virus Purification with the Zonal Ultracentrifuge, *Science.* 152 (1966) 1379–1381. doi:10.1126/science.152.3727.1379.
- [66] E. Hutchinson, E. Hutchinson, E. Fodor, Purification of influenza virions by haemadsorption and ultracentrifugation, *Protoc. Exch.* (2014). doi:10.1038/protex.2014.027.
- [67] B. Kalbfuss, M. Wolff, R. Morenweiser, U. Reichl, Purification of cell culture-derived human influenza A virus by size-exclusion and anion-exchange chromatography, *Biotechnol. Bioeng.* 96 (2007) 932–944. doi:10.1002/bit.21109.
- [68] T. Kröber, M.W. Wolff, B. Hundt, A. Seidel-Morgenstern, U. Reichl, Continuous purification of influenza virus using simulated moving bed chromatography, *J. Chromatogr. A.* 1307 (2013) 99–110. doi:10.1016/j.chroma.2013.07.081.
- [69] B. Kalbfuss, M. Wolff, L. Geisler, A. Tappe, R. Wickramasinghe, V. Thom, U. Reichl, Direct capture of influenza A virus from cell culture supernatant with Sartobind anion-exchange membrane adsorbers, *J. Membr. Sci.* 299 (2007) 251–260. doi:10.1016/j.memsci.2007.04.048.
- [70] J. Vajda, D. Weber, S. Stefaniak, B. Hundt, T. Rathfelder, E. Müller, Mono- and polyprotic buffer systems in anion exchange chromatography of influenza virus particles, *J. Chromatogr. A.* 1448 (2016) 73–80. doi:10.1016/j.chroma.2016.04.047.
- [71] T. Jarosch, A. Müller, M.W. Wolff, U. Reichl, *Hydrophobic Interaction Chromatography for purification of influenza virus*, 2011.
- [72] L. Opitz, A. Zimmermann, S. Lehmann, Y. Genzel, H. Lübben, U. Reichl, M.W. Wolff, Capture of cell culture-derived influenza virus by lectins: Strain independent, but host cell dependent, *J. Virol. Methods.* 154 (2008) 61–68. doi:10.1016/j.jviromet.2008.09.004.

Chapter 7: References

- [73] L. Opitz, S. Lehmann, U. Reichl, M.W. Wolff, Sulfated membrane adsorbers for economic pseudo-affinity capture of influenza virus particles, *Biotechnol. Bioeng.* 103 (2009) 1144–1154. doi:10.1002/bit.22345.
- [74] P. Marichal-Gallardo, M.M. Pieler, M. Wolff, U. Reichl, Steric exclusion chromatography for purification of cell culture-derived influenza A virus using regenerated cellulose membranes and polyethylene glycol, *J. Chromatogr. A.* (2016) in press. doi: 10.1016/j.chroma.2016.12.076.
- [75] D.P. Nayak, S. Lehmann, U. Reichl, Downstream processing of MDCK cell-derived equine influenza virus, *J. Chromatogr. B.* 823 (2005) 75–81. doi:10.1016/j.jchromb.2005.05.022.
- [76] H.G. Bahnemann, Inactivation of viral antigens for vaccine preparation with particular reference to the application of binary ethylenimine, *Vaccine.* 8 (1990) 299–303. doi:10.1016/0264-410X(90)90083-X.
- [77] O. Kistner, P.N. Barrett, W. Mundt, M. Reiter, S. Schober-Bendixen, F. Dorner, Development of a mammalian cell (Vero) derived candidate influenza virus vaccine, *Vaccine.* 16 (1998) 960–968. doi:10.1016/S0264-410X(97)00301-0.
- [78] C.E.J.J. Van, M. Weggeman, Virus purification methods, WO2005080556 A2, 2005. <http://www.google.de/patents/WO2005080556A2> (accessed November 13, 2015).
- [79] H.R. Cox, J. Van Der Scheer, The purification and concentration of influenza virus by means of alcohol precipitation, *J. Immunol. Baltim. Md* 1950. 56 (1947) 149–166.
- [80] A. Polson, A. Keen, C. Sinclair-Smith, I.G.S. Furminger, Polyethylene glycol purification of influenza virus with respect to aggregation and antigenicity, *Epidemiol. Infect.* 70 (1972) 255–265. doi:10.1017/S0022172400022312.
- [81] W. Cui, A. BEZAWADA, G. Zhu, P. TRAN, L. CHUNG, Methods for producing influenza vaccine compositions, WO2015017673 A1, 2015. <http://www.google.de/patents/WO2015017673A1> (accessed September 13, 2016).
- [82] J. Liu, R. Schwartz, M. Thompson, L.J.C. Maranga, S.S.-T. Hsu, M. Ghosh, A. Subramanian, Method of purifying influenza virus and removing MDCK cell DNA contaminants, US8357376 B2, 2013. <http://www.google.com/patents/US8357376> (accessed September 13, 2016).
- [83] Fluzone® Intradermal Quadrivalent Influenza vaccine. <http://www.fluzone.com/fluzone-intradermal-quadrivalent-vaccine.cfm> (accessed November 24, 2016).
- [84] Y.-F. Maa, M. Ameri, C. Shu, L.G. Payne, D. Chen, Influenza vaccine powder formulation development: spray-freeze-drying and stability evaluation, *J. Pharm. Sci.* 93 (2004) 1912–1923. doi:10.1002/jps.20104.

Investigation of influenza virus particle aggregation and purification with magnetic sulfated cellulose particles

- [85] D.G. Koutsonanos, M. del P. Martin, V.G. Zarnitsyn, S.P. Sullivan, R.W. Compans, M.R. Prausnitz, I. Skountzou, Transdermal Influenza Immunization with Vaccine-Coated Microneedle Arrays, *PLOS ONE*. 4 (2009) e4773. doi:10.1371/journal.pone.0004773.
- [86] Q. Zhu, V.G. Zarnitsyn, L. Ye, Z. Wen, Y. Gao, L. Pan, I. Skountzou, H.S. Gill, M.R. Prausnitz, C. Yang, R.W. Compans, Immunization by vaccine-coated microneedle arrays protects against lethal influenza virus challenge, *Proc. Natl. Acad. Sci.* 106 (2009) 7968–7973. doi:10.1073/pnas.0812652106.
- [87] S.P. Sullivan, D.G. Koutsonanos, M. del Pilar Martin, J.W. Lee, V. Zarnitsyn, S.-O. Choi, N. Murthy, R.W. Compans, I. Skountzou, M.R. Prausnitz, Dissolving polymer microneedle patches for influenza vaccination, *Nat. Med.* 16 (2010) 915–920. doi:10.1038/nm.2182.
- [88] Y. Kawaoka, G. Neumann, *Influenza Virus: Methods and Protocols*, 2012th ed., Humana Press, New York, 2012.
- [89] B. Kalbfuss, A. Knöchlein, T. Kröber, U. Reichl, Monitoring influenza virus content in vaccine production: Precise assays for the quantitation of hemagglutination and neuraminidase activity, *Biologicals*. 36 (2008) 145–161. doi:10.1016/j.biologicals.2007.10.002.
- [90] Avian influenza virus, Humana Press Inc, [S.l.], 2014.
- [91] J.J. Wolf, L. Wang, F. Wang, Application of PCR technology in vaccine product development, *Expert Rev. Vaccines*. 6 (2007) 547–558. doi:10.1586/14760584.6.4.547.
- [92] AR-9725A: Automating the Assessment of Cell Viability - Automating the Assessment of Cell Viability. <http://www.beckman.de/getattachment/ae61fb6d-7d30-4bcf-8202-ac0afdb06ff8/Automating%20the%20Assessment%20of%20Cell%20Viability> (accessed November 23, 2016).
- [93] M.M. Bradford, A rapid and sensitive method for the quantitation of microgram quantities of protein utilizing the principle of protein-dye binding, *Anal. Biochem.* 72 (1976) 248–254. doi:10.1016/0003-2697(76)90527-3.
- [94] V.L. Singer, L.J. Jones, S.T. Yue, R.P. Haugland, Characterization of PicoGreen Reagent and Development of a Fluorescence-Based Solution Assay for Double-Stranded DNA Quantitation, *Anal. Biochem.* 249 (1997) 228–238. doi:10.1006/abio.1997.2177.
- [95] Joint EMAEDQM workshop on improved potency assays for inactivated influenza vaccines - WC500130042.pdf. http://www.ema.europa.eu/docs/en_GB/document_library/Report/2012/07/WC500130042.pdf (accessed November 17, 2016).

Chapter 7: References

- [96] Microsoft PowerPoint - 4 - New Cells for New Vaccines 2 - September 2007 DNA L Mallet [Read-Only] [Compatibility Mode] - Mallet - NCNV II (2007).pdf. [https://www.regonline.com/custImages/240000/244811/Mallet%20-%20NCNV%20II%20\(2007\).pdf](https://www.regonline.com/custImages/240000/244811/Mallet%20-%20NCNV%20II%20(2007).pdf) (accessed November 17, 2016).
- [97] R.C. Dunlap, E.R. Brown, D.W. Barry, Determination of the viral particle content of influenza vaccines by electron microscopy, *J. Biol. Stand.* 3 (1975) 281–289. doi:10.1016/0092-1157(75)90032-3.
- [98] G.K. Hirst, M.W. Pons, Mechanism of influenza recombination, *Virology.* 56 (1973) 620–631. doi:10.1016/0042-6822(73)90063-9.
- [99] R. Floyd, D.G. Sharp, Aggregation of poliovirus and reovirus by dilution in water., *Appl. Environ. Microbiol.* 33 (1977) 159–167.
- [100] R. Floyd, D.G. Sharp, Viral aggregation: quantitation and kinetics of the aggregation of poliovirus and reovirus., *Appl. Environ. Microbiol.* 35 (1978) 1079–1083.
- [101] R. Floyd, D.G. Sharp, Viral aggregation: effects of salts on the aggregation of poliovirus and reovirus at low pH., *Appl. Environ. Microbiol.* 35 (1978) 1084–1094.
- [102] R. Floyd, Viral aggregation: mixed suspensions of poliovirus and reovirus., *Appl. Environ. Microbiol.* 38 (1979) 980–986.
- [103] I.A. Rudneva, V.P. Kovaleva, N.L. Varich, V.R. Farashyan, L.V. Gubareva, S.S. Yamnikova, I.A. Popova, V.P. Presnova, N.V. Kaverin, Influenza A virus reassortants with surface glycoprotein genes of the avian parent viruses: effects of HA and NA gene combinations on virus aggregation, *Arch. Virol.* 133 (1993) 437–450. doi:10.1007/BF01313781.
- [104] A.L. Ksenofontov, V.S. Kozlovskii, L.V. Kordyukova, V.A. Radyukhin, A.V. Timofeeva, E.N. Dobrov, Determination of concentration and aggregate size in influenza virus preparations from true UV absorption spectra, *Mol. Biol.* 40 (2006) 152–158. doi:10.1134/S0026893306010201.
- [105] J.N. Campbell, R.M. Eband, P.S. Russo, Structural Changes and Aggregation of Human Influenza Virus, *Biomacromolecules.* 5 (2004) 1728–1735. doi:10.1021/bm049878z.
- [106] W. Anderson, D. Kozak, V.A. Coleman, Å.K. Jämting, M. Trau, A comparative study of submicron particle sizing platforms: Accuracy, precision and resolution analysis of polydisperse particle size distributions, *J. Colloid Interface Sci.* 405 (2013) 322–330. doi:10.1016/j.jcis.2013.02.030.
- [107] J. Vajda, D. Weber, D. Brekel, B. Hundt, E. Müller, Size distribution analysis of influenza virus particles using size exclusion chromatography, *J. Chromatogr. A.* 1465 (2016) 117–125. doi:10.1016/j.chroma.2016.08.056.
- [108] K.L. Planken, H. Cölfen, Analytical ultracentrifugation of colloids, *Nanoscale.* 2 (2010) 1849. doi:10.1039/c0nr00215a.

Investigation of influenza virus particle aggregation and purification with magnetic sulfated cellulose particles

- [109] D.J. Scott, S.E. Harding, A.J. Rowe, *Analytical Ultracentrifugation: Techniques and Methods*, Royal Society of Chemistry, 2005.
- [110] A. Neumann, W. Hoyer, M.W. Wolff, U. Reichl, A. Pfitzner, B. Roth, New method for density determination of nanoparticles using a CPS disc centrifuge™, *Colloids Surf. B Biointerfaces*. 104 (2013) 27–31. doi:10.1016/j.colsurfb.2012.11.014.
- [111] L.B. Jr, S. Fitzpatrick, Size distribution analysis of recombinant adenovirus using disc centrifugation, *J. Ind. Microbiol. Biotechnol.* 20 (1998) 317–322. doi:10.1038/sj.jim.2900529.
- [112] S.-J. Shih, M. Yagami, W.-J. Tseng, A. Lin, Validation of a quantitative method for detection of adenovirus aggregation, *Bioprocess. J.* 9 (2011) 25–33.
- [113] M. Deschuyteneer, A. Elouahabi, D. Plainchamp, M. Plisnier, D. Soete, Y. Corazza, L. Lockman, S. Giannini, M. Deschamps, Molecular and structural characterization of the L1 virus-like particles that are used as vaccine antigens in Cervarix™, the AS04-adjuvanted HPV-16 and -18 cervical cancer vaccine, *Hum. Vaccin.* 6 (2010) 407–419. doi:10.4161/hv.6.5.11023.
- [114] M.M. Pieler, A. Heyse, M.W. Wolff, U. Reichl, Specific ion effects on the particle size distributions of cell culture-derived influenza A virus particles within the Hofmeister series, *Eng. Life Sci.* (2016) in press. doi:10.1002/elsc.201600153.
- [115] N.M. Bouvier, A.C. Lowen, Animal models for influenza virus pathogenesis and transmission, *Viruses*. 2 (2010) 1530–1563. doi:10.3390/v20801530.
- [116] V. Lohr, Y. Genzel, I. Behrendt, K. Scharfenberg, U. Reichl, A new MDCK suspension line cultivated in a fully defined medium in stirred-tank and wave bioreactor, *Vaccine*. 28 (2010) 6256–6264. doi:10.1016/j.vaccine.2010.07.004.
- [117] S. Kluge, D. Benndorf, Y. Genzel, K. Scharfenberg, E. Rapp, U. Reichl, Monitoring changes in proteome during stepwise adaptation of a MDCK cell line from adherence to growth in suspension, *Vaccine*. (2015). doi:10.1016/j.vaccine.2015.02.077.
- [118] B. Peschel, S. Frentzel, T. Laske, Y. Genzel, U. Reichl, Comparison of influenza virus yields and apoptosis-induction in an adherent and a suspension MDCK cell line, *Vaccine*. 31 (2013) 5693–5699. doi:10.1016/j.vaccine.2013.09.051.
- [119] M.M. Pieler, S. Frentzel, D. Bruder, M.W. Wolff, U. Reichl, A cell culture-derived whole virus influenza A vaccine based on magnetic sulfated cellulose particles confers protection in mice against lethal influenza A virus infection, *Vaccine*. 34 (2016) 6367–6374. doi:10.1016/j.vaccine.2016.10.041.
- [120] M. Wolff, M.M. Pieler, U. Reichl, Process for the preparation of magnetic sulfated cellulose particles, magnetic sulfated cellulose particles and its use, EP14175925.
- [121] E. De Gregorio, E. Caproni, J.B. Ulmer, Vaccine Adjuvants: Mode of Action, *Front. Immunol.* 4 (2013). doi:10.3389/fimmu.2013.00214.

Chapter 7: References

- [122] S. Stegemann, S. Dahlberg, A. Kröger, M. Gereke, D. Bruder, B. Henriques-Normark, M. Gunzer, Increased Susceptibility for Superinfection with *Streptococcus pneumoniae* during Influenza Virus Infection Is Not Caused by TLR7-Mediated Lymphopenia, *PLOS ONE*. 4 (2009) e4840. doi:10.1371/journal.pone.0004840.
- [123] J.M. Wood, G.C. Schild, R.W. Newman, V. Seagroatt, An improved single-radial-immunodiffusion technique for the assay of influenza haemagglutinin antigen: Application for potency determinations of inactivated whole virus and subunit vaccines, *J. Biol. Stand.* 5 (1977) 237–247. doi:10.1016/S0092-1157(77)80008-5.
- [124] C. Casterlain, C. Genot, Conformational changes of bovine serum albumin upon its adsorption in dodecane-in-water emulsions as revealed by front-face steady-state fluorescence, *Biochim. Biophys. Acta BBA - Gen. Subj.* 1199 (1994) 59–64. doi:10.1016/0304-4165(94)90096-5.
- [125] L. Jorgensen, E.H. Moeller, M. van de Weert, H.M. Nielsen, S. Frokjaer, Preparing and evaluating delivery systems for proteins, *Eur. J. Pharm. Sci.* 29 (2006) 174–182. doi:10.1016/j.ejps.2006.05.008.
- [126] E.M. Verdurmen, J.G. Albers, A.L. German, Polybutadiene latex particle size distribution analysis utilizing a disk centrifuge, *Colloid Polym. Sci.* 272 (1994) 57–63. doi:10.1007/BF00653310.
- [127] Y. Sugita, T. Noda, H. Sagara, Y. Kawaoka, Ultracentrifugation deforms unfixed influenza A virions, *J. Gen. Virol.* 92 (2011) 2485–2493. doi:10.1099/vir.0.036715-0.
- [128] B. Michen, T. Graule, Isoelectric points of viruses, *J. Appl. Microbiol.* (2010). doi:10.1111/j.1365-2672.2010.04663.x.
- [129] M.V. Peshwa, Y.-S. Kyung, D.B. McClure, W.-S. Hu, Cultivation of mammalian cells as aggregates in bioreactors: Effect of calcium concentration of spatial distribution of viability, *Biotechnol. Bioeng.* 41 (1993) 179–187. doi:10.1002/bit.260410203.
- [130] J.V. Rödig, E. Rapp, J. Bohne, M. Kampe, H. Kaffka, A. Bock, Y. Genzel, U. Reichl, Impact of cultivation conditions on N-glycosylation of influenza virus a hemagglutinin produced in MDCK cell culture, *Biotechnol. Bioeng.* 110 (2013) 1691–1703.
- [131] J.V. Roedig, E. Rapp, D. Höper, Y. Genzel, U. Reichl, Impact of Host Cell Line Adaptation on Quasispecies Composition and Glycosylation of Influenza A Virus Hemagglutinin, *PLoS ONE*. 6 (2011) e27989. doi:10.1371/journal.pone.0027989.
- [132] J.R. Wiśniewski, A. Zougman, N. Nagaraj, M. Mann, Universal sample preparation method for proteome analysis, *Nat. Methods*. 6 (2009) 359–362. doi:10.1038/nmeth.1322.
- [133] E.C. Hutchinson, P.D. Charles, S.S. Hester, B. Thomas, D. Trudgian, M. Martínez-Alonso, E. Fodor, Conserved and host-specific features of influenza virion architecture, *Nat. Commun.* 5 (2014). doi:10.1038/ncomms5816.

Investigation of influenza virus particle aggregation and purification with magnetic sulfated cellulose particles

- [134] S. Amrhein, K.C. Bauer, L. Galm, J. Hubbuch, Non-invasive high throughput approach for protein hydrophobicity determination based on surface tension, *Biotechnol. Bioeng.* 112 (2015) 2485–2494. doi:10.1002/bit.25677.
- [135] M.J. Gerl, J.L. Sampaio, S. Urban, L. Kalvodova, J.-M. Verbavatz, B. Binnington, D. Lindemann, C.A. Lingwood, A. Shevchenko, C. Schroeder, K. Simons, Quantitative analysis of the lipidomes of the influenza virus envelope and MDCK cell apical membrane, *J Cell Biol.* 196 (2012) 213–221. doi:10.1083/jcb.201108175.
- [136] J. Wang, B. Li, M.X. Wu, Effective and lesion-free cutaneous influenza vaccination, *Proc. Natl. Acad. Sci.* 112 (2015) 5005–5010. doi:10.1073/pnas.1500408112.
- [137] G.J.P. Fernando, X. Chen, T.W. Prow, M.L. Crichton, E.J. Fairmaid, M.S. Roberts, I.H. Frazer, L.E. Brown, M.A.F. Kendall, Potent Immunity to Low Doses of Influenza Vaccine by Probabilistic Guided Micro-Targeted Skin Delivery in a Mouse Model, *PLOS ONE.* 5 (2010) e10266. doi:10.1371/journal.pone.0010266.
- [138] H.J.H.B. Hirschberg, E. van Riet, D. Oosterhoff, J.A. Bouwstra, G.F.A. Kersten, Animal models for cutaneous vaccine delivery, *Eur. J. Pharm. Sci.* 71 (2015) 112–122. doi:10.1016/j.ejps.2015.02.005.

8 APPENDICES

8.1 Materials and equipment

Table 7 Chemicals used in this work

Chemical	Information
Ammonium chloride	≥99.5%, 09718-250G, Sigma-Aldrich Co. LLC.
Calcium chloride dehydrate	≥99.0%, C5080-500G, Sigma-Aldrich Co. LLC.
Chlorosulfonic acid	99%, 571024, Sigma-Aldrich Co. LLC.
Hydrogen chloride	37%, 100317, Merck KGaA
Lithium chloride	≥99.0%, 62476-100G-F, Sigma-Aldrich Co. LLC.
Magnesium chloride hexahydrate	≥99.0%, M2670-500G, Sigma-Aldrich Co. LLC.
Potassium chloride	≥99.0%, P9333-500G, Sigma-Aldrich Co. LLC.
Pyridine	≥99.9%, 494410, Sigma-Aldrich Co. LLC.
Sodium azide	≥99.0%, 71290, Sigma-Aldrich Co. LLC.
Sodium bromide	≥99.5%, 71329-250G, Sigma-Aldrich Co. LLC.
Sodium chloride	≥99.5%, S7653-250G, Sigma-Aldrich Co. LLC.
Sodium nitrate	≥99.0%, S8170-250G, Sigma-Aldrich Co. LLC.
Sodium phosphate dibasic	≥99.0%, S7907-500G, Sigma-Aldrich Co. LLC.
Sodium phosphate monobasic	≥99.0%, S8282-500G, Sigma-Aldrich Co. LLC.
Sucrose (saccharose)	≥99.0%, 1.07654.1000, Merck KGaA
Sulfuric acid	95-97% ,1.00731.1011, Merck KGaA

Investigation of influenza virus particle aggregation and purification with magnetic sulfated cellulose particles

Chemical	Information
Tris base	≥99.9%, T6791-500G, Sigma-Aldrich Co. LLC.
β-propiolactone	≥98.5%, 33672.01, Serva Electrophoresis GmbH

Table 8 Particle standards used in this work

Size	Information
1020 nm	PMMA-F-L2712, PMMA, 10 % w/v, SD = 0.040 μm, microParticles GmbH
105 nm	PMMA-R-KM215, PMMA, 5 % w/v, SD = 0.004 μm, microParticles GmbH
196 nm	PMMA-F-KM255, PMMA, 5 % w/v, SD = 0.004 μm, microParticles GmbH
239 nm	PVC, 0.3 – 0.5 % w/v in H ₂ O without detergent, LOT-QuantumDesign GmbH
286 nm	PMMA-FKM256, PMMA, 5 % w/v, SD = 0.007 μm, microParticles GmbH
50 nm	Lot. No. 11056C, PMMA, 1% w/v, Phosphorex Inc.,
652 nm	PMMA-F-L1055-2, PMMA, 5 % w/v, SD = 0.018 μm, microParticles GmbH
807 nm	PMMA-R-L1057-2, PMMA, 5 % w/v, SD = 0.019 μm, microParticles GmbH

Table 9 Magnetic particles used in this work

Type	Information
Magnetic macroporous bead cellulose particles	MG 200, 100 - 250 μm, Iontosorb
Magne™ protein A particles	20% w/v, G8781, Promega Corp.

Table 10 Molecular biology, cell culture and immunization experiments equipment used in this work

Type	Information
∅ 0,45 x 12 mm needle	466 5457, B. Braun Melsungen AG
1 mL syringe	9161406V, B. Braun Melsungen AG
3,3',5,5'-tetramethylbenzidine liquid substrate	T5569, Sigma-Aldrich Co. LLC.
96-well ELISA plates	MaxiSorp, Thermo Fisher Scientific Inc.

Chapter 8: Appendices

Type	Information
Adherent MDCK cells	ECACC 84121903
Anti-A/PR serum	03/242, NIBSC
Anti-mouse IgG (whole molecule)-peroxidase antibody	A3415, Sigma-Aldrich Co. LLC.
CpG adjuvant	19404498, Eurofins Genomics GmbH
dNTP set	R0182, Thermo Fisher Scientific Inc.
EpiSerf media	10732022, Thermo Fisher Scientific Inc.
Fetal calf serum	F7524, Sigma-Aldrich Co. LLC.
GMEM-BHK21 media	22100-093, Thermo Fisher Scientific Inc.
Influenza A/PR/8/34	3138, Robert Koch Institute
Isoflurane	N01AB06, Baxter AG
Lab-FMV-peptone	MC033, Lab M Ltd.
Mice	C57Bl/6, Harlan Laboratories
Monoclonal anti-influenza virus type A hemagglutinin antibody C102	3IH4, HyTest Ltd.
Oligo (dT)12-18 primer	18418-012, Thermo Fisher Scientific Inc.
Polyinosinic:polycytidylic acid adjuvant	High molecular weight, tlr1-pic, Invivogen
Random Primer	48190-011, Thermo Fisher Scientific Inc.
RNAlater RNA Stabilization Reagent	76106, Qiagen GmbH
RNase-free DNase	79254, Qiagen GmbH
RNeasy Mini Kit	74106, Qiagen GmbH
SMIF8 PGd media	M008-2b, Service Zellkultur Scharfenberg
SuperScript II Reverse Transcriptase	18064-071, Thermo Fisher Scientific Inc.
Trypsin	27250-018, Thermo Fisher Scientific Inc.
Xylazin	Ceva Tiergesundheit GmbH

Investigation of influenza virus particle aggregation and purification with magnetic sulfated cellulose particles

Table 11 General equipment used in this work

Device	Information
0.1 µm filter	SLVV033RS, Merck KGaA
0.2 µm bottle top filter	514-0340, VWR Int.
0.45 µm depth filter	CMMP9408YY, GE Water & Process Technologies
0.65 µm depth filter	CFAP9608YY, GE Water & Process Technologies
14 kDa MWCO dialysis tube	0653.1, cellulose, Carl Roth GmbH & Co. KG
5 µm depth filter	CFAP0508YY, GE Water & Process Technologies
750 kDa MWCO Sartoclon Slice 200 Hydrosart tangential flow filtration cassette	Prototype, Sartorius-Stedim Biotech GmbH
Äkta Explorer 100	GE Healthcare Bio-Sciences AB
ÄKTACrossflow tangential flow filtration system	GE Healthcare Bio-Sciences AB
Bioreactor	CT5-SK, 5L, Sartorius-Stedim Biotech GmbH
CPS DC24000 UHR disc centrifuge	CPS Instruments Inc.
Gradient injection needles	BN2015, 20ga needles, 38 mm needle length, CPS Instruments Inc.
Gradient injection syringes	8300013982, 2 mL (3mL) NORM-JECT syringe, Henke-Sass, Wolf GmbH
High speed centrifuge	Optima TM LE-80K, Beckman Coulter Inc.
Kimtech Science Precision Wipes	05511 7552, 4.4 x 8.4 in./po (11 x 21 cm), 280 pieces per box, Kimberly-Clark Professional
LightCycler 480 SYBR Green I Master reaction mix	Roche Diagnostics GmbH
LightCycler 480 system	Roche Diagnostics GmbH
Milli-Q Advantage A10 water purification system	Merck KGaA
NanoDrop ND-1000 spectrophotometer	Thermo Fisher Scientific Inc.
Roller bottles	680160, 850 cm ² , Greiner Bio One International GmbH
Sample injection syringe	1725 RNR, 250µL, Hamilton Company

Chapter 8: Appendices

Device	Information
Sulfated cellulose membrane adsorber	Prototype, 3 mL, Sartorius-Stedim Biotech GmbH
Tabletop Centrifuge	Avanti J-20XP, Beckman Coulter Inc.
Thermocycler	Peqlab Biotechnologie GmbH
UltiMate 3000 RSLCnano splitless LC system coupled online to a LTQ-Orbitrap Elite hybrid MS	Thermo Fisher Scientific Inc.
Water purification system	LCPAK0001, Merck KGaA
Zetasizer Nano ZS	Malvern Instruments Ltd.

8.2 Standard operating procedures used in this work

List of the standard operating procedures (SOP) used in this work of the bioprocess engineering group from the Max Planck Institute for Dynamics of Complex Technical Systems, Magdeburg.

Table 12 Standard operating procedures used in this work

Title	Version (Date)
Hemagglutination Assay	2.3 (26.02.2016)
Inactivation with β -Propiolactone	1.6 (21.03.2016)
Measurement of influenza virus particle size distributions with the CPS Disc Centrifuge DC24000	2.0 (02.11.2016)
Single-Radial-Immunodiffusion (SRID)-Assay Influenza A virus (strain A/Puerto Rico/8/1934 H1N1)	(24.02.2016)

8.3 Standard operating procedure for influenza virus particles size distribution measurements with the CPS Disc Centrifuge DC24000

Author: Michael M. Pieler

Version: Version 2.0 (02.11.2016)

8.3.1 Introduction

PSD of influenza VP are of great interest in influenza vaccines bioprocess development. Because of that, a standard operating procedure (SOP) was established for measuring influenza VP by DCS with the CPS disc centrifuge DC24000. The method is based on previous work on adeno-associated and influenza VP with several modifications [111,112]. The information obtained from VP PSD can help to optimize different processes where VP aggregates are a problem.

8.3.2 Information material

This SOP covers information for the PSD measurement method of VP. It is highly recommended to go through the following information material to obtain a deeper understanding of the CPS disc centrifuge system:

1. "Introduction to Differential Sedimentation" (Ian Laidlaw and Marc Steinmetz, "LSD_AUC_Chapter 14.PDF") [109]
2. "CPS Disc Centrifuge Operating Manual" ("manual10-2004.pdf" in English or "CPS-Handbuch deutsch 2009.pdf" in German)
3. "Determination of particle size distribution with assistance of the CPS DC24000 disc centrifuge" ("SOP_Disc_Centrifuge.doc" from CPS Instruments Inc.)

The information material, Excel, and Matlab files are enclosed to the SOP in the folder "SOP Data" or the ZIP-file "SOP_Data.zip".

8.3.3 Materials

8.3.3.1 Equipment

The equipment is outlined in Table 13.

Table 13 DCS disc centrifuge SOP equipment

Name	Info	Ordering info
CPS Disc Centrifuge DC24000	-	CPS Instruments Inc.
2x sample injection syringe	250 μ L, gas tight, for sample and standard particle injection	1725 RNR 250 μ L, Hamilton Company
9x 2 mL gradient injection syringes	reusable, for gradient injection	2 mL (3mL) NORM-JECT syringe Ref. 8300013982, Henke-Sass, Wolf GmbH
9x gradient injection needles	for 2 mL syringes, preferable no sharp needle, must be smaller than 38 mm	20ga needles #BN2015, CPS Instruments Inc.
Timer	suitable for a 10 min countdown	-
Kimtech Science Precision Wipes	tissue for cleaning	05511 7552, 4.4 x 8.4 in./po (11 x 21 cm), 280 pieces per box, Kimberly-Clark Professional

Note: All used needles must be equal or smaller than 38 mm in order to avoid scratching the surface of the centrifuge disc. Preferable, needles with a length of 38 mm should be used!

8.3.3.2 Chemicals

Chemicals needed for the disc centrifuge measurements are listed below with their ordering information.

Table 14 DCS disc centrifuge SOP chemicals

Name	Info	Ordering info
Sucrose (saccharose)	for density gradient ultracentrifugation	Merck KGaA, 1.07654.1000

8.3.3.3 Gradient buffers

The used GB depend on the sample which is going to be measured. Typically, it is best to use the same buffer the VP are suspended in. This can be problematic for VP samples in cell culture broth, as there is usually no cell culture supernatant available without VP. Therefore, a buffer as close as possible is needed and should be used, e.g., fresh cell culture media or a buffer which resembles the environment of the samples. However, PBS or dialysis puffer consisting of 50 mM Tris-HCl 150 mM NaCl pH 7.4 are usually sufficient.

Investigation of influenza virus particle aggregation and purification with magnetic sulfated cellulose particles

Low density GB:

The GB for the default measurement setup are:

1. 16 % w/v sucrose in corresponding buffer
2. 4 % w/v sucrose in corresponding buffer

Note: Prepare all sucrose-containing buffers used for the GB new. Do not store them for future use. The GB contains a lot of sucrose and is therefore a good media for microbial growth.

Example: 4 g or 16 g of sucrose dissolved in 100 mL PBS.

Note: If you dissolve a certain amount of sucrose in 100 mL or fill up to a certain amount of sucrose to 100 mL is not crucial. However, you should stick to one way of preparing the GB to enable comparability between different measurements. For ease of application and comparability dissolving the sucrose in a defined premeasured volume is encouraged, i.e., weigh in sucrose and mix with a defined volume of buffer.

High density GB:

High density GB are only needed for the VP density determination.

1. 20 % w/v sucrose in corresponding buffer
2. 8 % w/v sucrose in corresponding buffer

8.3.3.4 Standard particles

The standard particles are used to examine the gradient quality after injection, for in-run calibration, and for gradient or particle density measurements.

Table 15 DCS disc centrifuge SOP standard particles

Size in nm	Density in g mL ⁻¹ (material)	Solid content in weight %	Ordering info
239	1.385 (PVC)	0.3 – 0.5 %	LOT Quantum Design GmbH, Hr. Wittmer, wittmer@lot-qd.de, order in water (without detergent!)
105	1.19 (PMMA)	5%	Microparticles GmbH, PMMA-R-KM215

Note: Always pipette the standard particles into a new vessel, e.g., new Eppendorf tube, for routine usage in order to avoid contamination of the original vessel. Even small particulate contaminations can be detected by this measurement method and can interfere with the sample of interest!

8.3.4 Methods

8.3.4.1 Measurement procedure

Every measurement is based on a defined procedure including all parameters for the measurement and analysis with the proprietary CPS software.

Table 16 DCS disc centrifuge SOP standard procedures

Name	Description
Infl 4-16P	For measurements in a 4 to 16% sucrose gradient in 1x PBS puffer for VP (check and adapt VP density if needed!).
Infl Dia Buf	For measurements in a 4 to 16% sucrose gradient in dialysis buffer for VP (check and adapt VP density!).
Infl 3 4-16%	For measurements in a 4 to 16% sucrose gradient in 1x PBS puffer for the 239 nm particle standard.
Infl 4 8-20%	For measurements in a 8 to 20% sucrose gradient in 1x PBS puffer for the 239 nm particle standard.

The used standard parameters are outlined in the tables below.

Table 17 DCS disc centrifuge SOP sample parameters

Name	Description
RPM	set to max, i.e., 24 000 RPM, to fix it when measuring VP densities
Maximum diameter	2.0 microns = 2 000 nm
Minimum diameter	0.06 microns = 60 nm, can be reduced if needed but increases measurement time
Particle density	particle density of the measured particle species, i.e., influenza VP or standard particles
Particle refractive index	default set to 1.54

Table 18 DCS disc centrifuge SOP calibration standard parameters

Name	Description
Peak diameter	0.239 microns for the 239 nm calibration standard particle
Half height peak width	0.05 microns
Particle density	1.385 g mL ⁻¹

Investigation of influenza virus particle aggregation and purification with magnetic sulfated cellulose particles

Table 19 DCS disc centrifuge SOP fluid parameters

Name	Description
Fluid density for PBS	1.067 g mL ⁻¹
Fluid refractive index	1.355
Fluid viscosity	1.2 cps

If the VP density is not known or an exact value is not needed for the experiment a standard value between 1.16 and 1.20 g cm⁻³ can be selected for the measurement procedure [46,110].

Table 20 DCS disc centrifuge SOP observed VP densities

Name	Description	Density
A/PR _{ADH}	Produced in MDCK _{ADH} in GMEM	1.18 g mL ⁻¹
A/PR _{SUS}	Produced in MDCK _{SUS2} in SMIF8	1.17 g mL ⁻¹

8.3.4.2 Centrifuge cleaning

The cleanliness of the centrifuge is a prerequisite to obtain reliable data. This is especially important for the centrifuge disc and the optical detector.

Table 21 DCS disc centrifuge SOP cleaning the centrifuge

Step	Description
1	Remove stains from the outside of the centrifuge case with an ultrapure water-wetted tissue.
2	Clean the injection port. If necessary, disassemble the injection port from the door by unscrewing it. The centrifuge door can be removed after removal of the injection port to allow easier cleaning of the inside.
3	Clean the inside of the centrifuge with a ultrapure water-wetted tissue to remove residual buffer stains.

If sugar stains are hard to dissolve use warm ultrapure water!

Note: Great care must be taken during cleaning the disc to not scratch its surface. Scratches on the disc surface will impair the measurement quality up to making the disc centrifuge unusable! Therefore, the disc should be only touched with gloves and special wipes, i.e., Kimtech Science Precision Wipes!

Chapter 8: Appendices

Table 22 DCS disc centrifuge SOP cleaning the centrifuge disc

Step	Description
1	Put on gloves and wear them during the whole procedure to avoid getting fat stains from your hands on the centrifuge disc surface. Fat stains can lead to baseline instability and therefore invalid measurements!
2	Insert the sucking tool inside the injection hole of the white lid of the centrifuge disc and suck out the solution from the measurement. If no measurement was carried out this step is not applicable and you can proceed to step 3.
3	Remove the white lid with the removal tool by screwing it in the lid and lift it up.
4	Dry the inside of the centrifuge disc with a dry tissue. Use two tissues folded together a couple of times to touch the whole space inside the disc for best results. If no measurement was carried out this step is not applicable and you can proceed to step 5.
5	Use ultrapure water in a spray bottle to spray water into the centrifuge disc while turning it by hand with gloves so that the water can reach every part inside the disc.
6	Remove the liquid with the sucking tool.
7	Dry the inside of the centrifuge disc with a dry tissue. Use two tissues folded together a couple of times for best results.
8	Use an with ultrapure water-wetted tissue to clean the disc outside. If necessary, wet the tissue with more ultrapure water or use a new tissue.
9	Repeat steps 5 - 8 three times.
10	Use a dry tissue to remove residual water from the washing steps from the in- and outside of the centrifuge disc.
11	Wet a folded tissue with >99% ethanol and clean the in- and outside of the centrifuge disc to remove fat stains.
12	Clean also the white lid with a water-wetted tissue, then let it dry before cleaning it with >99% ethanol-wetted tissue.
13	Let the centrifuge disc and the white lid dry for at least 10 min. If you plan to immediately carry out another measurement, check if the residual ethanol is fully evaporated. If not, wait until the residual ethanol is fully evaporated! Residual alcohol can change the PSD of the VP and therefore leads to unreliable measurement data!
14	When the white lid and the centrifuge disc are clean and dry insert the white lid into the centrifuge disc and close the door.

Investigation of influenza virus particle aggregation and purification with magnetic sulfated cellulose particles

8.3.4.3 Gradient preparation

The gradient consists of nine layers with different sucrose concentrations ranging from high to low sucrose concentrations present in the two GB. The two GB are mixed in a 2 mL syringe for the preparation of each gradient layer. After that, each prepared gradient layer is injected one by one into the stable running centrifuge disc. The ratios of buffer A and B are shown in the table below.

Table 23 DCS disc centrifuge SOP gradient layer composition

Layer	Buffer A in mL	Buffer B in mL
1	1.6	0.0
2	1.4	0.2
3	1.2	0.4
4	1.0	0.6
5	0.8	0.8
6	0.6	1.0
7	0.4	1.2
8	0.2	1.4
9	0.0	1.6

Table 24 DCS disc centrifuge SOP gradient layer preparation

Step	Description
1	Load 2 mL syringe with the volume of the higher density buffer A according to Table 23.
2	Load the same 2 mL syringe with the volume of the lower density buffer B according to Table 23.
3	Mix the gradient in the syringe until no concentration differences are visible ("concentration smears"). The air should be removed from the syringe to obtain reproducible GB volumes. However, small bubbles do not disturb the measurements.
4	Repeat step 1 to 3 for every gradient layer for the nine gradient steps.

8.3.4.4 Standard preparation

The standard particles are diluted in the respective sample buffer before they are injected into the gradient. The dilution depends on the GB system used. Usually, 20 μ L of the original 1:1 239 nm standard solution diluted in 130 μ L, i.e., a 1:5 dilution, proved to be useful. Nevertheless, the dilution ratio can be adapted if not compatible with the used buffer. However, the standard particle

Chapter 8: Appendices

volume should be minimized as much as possible. Additionally, it is highly recommended to have at least 150 μL of the prepared diluted standard particle solution to have enough for the aspiration of 100 μL into the injection syringe.

Note: Dilution of the standard particles in the buffers should be carried out immediately before injection to avoid aggregation and therefore an invalid calibration. If aggregation tendencies are unknown for a specific buffer they have to be evaluated before carrying out measurements.

8.3.4.5 Virus particle measurements

The VP sample measurement is outlined in the table below. To obtain analyzable signals the influenza VP sample should have a concentration of at least 1 000 HAU $100 \mu\text{L}^{-1}$. However, this threshold value can vary depending on the VP sample. If the VP sample shows low absorption the contribution of the baseline drift is higher and the data has to be interpreted with caution.

Table 25 DCS disc centrifuge SOP sample measurement

Step	Description
1	Check if the centrifuge disc is clean and the white lid is inserted properly. The circle on the white lid should be at the same position of the circle on the centrifuge disc to avoid disc imbalances!
2	Close the centrifuge door.
3	Select the measurement procedure for the desired VP sample.
4	Start the centrifuge and wait until the desired RPM are reached and are stable, i.e., 24 000 RPM.
5	Inject gradient layer 1 to 9. One gradient layer injection should take approximately 1 to 2 s.
6	Start the 10 min countdown for gradient equilibration.
7	After 1 min (9 min of the countdown left) inject 100 μL of the diluted particle standard solution to assess gradient quality. Abort analysis after the standard particle peak was visible to return to the normal "Operate Analyzer" window. If the obtained peak is symmetric and narrow proceed with step 8, if peak is asymmetric proceed to step 13. Sometimes the GB drifts after the standard peak are visible and the software rejects the calibration. This can be ignored, because the calibration is carried out in step 10. Here we just want to observe the gradient quality by observing the standard peak form.
8	Wait until the full 10 min are over and prepare in the meantime everything for the next injection of the diluted particle standard solution and the sample.
9	Shortly before the 10 min countdown is over, exit the "Operate Analyzer" window and reopen it again for getting the exact present RPM for the measurement. The RPM value gets updated by closing and reopening the "Operate Analyzer" window.

Investigation of influenza virus particle aggregation and purification with magnetic sulfated cellulose particles

Step	Description
10	After the 10 min countdown, inject 100 μ L of the diluted particle standard solution and terminate the calibration after 1 min. We terminate the calibration because the calibration time depends on the procedure and buffer parameters and can vary from 1 min.
11	Inject 100 μ L of the prepared sample.
12	Wait until data acquisition is completed.
13	Stop the centrifuge.
14	Clean the centrifuge according to the “Centrifuge cleaning” section.

8.3.4.6 Gradient density measurements

To obtain accurate PSD the gradient density (and the VP particle density) has to be measured. Therefore, measurements with a standard particle mix with different but known sizes and densities (or with a VP sample spiked with both standard particles if the virus particle density has to be determined subsequently) is carried out in the GB of interest [110].

For that, the GB or the VP sample is spiked with the 105 nm and 239 nm standard particles. The standard particle mix is then measured like a conventional sample. The dilution should be as high as possible without compromising the peak in the size distribution. In general, a 1:8 to 1:16 dilution proved to be sufficient. A typical sedimentation time distribution is shown in Figure 9 with the indicated sedimentation times of both standards, i.e., $t_{Std105nm}$ and $t_{Std239nm}$.

The zoom tool in the CPS software can be used to obtain the retention time maxima (vague but for most applications sufficient) or the data can be exported as CSV and analyzed in Excel (more accurate, see “Excel” section for details).

Then, the gradient density can be determined from the measured sedimentation times of the standard particles by linear regression as outlined in Formula 3-5 in section 3.6.4 [110].

The Excel document “Gradient_Density_Calculator_v2.xlsx” can be used to calculate the gradient buffer density. Finally, the determined gradient density can be pasted into the used measurement procedure of the CPS software.

8.3.4.7 Virus particle density measurements

The VP sample is spiked with the 105 and 239 nm standard particles to derive the VP densities [110]. The spiked VP sample is measured in a 4 to 16% and 8 to 20% sucrose gradient. With the determined sedimentation times of the standard particles the gradient density can be derived (see previous section). Based on that and the sedimentation times of the VP in both gradients the VP density can be calculated.

Chapter 8: Appendices

The VP density can be determined from the measured sedimentation times of the VP in the 4 to 16% and the 8 to 20% sucrose gradient and the determined gradient densities (see previous section) by linear regression outlined in Formula 6-8 in section 3.6.5 [110].

The file "Density_Measurement_Example_R1_2xStd_B_105+239nm_Std.xlsx" can be used as a basis to calculate VP densities. The reported error of the VP density measurement method is < 4 % [110].

8.3.5 Validation

The validation data of the method can be found in the file "CPS_Vali_AR_v1.8_Final_1x-Measurement.xls" for single measurements and in "CPS_Vali_AR_v1.8_Final_3x-Measurement.xls" for triplicate measurements. If the system you are measuring is stable and you are familiar with the equipment and the method, the single measurement is sufficient.

8.3.6 Data analysis

8.3.6.1 Introduction

The PSD can be visualized in several ways with the CPS software. The following two options are encouraged:

1. Absorbance PSD
2. Weight PSD

The absorbance data helps to see small changes in the higher particle size ranges and is therefore interesting for the detection of small changes in the aggregation status. Nevertheless, the default option is to display the weight data (which is derived from the absorbance data).

The reason that the absorbance data representation shows higher sensitivity to larger particles is due to the fact that the absorbance increases with the particle size (see literature listed in the "Information material" section for a more detailed discussion on this topic).

Note: It is highly discouraged to compare absolute weight values. Especially, at low measured particle concentrations baseline instabilities can have a significant impact on the PSD. Because of that, the visualization of normalized size distributions is encouraged.

8.3.6.2 Excel

The measurement data can be also analyzed and visualized in Excel after the data has been exported into a CSV file via the CPS software.

Plot the PSD data according to file „PStest.xlsx“:

- The first column for weight, surface, number and absorbance is graphed using column A for the x-values and a linear x-axis scale.
- The second column for weight, surface, number and absorbance is graphed using column A for the x-values and a log x-axis scale.

Investigation of influenza virus particle aggregation and purification with magnetic sulfated cellulose particles

- The third column for weight, surface, number and absorbance is graphed using column A for the x-values and either a log or linear x-axis scale.

8.3.6.3 Matlab

For obtaining high quality figures you can visualize the PSD data in Matlab. Therefore, you can use the “CPS10.m” code file to load the PSD data into Matlab and to obtain an automatic overview of the measured samples. To run the code, navigate to the folder containing the file “CPS10.m” with “csv2cell.m” (subprogram for “CPS10.m”) and type “CPS10” to start the program. (Navigation over the Matlab command line can be done with the “cd” command to change the working directory, i.e., “cd \\afs\urz.uni-magdeburg.de\adsprof\abastian\Documents\CentrifDisc\Matlab”.) Then, select at least two data files in the dialog window for the data import and visualization.

To obtain optimized relative weight over log size plots you can run afterwards “Plot_LogWt_60_240nm.m” for showing the PSD from 60 to 240 nm, “Plot_LogWt_60_640nm.m” for 60 to 640 nm, or “Plot_LogWt_60_1040nm.m” for 60 to 1040 nm. The resulting figures can be used as a basis for publication grade figures.

To import other files after an import, type “clear,clc” to clear the workspace and screen. Then start again with “CPS10” for another import.

If you want to generate sedimentation time plots you can use “CPS_Time_v2.m” and “Plot_LogWt_Time_v1.m”.

8.3.7 Points to consider

- If you want to carry out overview measurements, you can use the gradient for up to three consecutive measurements without stopping the centrifuge and cleaning it. However, be aware that the obtained PSD will slightly vary from the one obtained by the validated method outlined in this document.
- If the VP density is not known and just one peak is visible it can be tricky to determine if the peak is of monomeric or dimeric nature.
- The buffer of the VP sample should have a lower density than the lightest layer of the gradient. Otherwise, streaming could be a problem and the obtained data is invalid.

8.4 Validation data of the virus particles size distribution measurement method with the CPS Disc Centrifuge DC24000

The validation of the PSD measurement method for VP was carried out with PMMA particles in the size range of approximately 50 to 1000 nm. The PMMA particles had a similar density with 1.19 kg m^{-3} compared to the VP. Due to the nature of the measurement system the variance at the lower and the upper limit were inhomogeneous. Therefore, a weighted regression was used, which is shown in Figure 32. The validation results for the single and triplicate measurements are shown in Table 27.

Table 26 Measurement data lower and upper detection limit

Measurement	Lower limit	Upper limit
nominal value	50.00	1020.00
1	46.67	1029.60
2	46.62	1009.63
3	47.01	1010.73
4	46.64	1020.60
5	46.61	1033.30
6	46.71	1031.99
7	46.67	1012.55
8	46.65	1015.98
9	46.95	1027.40
10	46.95	1023.95
Average	46.75	1021.57
Standard deviation	0.16	8.97
Variance	0.02	80.44

Investigation of influenza virus particle aggregation and purification with magnetic sulfated cellulose particles

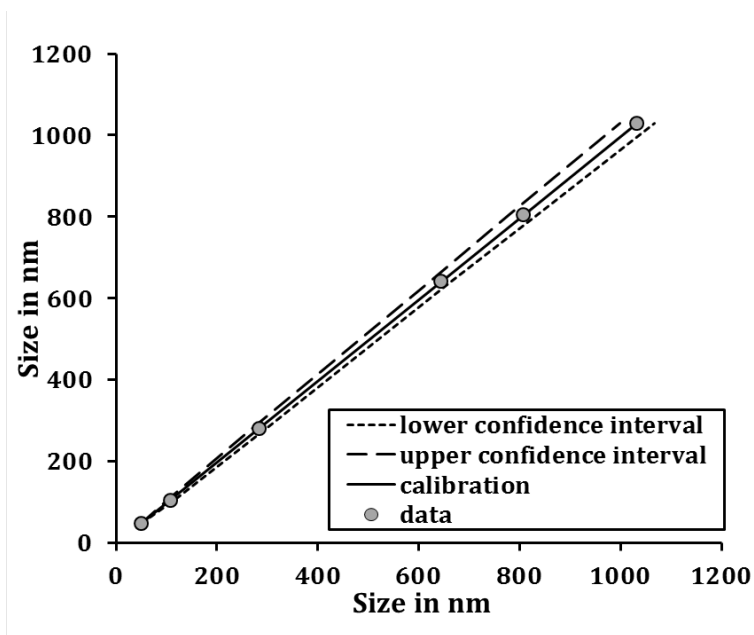


Figure 32 Weighted linear regression for single measurements

Table 27 Validation results for single measurement

Measurement setup	single	triplicate
Residual standard deviation in nm	0.52	0.42
Sensitivity in nm/nm	1.0001	0.9976
Process standard deviation in nm	0.52	0.42
Relative process standard deviation in %	0.99	0.80
Coefficient of determination (R^2)	0.9997	0.9999
Limit of detection in nm	1.70	1.37
Limit of quantitation in nm	5.16	4.17
Lower confidence interval in nm	0.83	0.67
Upper confidence interval in nm	35.02	26.20

8.5 Publications

The dissertation includes content that has already been published in or is submitted to international peer-reviewed scientific journals. Subsequently, the published and submitted publications are listed in detail, including the specific contribution of the author of this doctoral thesis. First authorship is indicated with “*”.

“Comparison of influenza virus particle purification using magnetic sulfated cellulose particles with an established centrifugation method for analytics”, A. Serve*, **M. M. Pieler***, D. Benndorf, E. Rapp, M. W. Wolff, U. Reichl, *Analytical Chemistry* 87.21 (2015): 10708-10711 [24]

Contributions: Michael M. Pieler and Anja Serve (Max Planck Institute for Dynamics of Complex Technical Systems, Bioprocess Engineering Group, Magdeburg, Germany) contributed equally to this work. The implementation of the MSCP production method, the MSCP production, the implementation of the MSCP purification methods, and the MSCP purifications were carried out by MMP. The influenza VP production (see section 3.3.3), the VP purification using centrifugation (see section 3.4.5), and the LC-MS/MS experiments (see section 3.6.6) were carried out by AS. MMP and AS carried out the experimental plan setup, the data analysis, and writing the manuscript.

“A cell-culture derived whole virus influenza A vaccine based on magnetic sulfated cellulose particles confers protection in mice against lethal influenza A virus infection”, **M. M. Pieler***, S. Frentzel*, D. Bruder, M. W. Wolff, U. Reichl, *Vaccine* 34.50 (2016): 6367–6374 [119]

Contributions: Michael M. Pieler (Max Planck Institute for Dynamics of Complex Technical Systems, Bioprocess Engineering Group, Magdeburg, Germany) and Sarah Frentzel (Institute of Medical Microbiology and Hospital Hygiene, Infection Immunology Group, University Hospital of the Otto-von-Guericke University Magdeburg, Germany) contributed equally to this work. The implementation of the MSCP production method, the MSCP production, the implementation of the MSCP experimental methods, the preparation of the VP samples, the preparation of the vaccines, and the implementation of the ELISA method were carried out by MMP at the Max Planck Institute for Dynamics of Complex Technical Systems, Magdeburg. The immunization and challenge experiments (see sections 3.5, 3.6.7, and 3.6.9) as well as the statistical data evaluation (see section 3.6.10.2) were carried out by SF at the Institute of Medical Microbiology and Hospital Hygiene, Infection Immunology Group, University Hospital of the Otto-von-Guericke University Magdeburg, Germany. MMP and SF carried out the experimental plan setup, the data analysis, and writing the manuscript.

Investigation of influenza virus particle aggregation and purification with magnetic sulfated cellulose particles

“Specific ion effects on the particle size distributions of cell culture-derived influenza A virus particles within the Hofmeister series”, **M. M. Pieler***, A. Heyse, M. W. Wolff, U. Reichl, Engineering in Life Sciences, in press [114]

Contributions: Michael M. Pieler (Max Planck Institute for Dynamics of Complex Technical Systems, Bioprocess Engineering Group, Magdeburg, Germany) and Anja Heyse (M.Sc. thesis, Otto-von-Guericke University Magdeburg, Germany) contributed to this work. The implementation of the PSD measurement method, the experimental methods, the experimental plan setup, the data analysis, and writing the manuscript were carried out by MMP. The preparation of the VP samples, the VP dialysis experiments, and the PSD measurements were carried out by MMP and AH.

“Chromatographic purification of cell culture-derived influenza A virus using regenerated cellulose membranes and polyethylene glycol”, P. Marichal-Gallardo*, **M. M. Pieler***, M. W. Wolff, U. Reichl, Journal of Chromatography A, in press [74]

Contributions: Michael M. Pieler and Pavel Marichal-Gallardo (Max Planck Institute for Dynamics of Complex Technical Systems, Bioprocess Engineering Group, Magdeburg, Germany) contributed equally to this work. The preparation of the VP samples and the PSD measurements were carried out by MMP. The chromatography was carried out by PMG. The implementation of the experimental methods, the experimental plan setup, the data analysis, and writing the manuscript were carried out by MMP and PMG.

8.6 Patents

“Method for the separation of virus compositions including depleting and purification thereof” (EP16174958, 2016, pending)

“Method for the production of a pharmaceutical composition like a vaccine and pharmaceutical composition” (EP15201000, 2015, pending)

“Method for the purification of virus compositions and virus compositions obtained” (EP15193102, 2015, pending)

“Process for the preparation of magnetic sulfated cellulose particles, magnetic sulfated cellulose particles and their use” (EP14175925, 2014, pending)

8.7 Attended conferences

8.7.1 Talks

M. M. Pieler, A. Serve, R. Hennig, D. Vázquez Ramírez, M. W. Wolff, U. Reichl, Max “Virus particle purification using magnetic sulfated cellulose particles” talk at the DECHEMA Himmelfahrtstagung conference, Koblenz, Germany, May 2016

M. M. Pieler, R. Hennig, N. Gebert, E. Rapp, M. W. Wolff, U. Reichl “Comparison of protein and glyco patterns of cell culture-derived influenza viruses purified by pseudo affinity ligands” talk at the 12th International PhD Seminar on Chromatographic Separation Science, Schleiden, Germany, February 2016

8.7.2 Posters

M. W. Wolff, **M. M. Pieler**, S. Frentzel, L. Fichtmüller, A. Bastian, D. Bruder, U. Reichl “Use of magnetic sulfated cellulose particles allows fast purification and blending of potent influenza vaccines in mice” poster at Recovery of Biological Products XVII, Fairmont Southampton, Bermuda, June 2016

M. M. Pieler, S. Frentzel, D. Bruder, M. W. Wolff, U. Reichl “Pseudo-affinity purification and formulation of a cell-culture derived whole influenza virus vaccine using magnetic sulfated cellulose particles” poster at the Vaccine Technology VI conference, Albufeira, Portugal, June 2016

M. M. Pieler, A. R. Fortuna, B. Hundt, M. W. Wolff, U. Reichl “Study of influenza virus aggregation during downstream processing” poster at the 34th International Symposium on the Separation of Proteins, Peptides and Polynucleotides, Würzburg, Germany, November 2014

M. M. Pieler, A. R. Fortuna, B. Hundt, M. W. Wolff, U. Reichl “Investigation of virus aggregation on performance of downstream processing in influenza vaccine manufacturing” at the 31. DECHEMA-Jahrestagung der Biotechnologen, Aachen, Germany, September 2014

M. M. Pieler, A. R. Fortuna, M. W. Wolff, U. Reichl “Investigation of virus aggregation on performance of downstream processing in influenza vaccine manufacturing” poster at the Recovery of Biological Products XVI conference, Rostock, Germany, July 2014

8.8 Supervised student projects

8.8.1 Master theses

A. Heyse (birth name Schenk), "Effect of Hofmeister salts on the aggregation status of cell culture-derived influenza virus particles concentrated by tangential flow filtration", Otto-von-Guericke University Magdeburg, 2015

The preparation of the VP samples, the VP dialysis experiments, and the PSD measurements were carried out by Anja Heyse (M.Sc. thesis, Otto-von-Guericke University Magdeburg, Germany) and Michael M. Pieler (Max Planck Institute for Dynamics of Complex Technical Systems, Bioprocess Engineering Group, Magdeburg, Germany).

N. Gebert, "Interaction of sulphated carbohydrates with influenza virus particles", Otto-von-Guericke University Magdeburg, 2015

The measurements of the MSCP dry weights, zeta potentials, and light microscopy pictures were carried out by Nicole Gebert (M.Sc. thesis, Otto-von-Guericke University Magdeburg, Germany).

8.8.2 Bachelor thesis

D. Kopp, "Neustrukturierung des Bioverfahrenstechnik-Praktikums – Upstream- und Downstream-Prozess eines rekombinanten Proteins (GFP) in E.coli", Otto-von-Guericke University Magdeburg, 2015

8.9 Curriculum vitae

Professional Experience

- 08.2013 – 12.2016 Doctoral Researcher in Downstream Processing
Bioprocess Engineering Group, Max Planck Institute for Dynamics of
Complex Technical Systems, Magdeburg, Germany
- 02.2013 – 07.2013 Research & Development in Microfluidics
Robert Bosch GmbH, Reutlingen and Gerlingen, Germany
- 02.2007 – 04.2011 Junior Finance Manager (working student)
A1 Telekom Austria AG, Vienna, Austria

Education

- 02.2010 – 12.2012 Master's Degree in Biotechnology
University of Natural Resources and Life Sciences, Vienna, Austria
Master's thesis: "Development of an SNP application based on real-time
high resolution melting analysis of surface immobilized nucleic acids"
- 09.2006 – 02.2010 Bachelor's Degree in Food Science and Biotechnology
University of Natural Resources and Life Sciences, Vienna, Austria
Bachelor's thesis: "Recombinant vaccines with focus on viral vaccines"
- 09.2005 – 05.2006 Military Service
Austrian army, military hospital, Vienna
- 09.2000 – 06.2005 High School in Electronics specializing in Biomedical Engineering
Technologisches Gewerbe-Museum, secondary technical and vocational
high school, Vienna, Austria

Internships/Jobs

- 05.2013 Clinical Institute of Laboratory Medicine
Medical University of Vienna/AKH Wien, Vienna, Austria
- 08.2006 Crude Fractionation
Baxter AG, Vienna, Austria
- 2003 – 2006 Yearly summer job
A1 Telekom Austria AG, Vienna, Austria

Chapter 8: Appendices

Additional publications before the dissertation

2013 “Development of an SNP application based on real-time high resolution melting analysis of surface immobilized nucleic acids”

M. M. Pieler, AV Akademikerverlag, Saarbrücken, Germany

ISBN-13: 9783639467437

Languages

German (native), English (business fluent)

Magdeburg, am 31.01.2017

Michael M. Pieler